Particle formation in RAFT-mediated emulsion polymerization

Please check the document version of this publication:

• A submitted manuscript is the version of the article upon submission and before peer-review. There can be important differences between the submitted version and the official published version of record. People interested in the research are advised to contact the author for the final version of the publication, or visit the DOI to the publisher's website.
• The final author version and the galley proof are versions of the publication after peer review.
• The final published version features the final layout of the paper including the volume, issue and page numbers.

Link to publication

Particle Formation in RAFT-mediated Emulsion Polymerization

Joost Sieger Kaspar Leswin

Particle Formation in RAFT-mediated

Emulsion Polymerization

PROEFSCHRIFT

ter verkrijging van de graad van doctor aan de
Technische Universiteit Eindhoven, op gezag van de
Rector Magnificus, prof.dr.ir. C.J. van Duijn, voor een
commissie aangewezen door het College voor
Promoties in het openbaar te verdedigen
op donderdag 21 juni om 14.00 uur

door

Joost Sieger Kaspar Leswin

geboren te Eindhoven

Dit proefschrift is goedgekeurd door de promotoren:

prof.dr. A.M. van Herk
en
prof.dr. R.G. Gilbert

Copromotor:
dr. J. Meuldijk

"Croyez ceux qui cherchent la vérité, doutez de ceux qui la trouvent." André Gide

Table of Contents

Summary

Particle formation in RAFT-mediated emulsion polymerization has been studied using reaction calorimetry. By measuring the heat flow during controlled feed *ab-initio* emulsion polymerization in the presence of amphipathic RAFT agents, particle formation by self-assembly of these species could be observed. Two different monomer systems, i.e. styrene and n-butyl acrylate, and various degrees of hydrophobicity of the initial macro-RAFT agents have been studied and compared.

The different macro-RAFT agents were synthesized by first forming a hydrophilic block of poly(acrylic acid) that would later on act as the electrosteric stabilizing group for the particles. Subsequently, different lengths of hydrophobic blocks were grown at the reactive end of the poly(acrylic acid) hydrophilic block via the RAFT-mediated controlled radical polymerization, either comprised of n-butyl acrylate or styrene.

Two processes govern particle formation: adsorption of macro-RAFT agents onto growing particles and formation of new particles by initiation of micellar aggregates or by homogeneous nucleation. Competition between these processes could be observed when monomers with a relatively high (n-butyl acrylate) or low (styrene) propagation rate coefficient were used.

A model describing particle formation has been developed and the results of model calculations are compared with experimental observations. Preliminary modeling results based on a set of reasonable physico-chemical parameters already showed good agreement with the experimental results. Most parameters used have been verified experimentally.

The development of the molecular weight distribution of the macro-RAFT agents has been analyzed by different techniques. Quantification of the particle formation process by analytical techniques was difficult, but qualitative insights into the fundamental steps

governing the nucleation process have been obtained. The amount of macro-RAFT agents initially involved in particle formation could be determined from the increase of molecular weight. The particle size distribution has been measured by capillary hydrodynamic fractionation, transmission electron microscopy and dynamic light scattering. From the data obtained from these particle-sizing techniques, the number of particles during the reaction could be monitored, leading to an accurate estimate for the particle formation time.

Upon implementation of the experimental data obtained for the surface active macro-RAFT systems, the model demonstrated to be very sensitive towards the "headgroup" area of the macro-RAFT species. Three nucleation cases based on the initial surface activity of the macro-RAFT species in the aqueous phase are proposed to explain the deviations from the assumptions of the nucleation model. Even though the macro-RAFT species have a narrow molecular weight distribution, they are nevertheless made up of a distribution of block lengths of polystyrene upon a distribution of block lengths of poly(acrylic acid). The resulting differences in initial surface activity are the most probable reason for the observed differences between model calculations and experimental results for the nucleation time and particle size distribution of the final latex product.

With the procedure described above, latexes have been synthesized without using conventional surfactants and the mechanisms involved in the particle formation for these systems have been elucidated. The results of this work enable production of latex systems with well defined molecular mass distributions and narrow particle size distributions. Furthermore, the technique based on the application of amphipathic RAFT agents is promising for the production of complex polymeric materials in emulsion polymerization on a technical scale.

Samenvatting

De deeltjesvorming bij door RAFT gecontroleerde radicaalpolymerisatie in emulsie is bestudeerd met behulp van reactiecalorimetrie. Door nauwkeurig de warmteproductiesnelheid te meten gedurende de *ab-initio* emulsiepolymerisatie kan deeltjesvorming door aggregatie van de oppervlakte-actieve macro-RAFT moleculen worden waargenomen. Voor de monomeren styreen en n-butylacrylaat zijn in aanwezigheid van de van deze monomeren afgeleide macro-RAFT-moleculen de deeltjesvorming en het vervolg van het emulsiepolymerisatieproces onderzocht.

De verschillende macro-RAFT-moleculen zijn gesynthetiseerd door eerst een hydrofiel blok van poly(acrylzuur) te vormen. Dit hydrofiele blok zorgt in het emulsiepolymerisatieproces voor de colloïdale stabiliteit van de latexdeeltjes. Vervolgens is door middel van RAFT-gecontroleerde radicaalpolymerisatie een hydrofoob blok van polystyreen of van poly(n-butylacrylaat) aan de hydrofiele macro-RAFT-moleculen gegroeid. Er zijn macro-RAFT-moleculen gesynthetiseerd met verschillende lengten van het hydrofobe blok.

Tijdens de emulsiepolymerisatie worden de macro-RAFT-moleculen door twee processen verbruikt: enerzijds door bij te dragen aan vorming van nieuwe deeltjes, anderzijds door aan het oppervlak van bestaande deeltjes geadsorbeerd te worden. De vorming van nieuwe deeltjes kan door homogene dan wel micellaire nucleatie plaats vinden. De competitie tussen de twee verbruiksprocessen kon worden bestudeerd door te werken met monomeren met sterk verschillende propagatiesnelheidscoëffiënten (k_p); styreen heeft een relatief lage k_p en n-butylacrylaat een relatief hoge.

Er is een model ontwikkeld dat de deeltjesvorming beschrijft voor de toegepaste macro-RAFT-moleculen. De resultaten van modelberekeningen zijn vergeleken met experimentele waarnemingen. Berekeningen op basis van fysisch-chemisch redelijke aannamen kwamen

goed overeen met experimentele resultaten. Tijdens dit onderzoek zijn deze aannamen experimenteel geverifieerd.

De ontwikkeling van de molecuulgewichtsverdeling van de macro-RAFT-moleculen gedurende de reactie is onderzocht met behulp van verschillende analysetechnieken. Een kwantitatief antwoord op de vraagstelling aangaande de duur van het deeltjesvormingsproces bleek moeilijk te geven. Er is echter wel kwalitatief inzicht verkregen in de fundamentele stappen die bepalend zijn in het deeltjesvormingsproces. Het aantal macro-RAFT-moleculen dat bij de initiële deeltjesvorming betrokken was, kon met behulp van chromatografische technieken worden vastgesteld. De deeltjesgrootteverdeling is geanalyseerd met behulp van capillaire hydrodynamische fractionering, transmissie elektronenmicroscopie en dynamische lichtverstrooiing. Op basis van de resultaten van deze deeltjesgrootte analyses kon een nauwkeurige schatting worden gemaakt van de nucleatietijd.

Bij de implementatie van de verkregen experimentele resultaten in het nucleatiemodel is gebleken dat de uitkomst van de modelberekeningen zeer gevoelig is voor het specifieke oppervlak van de macro-RAFT-moleculen die bij de deeltjesvorming betrokken zijn. Ter verklaring van de afwijkingen van het model ten opzichte van de experimentele resultaten zijn drie situaties, gebaseerd op de initiële oppervlakteactiviteit van het macro-RAFT-molecuul, gepresenteerd. Want hoewel de macro-RAFT-moleculen een smalle molecuulgewichtsverdeling hebben, zijn zij desalniettemin opgebouwd uit een verdeling van hydrofobe bloklengten bovenop een verdeling van hydrofiele bloklengten, die tezamen een grote verscheidenheid aan oppervlakteactiviteit voortbrengen.

Met de beschreven emulsiepolymerisatietechniek zijn latexproducten verkregen zonder gebruik te maken van conventionele zepen. De mechanismen die een rol spelen bij het nucleatieproces zijn ten opzichte van de reeds in de literatuur gerapporteerde kennis verder opgehelderd. De resultaten van dit werk maken het mogelijk latexproducten te produceren

met zowel een goed gedefinieerde molecuulgewichtsverdeling als een smalle deeltjesgrootteverdeling. Bovendien is het gebruik van amfifiele macro-RAFT-moleculen een veelbelovende techniek voor het produceren van complexe polymere materialen in emulsies op een technische schaal.

Glossary

Acronyms

AA	Acrylic acid
BA	Butyl acrylate
C(Z)E	Capillary (Zone) Electrophoresis
CHDF	Capillary Hydrodynamic Fractionation
CMC	Critical micelle concentration
DLS	Dynamic light scattering
DLVO	Theory of stability of lyophobic dispersions as developed by Derjaguin and Landau and independently by Verwey and Overbeek
DP	Degree of polymerization
DRI	Differential refractive index
Dx	Dioxane
EOF	Electro-osmotic flow
ESI-MS	Electrospray ionization mass-spectrometry
HDC	Hydrodynamic chromatography
HPLC	High performance liquid chromatography
HQ	Hydroquinone
HUFT	Homogeneous nucleation model described by Hansen and Ugelstadt as well as by Fitch and Tsai
LAC	Liquid adsorption chromatography
MALDI-ToF MS	Matrix-assisted laser desorption ionization time-of-flight mass-spectrometry
MeHQ	Hydroquinone monomethyl ether
MWD	Molecular weight distribution
PDI	Polydispersity index
PFG	Column material for use with fluorinated solvents
PG	Propylene glycol
PLP-SEC	Pulsed laser polymerization in combination with SEC
PMMA	Poly(methyl methacrylate)
PSD	Particle size distribution
PVA	Poly(vinyl alcohol)
RAFT	Reversible addition-fragmentation chain transfer
SANS	Small angle neutron scattering
SDS	Sodium dodecyl sulfate
SEC	Size exclusion chromatography
STY	Styrene
(cryo-)TEM	(cryogenic) Transmission electron microscopy
THF	Tetrahydrofuran
UV	Ultra-violet
V-501	4,4'-Azobis(4-cyanopentanoicacid) also known as 4,4'-Azobis(4-cyanovalericacid)

Symbols

symbol	definition	Typical units
Γ	Interfacial tension at the latex particle water surface	10^{-3} N s^{-1}
ρ	Average number of radicals entering a particle	s^{-1}
ρ_L	Density of the latex particles	g L^{-1}
ρ_M	Density of monomer	kg m^{-3}

symbol	definition	Typical units
ρ_P	Density of polymer	kg m^{-3}
φ_p	Volume fraction of polymer in the polymer solution constituting the latex particles	
χ	Flory-Huggins interaction parameter	
A	Heat exchange area	m^2
A_E	Specific surface area of surfactant	m^2
A_S	Area of a particle	m^2
A_{SDS}	Total surface covered by SDS	m^2 g^{-1}
C	Total concentration of added surfactant	mol L^{-1}
d_n	Number average diameter	10^{-9} m
d_{vv}	Volume weighted average diameter	10^{-9} m
d_z	Intensity weighted average diameter	10^{-9} m
[I]	Initiator concentration	mol L^{-1}
k	Exit rate of radicals from a particle	s^{-1}
K_d	Initiator dissociation rate coefficient	s^{-1}
K_p	Propagation rate coefficient	L mol^{-1} s^{-1}
$K_{p,W}$	Propagation rate coefficient in the water phase	L mol^{-1} s^{-1}
K_t	Termination rate coefficient	L mol^{-1} s^{-1}
$K_{t,W}$	Termination rate coefficient in the water phase	L mol^{-1} s^{-1}
m	Concentration of polymer	g L^{-1}
M_0	Molecular weight of monomer	kg mol^{-1}
m_{M^0}	Mass of monomer per total volume	g L^{-1}
$[M]_p$	[Monomer] in the particles	mol L^{-1}
$[M]_W$	[Monomer] in the water phase	mol L^{-1}
$\bar{n}$	Time \<number\> of free radicals per particle	
N_A	Avogadro's number	mol^{-1}
N_c	Number concentration of particles	L^{-1}
n_{cap}	Number of RAFT capped chains per particle	
n_{M^0}	Moles of monomer per unit volume of water	mol L^{-1}
$n_{macro\text{-}RAFT}$	Number of macro-RAFT molecules	
N_p	Number of particles	
Q_c	Calibration heat	W
r_u	Average radius of the unswollen particles	10^{-9} m
S_a	Titrated soap adsorbed on the latex particles	mol g^{-1}
T_a	Corrected jacket temperature	°C
T_g	Glass transition temperature	°C
T_j	Temperature of the surrounding jacket oil	°C
T_r	Temperature of the reaction mixture	°C
U	Overall heat transfer coefficient	W m^{-2}K^{-1}
V_s	Monomer swollen volume	m^3
V_{sM}	Partial molar volume of monomer	m^3
V_W	Volume of water	L
X_{crit}	Critical degree of polymerization	
$\bar{X}_n$	Number-average degree of polymerization of chains	
z	Degree of polymerization necessary for a initiator derived radical to become surface active enough to enter a particle	

Chapter 1

Introduction

1.1 *Colloidal stability of aqueous polymer dispersions*

A colloid is a heterogeneous system consisting of small "particles" distributed more or less uniformly throughout a continuous phase. Thomas Graham coined the term colloid (glue-like) for these kinds of systems in 1861. Milk is a nice example of a natural colloid, an emulsion of fat in water, electrostatically stabilized by phosphate groups of the protein casein. However, the formation of cream on top of milk indicates that casein is not the best of stabilizers, since the cream is formed by coalescence of fat into oil based droplets floating on the surface[1].

In the industrially important suspension and emulsion polymerization process, surfactants are used to stabilize colloidal polymer particles. These surfactants stabilize "particles" either by electrostatic repulsion or steric repulsion, a combination of electrostatic and steric stabilization is referred to as electrosteric stabilization. The overall stability of a colloidal system depends on the total interaction energy curve for the system, i.e. the sum of the Van der Waals attractive and the electrostatic repulsive energy terms as a function of the distance of separation of the particles[2], this is known for electrostatic stabilization as the DLVO theory[3].

1.2 *Emulsion Polymerization*

Emulsion polymerization is employed in industry to produce latexes, i.e. dispersions of submicron polymer particles in water. Latex products are applied in coatings, paints, adhesives and resins. Starting from monomer-in-water dispersions in aqueous surfactant solutions (above the CMC), dispersions of polymer particles ranging generally from 50 to 500 nm in diameter are obtained after polymerization starting in micelles. The heterogeneous medium of emulsion polymerizations is a strong benefit for large scale exothermic polymerization reactions. The aqueous continuous phase enables relatively good heat transfer to the reactor wall during polymerization. With the monomer swollen particles acting as micro-reactors, polymer of a high degree of polymerization can be obtained due to compartmentalization. However, since all polymer is formed inside the colloidal particles, the resulting latex will still be easily processable. A more detailed mechanistic discussion of emulsion polymerization is given in chapter 3 and in literature[4, 5].

1.3 *Controlled radical polymerization*

In free radical emulsion polymerizations the typical growth lifetime of a radical, i.e. a growing polymer chain, is in the order of a second, whereas the reaction will take in many cases hours to go to completion. In this way control over chain architecture of the polymer, e.g. the formation of block copolymers is hard or even impossible to accomplish. Swarc first described the concept of controlled or living polymerization[6, 7]. Better control over the chain architecture of the polymer can be achieved by minimizing the termination of the propagating radicals. This minimization of termination events can be performed in various ways. In the last decennium two main mechanisms for controlled radical polymerization were developed, one employs the formation of reversible termination products (Nitroxide Mediated Polymerization[8], Atom Transfer Radical Polymerization[9]) and the other is based on the

transfer of radical activity reversibly between polymeric chains (Reversible Addition-Fragmentation chain Transfer[10], Macromolecular Design via Inter-exchange of Xanthate[11] and degenerative transfer). Distributing the active propagating time of a polymeric chain over the time it takes for the reaction to go to completion is the key to success for all controlled radical polymerization techniques. However, the price to pay for this control is increased reaction times as the number of propagating chains at any given time is reduced.

Reversible Addition-Fragmentation chain Transfer (RAFT) polymerization has demonstrated to be one of the most versatile techniques to implement "living" radical polymerization. A RAFT mediated radical polymerization is carried out with the same ingredients as a standard free radical polymerization, except for the presence of a thiocarbonylthio compound, see structure 1 in Figure 1.1. This compound acts as an efficient transfer agent, the so called RAFT agent. The RAFT agent confers controlled characteristics to the polymerization. RAFT polymerization has the added benefit that it is compatible with a wide range of monomers. Dithioesters, dithiocarbamates,[12] xanthates[13] and trithiocarbonates[14, 15] are examples of RAFT agents with different molecular structures that have been successfully used as chain transfer agents[16, 17].

Figure 1.1 shows the currently accepted simplified RAFT mechanism, not taking into account retardation affects as discussed in literature[18]. For RAFT polymerization, a conventional initiator is used to start the polymerization. The RAFT agent reacts with a propagating macroradical ($P_n\cdot$) to form a dormant polymeric species and a radical based on the leaving group (1 chain transfer). The leaving radical species ($R\cdot$) can propagate to form a polymeric species itself (2 reinitiation). Upon reaction of the polymeric dormant RAFT moiety with another macroradical the equilibrium reaction can transfer the radical activity back to the initial macroradical (3 chain equilibrium). By working with a large ratio of RAFT agent

3

concentration to initiator concentration, termination can be minimized and optimal controlled radical conditions are attained. By this mechanism and under the right conditions various polymeric structures can be synthesized such as blocks, stars and brushes.
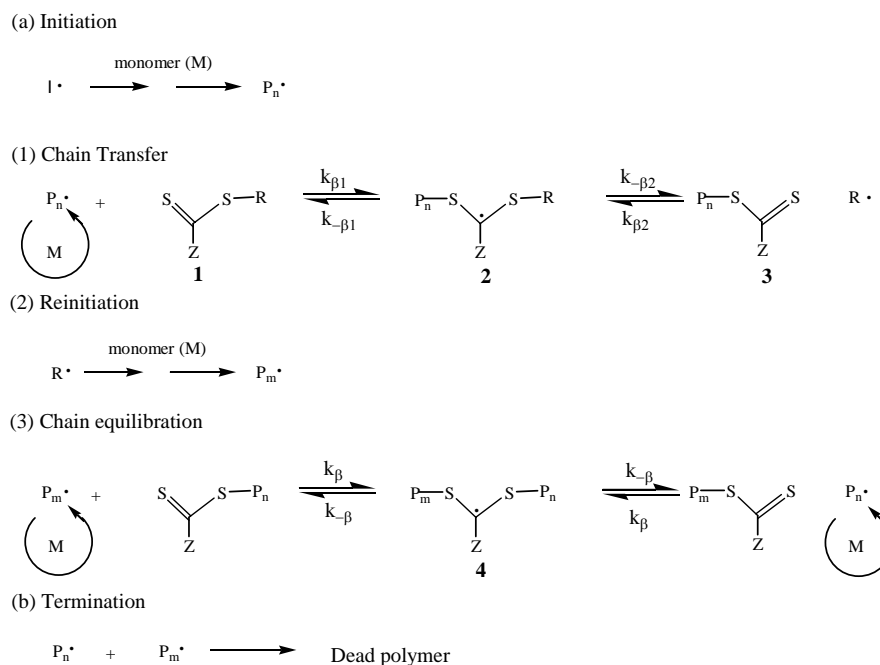
Figure 1.1: Schematic representation of the RAFT process.

1.4 *Controlled radical polymerization in heterogeneous media*

The use of RAFT polymerization in bulk and solution has been well developed[10, 19]. However, the initial use of RAFT in emulsion polymerization was accompanied by a lot of stability problems[20], lack of molecular weight control and very low polymerization rates. The origin of these problems is transport[21] of the predominantly hydrophobic RAFT species to the locus of polymerization in emulsion polymerization, i.e. the micelles for *ab-initio* reactions or the particles in seeded reactions. This was demonstrated by Prescott et al.[22] by performing successful RAFT mediated emulsion polymerization in a seeded system, when acetone was used for transport of the RAFT agents from the monomer droplets through the aqueous phase

to the particles. However, the application of this technique is restricted to small scale laboratory experiments.

1.5 *Amphipathic macro-RAFT agents in emulsion*

A technique based on the employment of water soluble RAFT agents was developed within the Key Centre for Polymer Colloids at the University of Sydney and reported by Ferguson et al.[23, 24] (A NMP system based on the same principle has been developed by Delaittre et al.[25]) These RAFT agents are initially dissolved in the aqueous phase, see Figure 1.2, upon aqueous phase controlled polymerization of hydrophobic monomers they will grow surface active and assemble into macro-RAFT aggregates. These assemblies of macro-RAFT molecules can subsequently act as the precursors for particle formation upon entry of a surface active (z-meric) radical species. By performing these reactions under controlled slow monomer addition, droplet polymerization can be prevented.
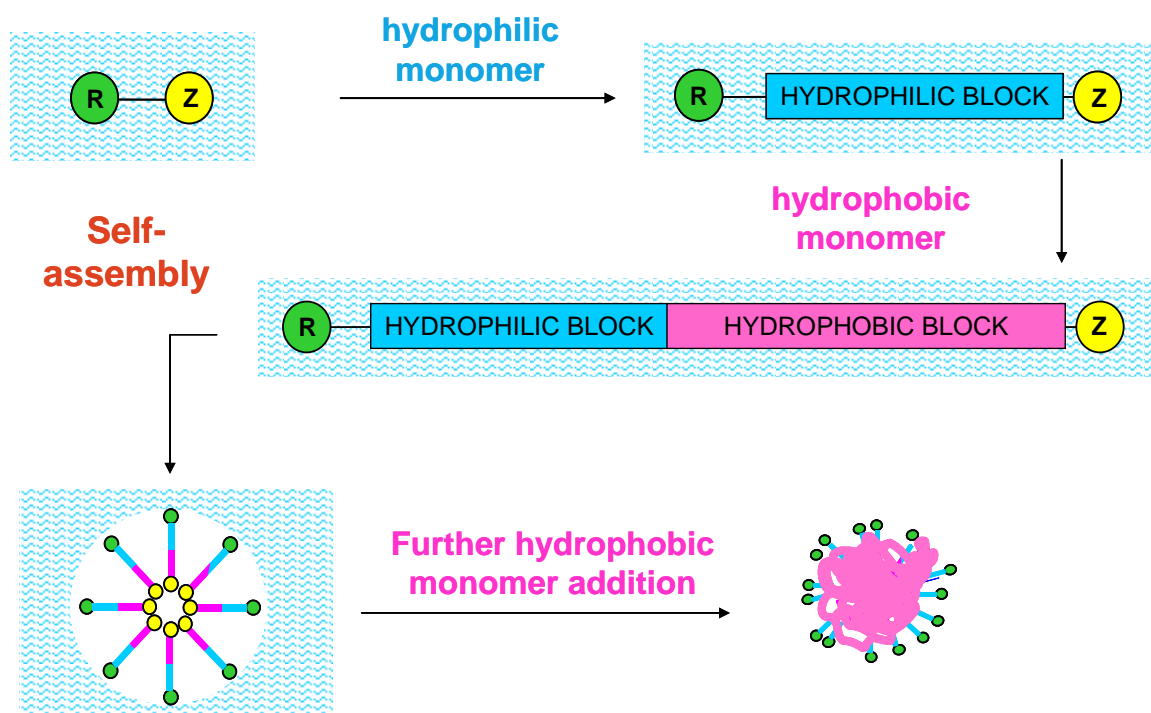
Figure 1.2: Process used to create particles with amphipathic macro-RAFT agents, reproduced from Ferguson et al.[23]

Application of the amphipathic RAFT system not only allows one to form latexes from *ab-initio* emulsion polymerization with narrow molecular weight distributions, it also works as a reactive surfactant. The hydrophilic block of the macro-RAFT agent will act as a stabilizer for the colloidal polymer particles, making the use of free labile surfactant obsolete.

1.6 *Scope of this thesis*

The main objective of this research project is to elucidate the nucleation process for RAFT mediated emulsion polymerizations, so that eventually the amphipathic RAFT system can be employed to not only make polymer of a controlled structure and molecular weight distribution but also with a narrow particle size distribution around a predefined size.

Calorimetry was the main tool to study the semi-batch emulsion polymerization online in the presence of amphipathic RAFT agents. The calorimetric data for systems with amphipathic macro-RAFT agents of varying degree of surface activity are discussed in chapter 2. However, for a full understanding of the nucleation process and the mechanisms governing it, time evolution of the molecular weight distribution and the particle size distribution is required.

The results of analytical work on the molecular characterization of the initial macro-RAFT agent and the time-evolution of the MWD for these RAFT species are reported in chapter 4. The analysis of the particle size distribution and some other important physico-chemical properties, the specific surface area of the macro-RAFT agent and surface tension of the latex during the reaction are reported in chapter 5.

Based on previous work and preliminary calorimetric results a model for nucleation was developed within the Key Centre for Polymer Colloids, the full derivation of the expression for particle numbers and the agreement with experimental data based on calculations with

physically reasonable parameters is provided in chapter 3. In the final chapter the obtained

results for the model parameters for the amphipathic RAFT system are implemented and the

results are discussed.

1.7 *References*

1. Atkins, P.; de Paula, J., *Atkins' Physical Chemistry, 7th Edition*. 2002;
2. Munday, D. L., *Surfaces, interfaces and colloids-principles and applications, second edition, edited by D. Myers*. 2000; Vol. 51.
3. Verwey, E. J. W.; Overbeek, J. T. G., *Theory of the Stability of Lyophobic Colloids*. 1948;
4. van Herk, A.; Editor, *Chemistry and Technology of Emulsion Polymerisation*. 2005;
5. Gilbert, R. G., Emulsion Polymerization. In 1995; p 384.
6. Szwarc, M. *Journal of Polymer Science, Part A: Polymer Chemistry* **1998,** 36, ix.
7. Szwarc, M. *Nature* **1956,** 178, 1168-9.
8. Georges, M. K.; Veregin, R. P. N.; Kazmaier, P. M.; Hamer, G. K. *Macromolecules* **1993,** 26, 2987-8.
9. Wang, J.-S.; Matyjaszewski, K. *Journal of the American Chemical Society* **1995,** 117, 5614-15.
10. Chiefari, J.; Chong, Y. K.; Ercole, F.; Krstina, J.; Jeffery, J.; Le, T. P. T.; Mayadunne, R. T. A.; Meijs, G. F.; Moad, C. L.; Moad, G.; Rizzardo, E.; Thang, S. H. *Macromolecules* **1998,** 31, 5559-5562.
11. Corpart, P.; Charmot, D.; Biadatti, T.; Zard, S.; Michelet, D. Block polymer synthesis by controlled radical polymerization. 98-FR1316, 9858974, 19980623., 1998.
12. Mayadunne, R. T. A.; Rizzardo, E.; Chiefari, J.; Chong, Y. K.; Moad, G.; Thang, S. H. *Macromolecules* **1999,** 32, 6977-80.
13. Destarac, M.; Charmot, D.; Franck, X.; Zard, S. Z. *Macromolecular Rapid Communications* **2000,** 21, 1035-1039.
14. Mayadunne, R. T. A.; Rizzardo, E.; Chiefari, J.; Krstina, J.; Moad, G.; Postma, A.; Thang, S. H. *Macromolecules* **2000,** 33, 243-5.
15. Lai, J. T.; Filla, D.; Shea, R. *Macromolecules* **2002,** 35, 6754-6756.
16. Sprong, E.; Leswin, J. S. K.; Lamb, D. J.; Ferguson, C. J.; Hawkett, B. S.; Pham, B. T. T.; Nguyen, D.; Such, C. H.; Serelis, A. K.; Gilbert, R. G. *Macromolecular Symposia* **2006,** 231, 84-93.
17. de Brouwer, H.; Tsavalas, J. G.; Schork, F. J.; Monteiro, M. J. *Macromolecules* **2000,** 33, 9239-9246.
18. Barner-Kowollik, C.; Buback, M.; Charleux, B.; Coote, M. L.; Drache, M.; Fukuda, T.; Goto, A.; Klumperman, B.; Lowe, A. B.; McLeary, J. B.; Moad, G.; Monteiro, M. J.; Sanderson, R. D.; Tonge, M. P.; Vana, P. *Journal of Polymer Science, Part A: Polymer Chemistry* **2006,** 44, 5809-5831.
19. Moad, G.; Chiefari, J.; Chong, Y. K.; Krstina, J.; Mayadunne, R. T. A.; Postma, A.; Rizzardo, E.; Thang, S. H. *Polymer International* **2000,** 49, 993-1001.
20. Uzulina, I.; Kanagasabapathy, S.; Claverie, J. *Macromolecular Symposia* **2000,** 150, 33-38.
21. Prescott, S. W.; Ballard, M. J.; Rizzardo, E.; Gilbert, R. G. *Australian Journal of Chemistry* **2002,** 55, 415-424.

22. Prescott, S. W.; Ballard, M. J.; Rizzardo, E.; Gilbert, R. G. *Macromolecules* **2002,** 35, 5417-5425.
23. Ferguson, C. J.; Hughes, R. J.; Nguyen, D.; Pham, B. T. T.; Gilbert, R. G.; Serelis, A. K.; Such, C. H.; Hawkett, B. S. *Macromolecules* **2005,** 38, 2191-2204.
24. Ferguson, C. J.; Hughes, R. J.; Pham, B. T. T.; Hawkett, B. S.; Gilbert, R. G.; Serelis, A. K.; Such, C. H. *Macromolecules* **2002,** 35, 9243-9245.
25. Delaittre, G.; Nicolas, J.; Lefay, C.; Save, M.; Charleux, B. *Chemical Communications (Cambridge, United Kingdom)* **2005**, 614-616.

Chapter 2

Calorimetric study of particle formation

Abstract: *Ab-initio RAFT-mediated emulsion polymerizations with controlled monomer feed have been studied by reaction calorimetry. This online monitoring technique provided detailed information about the onset of the nucleation period in the semi-batch process for both the styrene and n-butyl acrylate reactions. The polymerizations were carried out under controlled radical conditions by employing amphipathic (polymeric macro-)RAFT agents of various degrees of surface activity. For the n-butyl acrylate system a clear trend could be observed: the more surface active initial macro-RAFT agent always led to earlier commencement of nucleation. For styrene no such trend was observed this could possibly be due to inhibition effects that apparently do not have such a big influence in the highly reactive n-butyl acrylate system. However, for both monomer systems the more surface active polymeric macro-RAFT agents led to a more rapid initial polymerization rate. These macro-RAFT agents also adjusted more quickly than the hydrophilic macro-RAFT agents to an increased monomer feed, indicating the presence of more particles.*

2.1 *Introduction*

2.1.1 Heat of polymerization

The propagation step of a radical polymerization of vinyl monomers is schematically represented below.
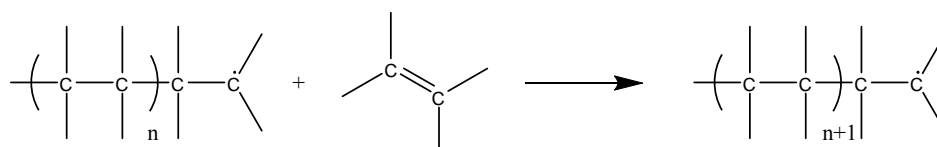
Figure 2.1: Propagation step in free radical polymerisation for vinyl monomers.

The energy gained by converting the double bond into two single bonds is high ($\Delta H \ll 0$). Literature values for the enthalpies of polymerization determined by calorimetry in the liquid state for the monomers studied here, styrene and n-butyl Acrylate have been reported as respectively between 68.5 and 73 kJ mol^{-1} (at 26.9 °C[1, 2]) and 78 kJ mol^{-1} (at 74.5 °C[1, 3]). These variations in the polymerization enthalpies are due to differences in reaction phases, temperature and environment of the measurements, so preferably one should use the literature values obtained for a system as close as possible to the system under investigation[4]. By monitoring the generated heat during a reaction one can obtain polymerization rates. This is valid since the vast majority (by number) of the reactions taking place in a free-radical polymerization comprise propagation, typically orders of magnitude more than termination, initiation and transfer. Because of the presence of macro-RAFT agents in the investigated systems an even larger number of addition and fragmentation reactions is taking place. However, this does not result in any net heat effects since with every addition step a similar bond is broken by fragmentation, see Figure 1.1.

2.1.2 Kinetics of Emulsion Polymerization

The rate of polymerization in a latex particle depends on the monomer concentration in the latex particles ($[M]_p$), the time average number of free radicals per particle ($\bar{n}$) and the propagation rate coefficient for the monomer (k_p). Since every particle is basically a mini-reactor in an emulsion polymerization, the overall rate of an emulsion polymerization increases generally with an increasing number of particles (N_p). For a constant volume batch process this is demonstrated by the following equation for the conversion rate. In equation (2.1) the number concentration of particles $N_c = N_p/V_w$, where V_w is the volume of water in the reactor[5].

$$\frac{dx}{dt} = \frac{k_p [M]_p \bar{n} N_c}{n_{M^0} N_A}$$

(2.1)

Here $n_{M^0} = m_{M^0} / (M_0 V_W)$ is the initial number of moles of monomer present per unit volume of water in the reactor. Equation (2.1) holds for all batch emulsion polymerizations. However, one should take into account the changing of various parameters during the reaction, e.g. $[M]_p$ will depend on the particle diameter and the value of the apparent k_p will change with conversion.

2.1.3 Reaction calorimetry

Reaction calorimetry is, together with dilatometry, one of the most precise techniques to study emulsion polymerization kinetics[4]. Reaction calorimetry can be used in many circumstances where dilatometry cannot, e.g. obtaining accurate rate data while one or more components are being fed into the system. The present controlled feed experiments with the amphipathic RAFT agents are carried out under such semi-batch conditions. Successful use

11

of a reaction calorimeter has been reported for monitoring emulsion polymerization kinetics[4, 6-16], nucleation effects[17-19], control of molecular weight[20] and other processes[21-23].

A commercial reaction calorimeter (RC1e, HP60 reactor, Mettler-Toledo GmbH, Switzerland) was used in this study. The characteristics and operational possibilities of this equipment have been described in detail in literature[10]. The calorimeter accurately measures the temperatures of the reaction mixture (T_r) and of the surrounding jacket oil (T_j) to determine the heat flow generated or absorbed within the reactor (see schematic representations in Figure 2.2 and Figure 2.3; both images were reproduced from the Mettler Toledo WinRC software with their approval). The system can be calibrated by introducing an accurately known amount of heat to a non-reacting fluid by an electrical heater. In the absence of any other heat effects the overall heat transfer coefficient (U) and the heat exchange area (A) can be determined from the following heat balance for the system:

$$UA\int (T_r - T_a)\, dt = \int Q_c\, dt \qquad (2.2)$$

Here Q_c represents the calibration heat and T_a is the corrected jacket temperature, a term introduced to take into account the appreciable heat capacity of the reactor wall during non-isothermal operation (see Figure 2.3); in the isothermal mode T_j is equal to T_a.
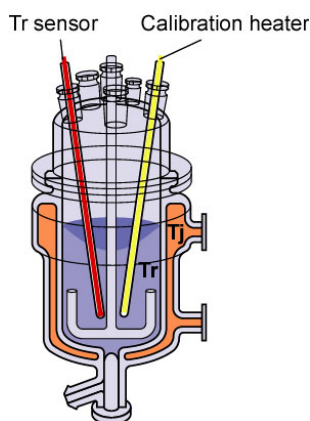
Figure 2.2: Principle of measurement of the Mettler Toledo RC-1e reactor.
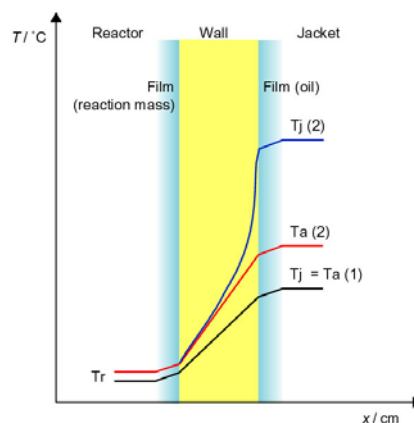
Figure 2.3: T_a, the corrected jacket temperature.

All measurements in the RC-1e are measured with respect to a baseline. The baseline is related to the heat flow through the reactor wall for the same system in the absence of reaction. This heat flow incorporates aspects like specific heat and energy dissipation due to stirring. The accuracy of the measurements is governed to a large extent by the stability of the baseline.

2.1.4 Objectives

This chapter describes the results of particle formation in RAFT-mediated emulsion polymerization investigated by reaction calorimetry. By measuring the heat flow during controlled feed *ab initio* emulsion polymerization the mechanism of particle formation by self-assembly of the amphipathic macro-RAFT agents can be studied. Two different monomer systems and various gradations of hydrophobicity of the initial macro-RAFT agents have been analysed and compared.

2.2 *Experimental*

Various polymeric amphipathic macro-RAFT agents were synthesized starting from an amphipathic RAFT agent with a butyl Z-group and a propanoic acid leaving group (see Figure 2.4). These macro-RAFT agents were subsequently used in controlled feed calorimetric experiments. Details of all reaction steps are now given.

2.2.1 Chemicals

The RAFT agent 2-butyl(((butylsulfanyl)carbonothioyl)sulfanyl)propanoic acid, see Figure 2.4, was used as supplied by Dulux Australia; the procedure for synthesis of this RAFT agent is described in literature[24, 25]. Acrylic acid (AA, Aldrich ≥ 99%) was distilled under reduced pressure in the presence of copper (Copper fine powder extra pure, Merck) and stored in the

dark before use at 7 °C. The monomers styrene, (STY, Aldrich 99+%) and n-butyl acrylate

(BA, Aldrich 99+%) were purified by filtration through a column filled with inhibitor-

remover replacement packing, for respectively removing tert-butylcatechol and removing

hydroquinone (HQ) and hydroquinone monomethyl ether (MEHQ) (Aldrich). The solvents

Propylene Glycol (PG, BASF), 1,4-Dioxane (Dx, Merck HPLC grade), were used as

received. All water used during the BA experiments was Milli Q demineralized water. The

water used for the styrene experiments was obtained from a Millipore Elix system. The

initiator 4,4'-Azobis(4-cyanopentanoic acid) (V-501, Fluka >98%) and sodium hydroxide

(NaOH, Merck ≥ 98%) were used as received. Only high purity Argon was used for

deoxygenation.
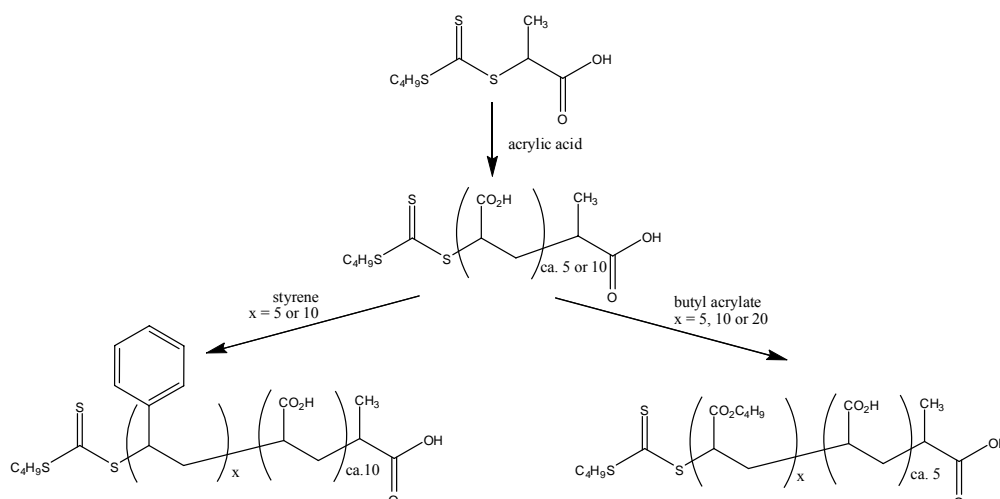
Figure 2.4: Synthesis steps of amphipathic macro-RAFT agents that were subsequently used in controlled feed experiments growing x to a length of about 300 monomeric units.

2.2.2 Synthesis of hydrophilic macro-RAFT agent

The RAFT agent and an equivalent amount of moles of NaOH, the hydrophilic monomer

Acrylic Acid (AA), initiator V-501 and Milli-Q demineralized water, Propylene Glycol (PG)

or Dioxane (Dx) were added together in a round-bottom flask to obtain a 40 % (w/w) solid

content at full conversion (see Table 2.1 for the molar ratios applied). This mixture was

capped with a rubber septum and degassed by purging with high purity Argon while stirring

with a magnetic stirrer bar. Subsequently it was heated to the reaction temperature of 60 °C,

where it was left for 2.5 hours while stirring. The resulting macro-RAFT agent was analysed

by electrospray-MS. The scale of the reaction will be discussed in 2.3.1

Table 2.1: Molar ratios for preparation of both hydrophilic and amphipathic macro-RAFT agents.*

Macro-RAFT agents	RAFT	Monomer	Initiator V-501	Buffer NaOH	Solvent H_2O/Dx/PG	Solids @ full conv.
Hydrophillic	Dulux RAFT agent	5 or 10 (AA)	0.5	1 (only in H_2O)	H_2O/Dx/PG	0.4
Amphipathic	Hydrophilic macro-RAFT	5, 10 or 20 (STY or BA)	0.5		Dx/PG	0.4

*RAFT agent 25-75 $\cdot 10^{-3}$ mol

2.2.3 Synthesis of amphipathic macro-RAFT agent

Part of the previously formed macro-RAFT agent was converted into polymeric amphipathic

macro-RAFT agents by growing a hydrophobic block of various lengths of either n-butyl

acrylate or styrene onto it. The procedure for the synthesis is similar to that of the initial

hydrophilic RAFT agent (see paragraph 2.2.2). Now the amphipathic RAFT agent with the

hydrophilic block of acrylic acid is the starting RAFT agent. Once again all ingredients were

added together in a round-bottom flask and degassed with high purity argon while stirring.

The reaction with n-butyl acrylate was started by heating up to 60 °C and this was maintained

for 2.5 hours. The styrene experiments were performed at 70 °C in overnight runs. After the

synthesis of styrene based macro-RAFT agents in 1,4-dioxane, the solvent was evaporated in

a vacuum oven at 40 °C. The product was a dry yellow powder.

2.2.4 Controlled feed RC-1 experiments

A typical procedure on the basis of a styrene polymerisation is described below (see Table

2.2). The macro-RAFT agent was dissolved in 760 mL of 0.05 M NaOH solution in a 1 L

beaker. This mixture was stirred for about 15 minutes, before it was added to the RC-1

reaction vessel. The Mettler Toledo RC-1e was equipped with a 1.8 L Hastelloy vessel and stainless steel double jacketed lid. A propeller stirrer, temperature probe and calibration heater were fixed to the lid. (BA experiments were performed with Kalrez® perfluoroelastomer O-rings to prevent swelling of the O-rings with the monomer.) The closed loop addition mechanism consisted of Prominent pumps and Mettler Toledo balances connected to two RD10 control units. After closing the reactor, the macro-RAFT solution was deoxygenated for the first time by introducing high purity Argon to the reactor while stirring for four minutes, the pressure was released by venting for 1 minute while still keeping a positive Argon overpressure. This 5 minute cycle was repeated three times, after which the reactor was heated to reaction temperature of 80 °C and the stirring speed was set at 500 rpm. Subsequently the reaction mixture was calibrated using the inbuilt calibration procedure. After calibration a 90 minute time interval was programmed to allow the mixture to return to the reaction temperature and for another deoxygenation process (4 cycles) to take place, after which the reaction could establish a flat baseline. The initiator was dissolved in 100 mL of 0.35 M NaOH solution in a flask equipped with a rubber septum. Before addition to the reaction mixture the initiator solution was deoxygenated by purging with high purity argon. A balloon filled with high purity Argon was attached to the bottle containing the initiator solution to keep a positive Argon pressure while the initiator solution was being pumped into the reactor. The monomer was treated in the same way. The actual reaction phase was started by the addition of 50 ml of the initiator solution, after which a 25 minute pause was introduced to allow the reaction to come back to baseline. Subsequently the monomer feed was started by adding 15 grams of styrene over a period of four hours using the closed loop feeding setup. The heat effect of the monomer dosing was accounted for by calculating the heat necessary to warm up the monomer to reaction temperatures assuming a low constant temperature (25 °C) of the monomer and with the heat capacity values from literature[26]. The

Styrene feed rate was increased to 141 grams in the next five hours. A further two hours were allowed after the completion of the monomer feed for the reaction to go to complete conversion and return back to baseline. The resulting latex went through another calibration procedure and was afterwards cooled down to room temperature and the stirring was slowed down to 100 rpm.

Table 2.2: Experimental conditions for the controlled feed RC-1e experiments in the presence of macro-RAFT agents, respectively 5AA+10BA and 10AA+10STY, with a final RAFT/monomer ratio of 1:300.

Conditions	n-Butyl Acrylate		Styrene	
Temperature	60 °C		80 °C	
Agitation	Anchor @ 300 rpm		Propeller @ 500 rpm	
Initiator solution				
V-501	$2.0 \cdot 10^{-3}$ mole	0.56 g	$2.50 \cdot 10^{-3}$ mole	0.67 g
NaOH	$0.8 \cdot 10^{-2}$ mole	0.32 g	$1.75 \cdot 10^{-2}$ mole	0.70 g
H_2O	50 g		50 g	
Macro-RAFT solution				
H_2O	760 g		760 g	
NaOH	$1.6 \cdot 10^{-2}$ mole	0.64 g	$3.75 \cdot 10^{-2}$ mole	1.50 g
Macro-RAFT	$4.0 \cdot 10^{-3}$ mole	15.2 g PG mix	$5.00 \cdot 10^{-3}$ mole	8.67 g
Feeds				
Slow feed	15 g per 2 hours		12.43g per 4 hours	
Fast feed	141 g per 4 hours		142.95 g per 5 hours	

2.3 *Results & Discussion*

2.3.1 Synthesis of macro-RAFT agents

A trithiocarbonate RAFT agent was used to prepare a macro-RAFT comprising, on average, five or ten acrylic acid units. This was first performed at similar conditions as described by Ferguson et al.[24]. However, the reactions in the RC-1e are on a significantly larger scale. Firstly, the available RC-1e has a minimum load of about 650 mL in the reactor, because with a lower volume the temperature probe and calibration heater are not submerged. Secondly, there is a minimum concentration of RAFT agent and monomer required to produce an observable heat flow. This level was estimated from the noise level in a blank run to be around 0.5 Watt; under starved conditions this is equivalent to a feed of $7.7 \cdot 10^{-6}$ mole Styrene per second or 2.67 gr Styrene per hour. In order to perform repeat experiments with macro-

RAFT agents of the exact same composition, the first synthesis step had to be scaled up. An initial attempt at a 100 mL scale, in a 250 ml round-bottom flask heated by an oil-bath and stirred magnetically failed. The increased reaction volume to surface ratio resulted in insufficient temperature control over the reaction, resulting in increased temperatures and pressures and subsequent venting via the rubber septum. The system was in a self accelerating loop, with increasing polymerization rates, resulting in higher viscosities, less temperature control etc… Not only did the reaction run under uncontrolled conditions, also the polymerization itself was not controlled, as evidenced by formation of a high viscosity polymeric product which indicates the formation of high molecular weight poly(acrylic acid). After this initial failure, the reaction was thereafter successfully performed with increased agitation by magnetic stirring and targeted at lower solid contents at complete conversion..

Electrospray mass spectrometry (ESI-MS) was carried out on the successfully synthesized initial hydrophilic macro-RAFT agent; it confirmed the formation of the macro-RAFT agent with a relatively narrow molecular weight distribution (see Figure 2.5). The product of the subsequent polymerisation with n-butyl acrylate was characterized in the same way (see Figure 2.6). These are two examples for a range of successfully synthesized macro-RAFT agents. Although ESI-MS cannot be used to obtain a quantitative characterisation of the macro-RAFT agent, it does provide insight into the distribution of the different macro-RAFT molecules. A more in depth discussion of the polymer characterisation techniques used can be found in chapter 4.
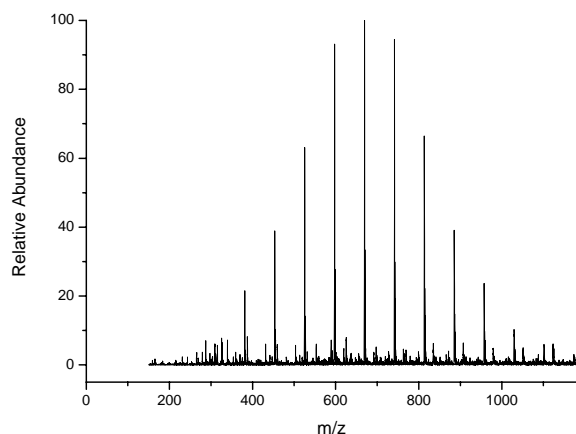
Figure 2.5: Electrospray mass spectrum of macro-RAFT agent designed to contain five AA units.
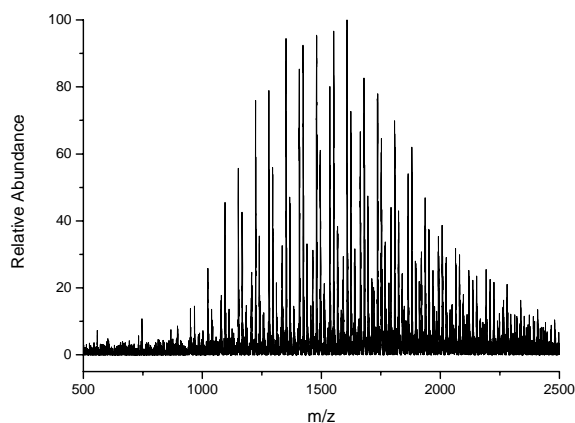
Figure 2.6: Electrospray mass spectrum of macro-RAFT agent designed to contain five AA groups and 10 BA units.

2.3.2 Calorimetric reactions

The synthesized macro-RAFT agents were used in controlled feed calorimetric experiments in the RC-1e calorimetric reactor. These experiments all showed the same basic behaviour during the reaction (see Figure 2.7). Initially all macro-RAFT agents were dissolved in the aqueous phase, with a low amount of monomer present during the initial slow feed phase. Therefore a low polymerization heat flow was observed if any. Subsequently the start of particle formation was clearly visible as a sharp increase in the heat flow. The reservoir of unreacted monomer in the system was quickly converted into polymer. The conversion rate depends on the number of particles in the system. Once all monomer added so far was converted, the polymerisation continued under starved conditions. After two (BA) or four (STY) hours the feed rate was increased, the heat production quickly followed the feed rate and continued at the elevated level under starved conditions. This is proven by the immediate drop of the heat flow back to the baseline once the feed was stopped.
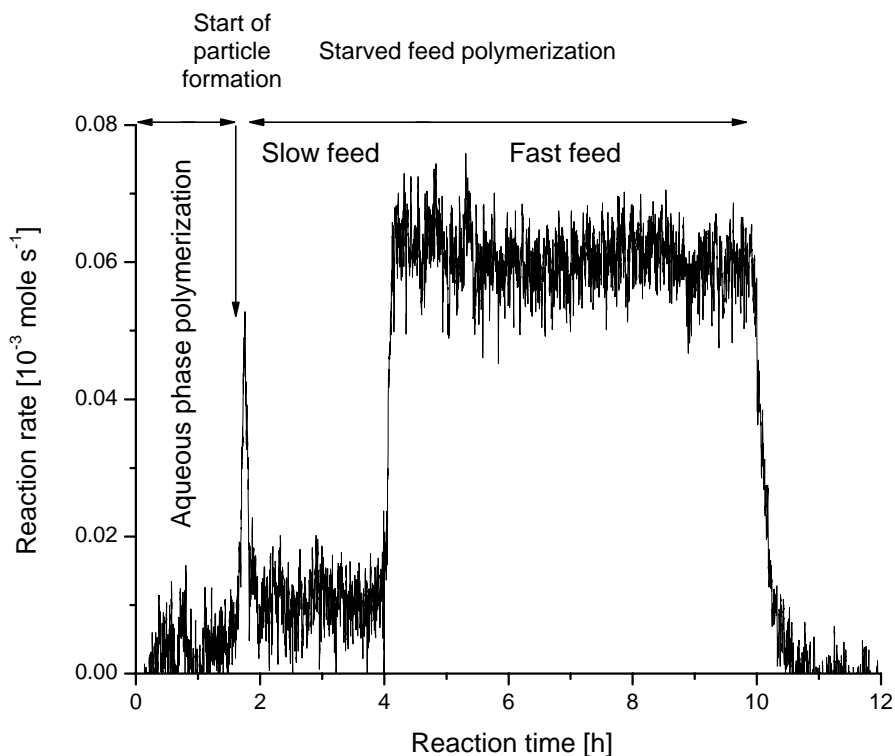
Figure 2.7: Different stages in controlled feed RAFT-mediated emulsion polymerization of styrene.

Figure 2.7 clearly demonstrates that calorimetric measurements are a good method to observe the start of particle formation in *ab initio* emulsion polymerisations. However, since the emulsion polymerisation in the presence of amphipathic RAFT agents has to be performed under controlled feed conditions to prevent droplet polymerisation, it is impossible to observe the duration of the particle formation period. The calorimetric data also revealed that even though the monomer is fed at a very low rate initially for all reactions, the monomer added before the start of particle formation is more than can be dissolved in the aqueous phase. So, either there are some monomer droplets present or the monomer is distributed over the micelles already present. This becomes particularly important when modelling these systems (see chapter 3).

2.3.3 Macro-RAFT agents compared

Macro-RAFT agents of various degrees of hydrophobicity have been synthesized and used in calorimetric experiments. Figure 2.8 provides an overview of the results.
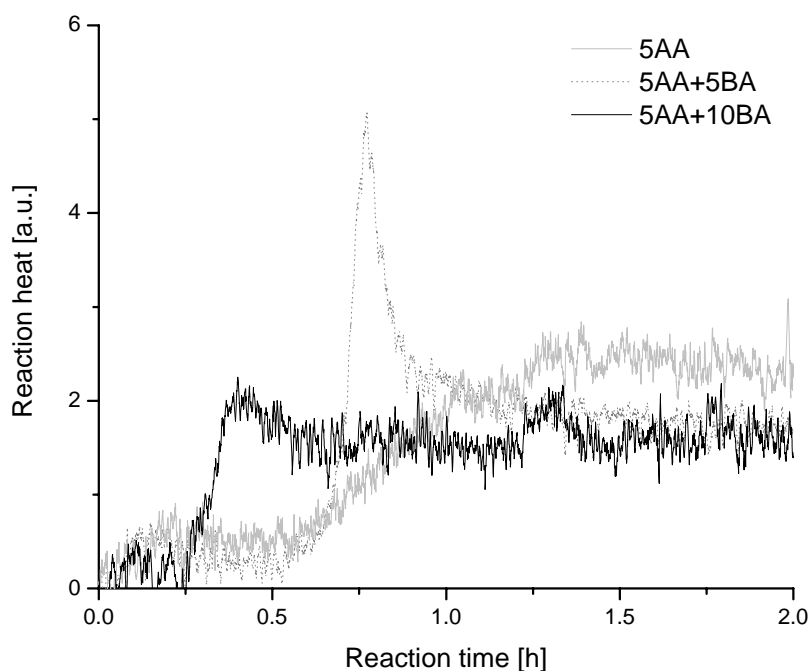
Figure 2.8: Initial particle formation compared for different degrees of hydrophobicity of macro-RAFT agents in n-butyl acrylate controlled feed experiments.

For both the n-butyl acrylate as well as the styrene based experiments there was no difference in the behaviour after particle formation in the fast feed regime. During all reactions the rate of monomer consumption was equal to the feed rate. However, a clear trend could be observed at the start of the reaction in the slow feed regime of the n-butyl acrylate experiments (see Figure 2.8). The more hydrophobic the initial RAFT agent was, the earlier the particle formation started. For the more hydrophobic macro-RAFT agents this was followed by a quick consumption of the monomer added up to that time, while the hydrophilic macro-RAFT took more than an hour to do so. This indicates fast particle formation for the most hydrophobic macro-RAFT agents that are probably already present as micelles at the start of the nucleation stage.

For the styrene polymerizations no such clear trend in the starting time of the particle formation was observed (see Figure 2.9 and Figure D and E in Appendix I). This could possibly be due to inhibition.
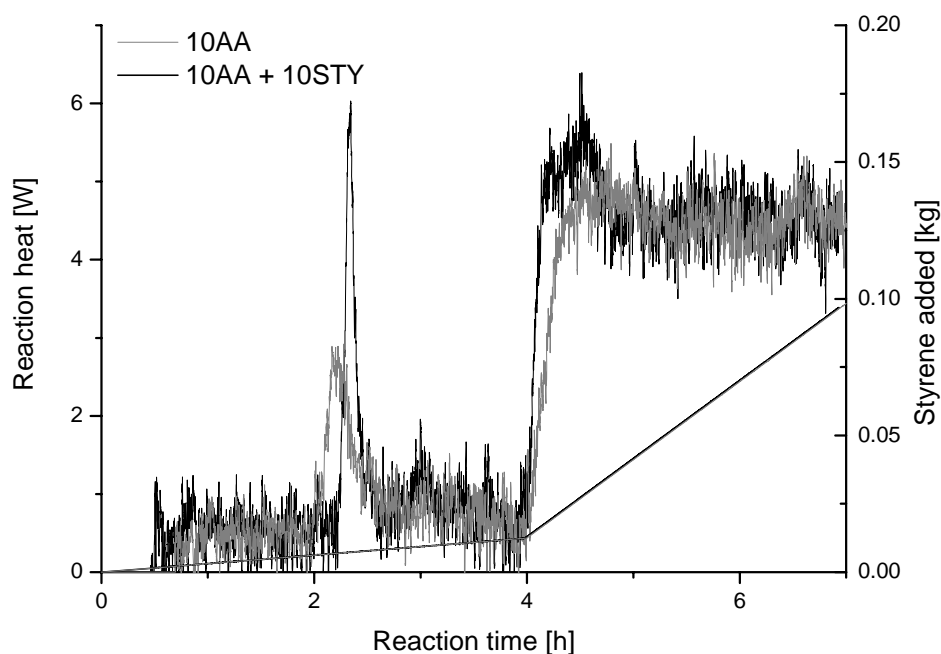
Figure 2.9: Initial particle formation compared for different degrees of hydrophobicity of macro-RAFT agents in styrene controlled feed experiments.

However, a clear difference could be observed in the rate of monomer consumption once particle formation started, indicating the formation of more particles. A similar behaviour can be observed once the feed rate is increased to the fast feed regime; the system with the more hydrophobic macro-RAFT agents, i.e. 10AA+10STY, adapts quicker to a new feed regime. In Table 2.3 all observations for the different macro-RAFT agents are collected, showing the trends in calorimetric data. More supporting calorimetric data for the reactions discussed here can be found in appendix 1.

Table 2.3: Start of particle formation and duration to monomer consumption for various macro-RAFT agents.

Monomer system	Macro-RAFT agent	Start particle formation [h:mm]	Time monomer consumption [h:mm]
BA	5AA	0:33	0:53
BA	5AA+5BA	0:36	0:36
BA	5AA+10BA	0:15	0:19
STY	10AA	1:56	0:52
STY	10AA+10STY	2:13	0:21

2.3.4 Use of more hydrophobic macro-RAFT agents

All macro-RAFT agents used in this project had to be soluble in water or at least in a NaOH solution to perform *ab initio* emulsion polymerizations. However, by dissolving more hydrophobic macro-RAFT agents e.g. 5AA+20BA in an organic medium such as a monomer, these macro-RAFT agents can be used to perform mini-emulsion experiments with RAFT control in the absence of any added surfactant or co-surfactant. One of these reactions was successfully performed in the RC-1e; see Figure 2.10, resulting in a stable latex with a similar amount of particles as droplets at the start of the reaction. This was verified by light scattering (monomer droplets) and by CHDF measurement of the latex particles. In normal mini-emulsion experiments where the colloidal system is insufficiently stabilized, the monomer droplets will undergo Ostwald ripening, where monomer is transferred from the smaller droplets to the bigger ones resulting in fewer and larger particles after polymerization. For this system an increased number of particles is observed, see Table 2.4, but that is most likely due to the overestimation of the average droplet size by DLS.
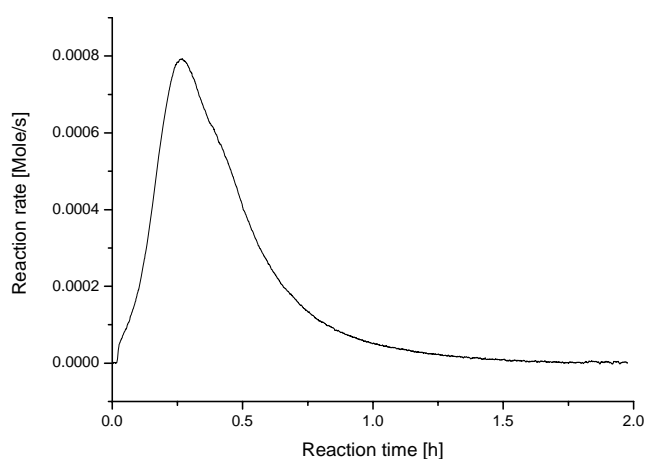
Figure 2.10: Mini-emulsion polymerisation in the presence of "super" hydrophobic macro-RAFT agent (5AA+20BA).

Table 2.4: Particle number before and after mini-emulsion with 5AA+20BA macro-RAFT.

	\<Radius\> [nm] by weight	Particle/droplet number
Droplets (DLS)	86	6.7×10^{16}
Particles (CHDF)	56	2.0×10^{17}

2.3.5 Sensitivity of RC-1e

As mentioned in the introduction, the accuracy of the calorimetric measurements is dependent on the stability of the baseline. This is particularly important when measuring such low heat flows as in the controlled feed experiments. It was only after a repeated drop in the baseline at similar times that the importance of the air flow over the reactor was recognized as an important factor. The RC-1 reactions including the calibration phases took more than a working day, so in the evening when other fume hoods were switched off, the airflow over the reactor increased. This resulted in a slight drop of the baseline. This effect became obvious when the sash level was lowered during the reaction, resulting in an increased airflow and big drop in the baseline level. Subsequent reactions were all carried out with constant sash levels.

2.4 *Conclusions*

Block copolymeric macro-RAFT agents with varying degrees of hydrophobicity have been successfully synthesized in a two step procedure. Care should be taken to have enough cooling capacity during the formation of the hydrophilic macro-RAFT, to prevent uncontrolled reactions of acrylic acid due to its extremely high propagation rate coefficient[27].

The controlled feed calorimetric experiments with n-butyl acrylate showed a clear trend. The more hydrophobic the macro-RAFT agent, the earlier the particle formation stage started and the quicker all monomer added up to that moment was consumed. For the styrene experiments a trend in starting times could not be observed, possibly due to inhibition. However, the faster consumption of the monomer added so far was also clearly visible for this monomer system. The faster consumption of monomer indicates more particles in the

reaction mixture, so more hydrophobic macro-RAFT agents form particles faster, possibly by the formation of micelles in an early stage of the reaction.

Calorimetric measurements proved to be an effective tool for monitoring the start of the particle formation process in emulsion polymerizations. The duration of the particle formation stage could not be determined by calorimetry since the reactions had to be run under controlled feed conditions to prevent droplet polymerization. Other methods have to be used to determine this reaction parameter.

2.5 *References*

1.   Joshi, R. M. *Journal of Polymer Science* **1962,** 56, 313-38.
2.   McCurdy, K. G.; Laidler, K. J. *Canadian Journal of Chemistry* **1964,** 42, 818-24.
3.   Dainton, F. S.; Ivin, K. J.; Walmsley, D. A. G. *Transactions of the Faraday Society* **1960,** 56, 1784-92.
4.   Lamb, D. J.; Fellows, C. M.; Morrison, B. R.; Gilbert, R. G. *Polymer* **2005,** 46, 285-294.
5.   Gilbert, R. G., Emulsion Polymerization. In 1995; p 384.
6.   Lamb, D. J.; Fellows, C. M.; Gilbert, R. G. *Polymer* **2005,** 46, 7874-95.
7.   De La Rosa, L. V.; Sudol, E. D.; El-Aasser, M. S.; Klein, A. *Journal of Polymer Science, Part A: Polymer Chemistry* **1999,** 37, 4073-4089.
8.   De La Rosa, L. V.; Sudol, E. D.; El-Aasser, M. S.; Klein, A. *Journal of Polymer Science, Part A: Polymer Chemistry* **1999,** 37, 4066-4072.
9.   De La Rosa, L. V.; Sudol, E. D.; El-Aasser, M. S.; Klein, A. *Journal of Polymer Science, Part A: Polymer Chemistry* **1999,** 37, 4054-4065.
10.   de la Rosa, L. V.; Sudol, E. D.; El-Aasser, M. S.; Klein, A. *Journal of Polymer Science, Part A: Polymer Chemistry* **1996,** 34, 461-73.
11.   Ozdeger, E.; Sudol, E. D.; El-Aasser, M. S.; Klein, A. *Journal of Polymer Science, Part A: Polymer Chemistry* **1997,** 35, 3837-3846.
12.   Ozdeger, E.; Sudol, E. D.; El-Aasser, M. S.; Klein, A. *Journal of Polymer Science, Part A: Polymer Chemistry* **1997,** 35, 3827-3835.
13.   Ozdeger, E.; Sudol, E. D.; El-Aasser, M. S.; Klein, A. *Journal of Polymer Science, Part A: Polymer Chemistry* **1997,** 35, 3813-3825.
14.   Blythe, P. J.; Klein, A.; Phillips, J. A.; Sudol, E. D.; El-Aasser, M. S. *Journal of Polymer Science, Part A: Polymer Chemistry* **1999,** 37, 4449-4457.
15.   Kemmere, M. F.; Meuldijk, J.; Drinkenburg, A. A. H.; German, A. L. *Polymer Reaction Engineering* **2000,** 8, 271-297.
16.   Kemmere, M. F.; Meuldijk, J.; Drinkenburg, A. A. H.; German, A. L. *Journal of Applied Polymer Science* **2000,** 79, 944-957.
17.   Blythe, P. J.; Klein, A.; Sudol, E. D.; El-Aasser, M. S. *Macromolecules* **1999,** 32, 6952-6957.
18.   Blythe, P. J.; Morrison, B. R.; Mathauer, K. A.; Sudol, E. D.; El-Aasser, M. S. *Macromolecules* **1999,** 32, 6944-6951.

19. Blythe, P. J.; Klein, A.; Sudol, E. D.; El-Aasser, M. S. *Macromolecules* **1999,** 32, 4225-4231.
20. Vicente, M.; Leiza, J. R.; Asua, J. M. *AIChE Journal* **2001,** 47, 1594-1606.
21. Wang, X.; Sudol, E. D.; El-Aasser, M. S. *Macromolecules* **2001,** 34, 7715-7723.
22. Wang, X.; Sudol, E. D.; El-Aasser, M. S. *Langmuir* **2001,** 17, 6865-6870.
23. Wang, X.; Sudol, E. D.; El-Aasser, M. S. *Journal of Polymer Science, Part A: Polymer Chemistry* **2001,** 39, 3093-3105.
24. Ferguson, C. J.; Hughes, R. J.; Nguyen, D.; Pham, B. T. T.; Gilbert, R. G.; Serelis, A. K.; Such, C. H.; Hawkett, B. S. *Macromolecules* **2005,** 38, 2191-2204.
25. Ferguson, C. J.; Hughes, R. J.; Pham, B. T. T.; Hawkett, B. S.; Gilbert, R. G.; Serelis, A. K.; Such, C. H. *Macromolecules* **2002,** 35, 9243-9245.
26. Brandrup, J.; Immergut, E. H.; Editors, *Polymer Handbook, Fourth Edition.* 1998;
27. Lacik, I.; Beuermann, S.; Buback, M. *Macromolecular Chemistry and Physics* **2004,** 205, 1080-1087.

Chapter 3

Particle formation mechanism

Abstract: *A model inspired by Smith and Ewart's nucleation theory has been derived for the particle formation mechanism of the amphipathic macro-RAFT system under controlled feed conditions. It is assumed that the preformed amphipathic macro-RAFT molecules are present in the form of micellar assemblies at the start of nucleation. Entry by z-meric species initiates particle formation by growing the macro-RAFT agents to such a degree of polymerization of the hydrophobic block that the macro-RAFT is no longer labile. Remaining labile macro-RAFT assemblies will be cannibalized by the growing particles. Cessation of nucleation is assumed once all macro-RAFT agents are adsorbed onto the particles and are no longer labile. A first implementation of the model using physically reasonable parameters shows promising results. However, it is important to verify the various parameters experimentally before any mechanistic postulates can be confirmed or refuted.*

3.1 *Introduction*

A mathematical model describing particle formation by self-assembly of amphipathic RAFT agents has been developed within the Key Centre for Polymer Colloids. This model is based on previously reported research[1], on preliminary results by Sprong et al.[2] and on the calorimetric data described in chapter 2.

3.2 *Conventional emulsion polymerization*

Before discussing the particular conditions for the amphipathic macro-RAFT system it is important to know which fundamental reaction steps are involved in nucleation for conventional emulsion polymerization. The mechanistic fundamentals of particle nucleation in conventional emulsion polymerization have been laid down by the pioneering work of Harkins[3] and Smith and Ewart[4]. In their theory, as illustrated in Figure 3.1, particle formation starts by aqueous-phase radicals entering ('stinging') surfactant micelles ("micellar entry").
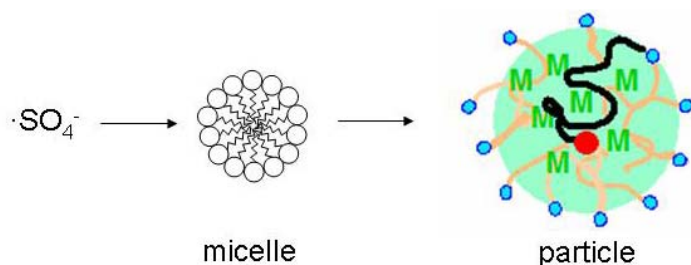
Figure 3.1: Micellar entry according to Smith and Ewart.

However, the model developed by Smith and Ewart is of limited validity, it only holds for very hydrophobic monomers combined with surfactant systems at super micellar concentration with a low CMC. Emulsion polymerizations not obeying these prerequisites deviate in the experimentally found particle numbers and show e.g. a stronger dependency on the surfactant concentration. For a better qualitative and quantitative agreement with experiments the model has to allow for aqueous phase events[5] and homogeneous nucleation.

Homogeneous nucleation has been described by Hansen and Ugelstadt[6], as well as by Fitch and Tsai[7], in the so called HUFT model. The main conclusion of the HUFT theory is that particles may be formed by three different mechanisms, by themselves or in a combination of nucleation mechanisms[8]. These mechanisms are:

- Precipitation of growing radicals from the aqueous phase (homogeneous nucleation)

- Nucleation by "stinging" of surfactant micelles (as in the Smith-Ewart theory)

- Nucleation in monomer droplets (droplet polymerization).

These nucleation mechanisms are illustrated for the amphipathic RAFT system in Figure 3.2.

The HUFT model describes transfer of radical species from the bulk aqueous phase to the particle/micellar surface as the rate determining factor for micellar nucleation. Hawkett et al.[9] introduced the concept of a critical degree (z-meric species) of surface activity necessary for a radical species to enter a particle/micelle. Maxwell and Morrisson[10] realized, based on the experimental work of Trau et al.[11], that not entry of a z-mer was the rate determining step but aqueous phase polymerization to attain this critical surface activity.

The possible fates of a radical species before nucleation can be described by the following. An aqueous-phase radical generated by decomposition of the initiator can undergo propagation steps in the aqueous phase until it becomes sufficiently surface active (z-meric length, e.g. DP of 2 for styrene with a persulfate based radical). Providing the radical does not terminate in the aqueous phase, it will be transferred rapidly to the surface of a particle or micelle once the DP of z has been attained. This transfer step is extremely fast and other fates of the z-meric radical in the aqueous phase have much larger time constants and are therefore negligible. At the surface of the particle or micelle, the z-mer can either desorb again or propagate. Radicals of a DP less than z may adsorb on the surface of a particle or micelle.

However, these oligomers will desorb again before additional propagation occurs. A z-meric species is surface active and the adsorption strength represented by the adsorption isotherm for these z-meric species dictates a longer residence time on the surface. An adsorbed species of this critical length (z) is therefore far more likely to propagate and therefore forms a long polymer chain inside a micelle or particle.

For a system obeying zero-one kinetics like styrene, where radical entry in a particle that already contains a propagating radical results essentially in instantaneous termination, a radical species has various options[5]. It can further propagate, terminate or undergo radical transfer to e.g. monomer or polymer. Upon transfer to monomer a short labile radical is formed that can leave the particle (i.e. exit). The fate of these radicals can be summarized by the following limiting cases, a more detailed description has been given by Gilbert[5]:

Limit 1   Complete termination in the aqueous phase.

Limit 2   Complete re-entry of desorbed free radicals. This limit can be subdivided into:

              2a Propagation is more likely than escape.

              2b Escape is much more likely.

Limit 3   Termination is rate-determining.

For each of these limiting cases the time average number of radicals per particle, $\bar{n}$, can be calculated based on the limiting events. So an expression is obtained describing radical loss[5].

In the absence of micelles (or particles below a sufficient concentration), the surface active radical species can further propagate to an even more hydrophobic species, with the so called j-crit length. When the j-crit length is reached the radical species becomes insoluble in the aqueous phase and will form a particle by a coil-globule transition, this process is referred to as homogeneous nucleation.

3.3 *Nucleation in amphipathic RAFT systems*

For the preformed amphipathic macro-RAFT agents (e.g. 5AA+10BA and 10AA+10STY) the nucleation possibilities, see Figure 3.2, were limited to either micellar entry or homogeneous nucleation by running experiments under controlled feed conditions to minimize the number of monomer droplets in the system. For the amphipathic species, which are already surface active, homogeneous nucleation is far less likely since aggregates will already have formed at the start of the polymerization. Initially it was postulated that nucleation was due to the self-assembly of di-blocks into rigid micelles which simply keep on growing[12]. However, this point of view was refuted based on the fact that the number of RAFT molecules found per particle (in the range of 2000-4000 RAFT agents per particle) was much higher[2] than the typical aggregation number of these kind of surface active species[13] (typically around 100).
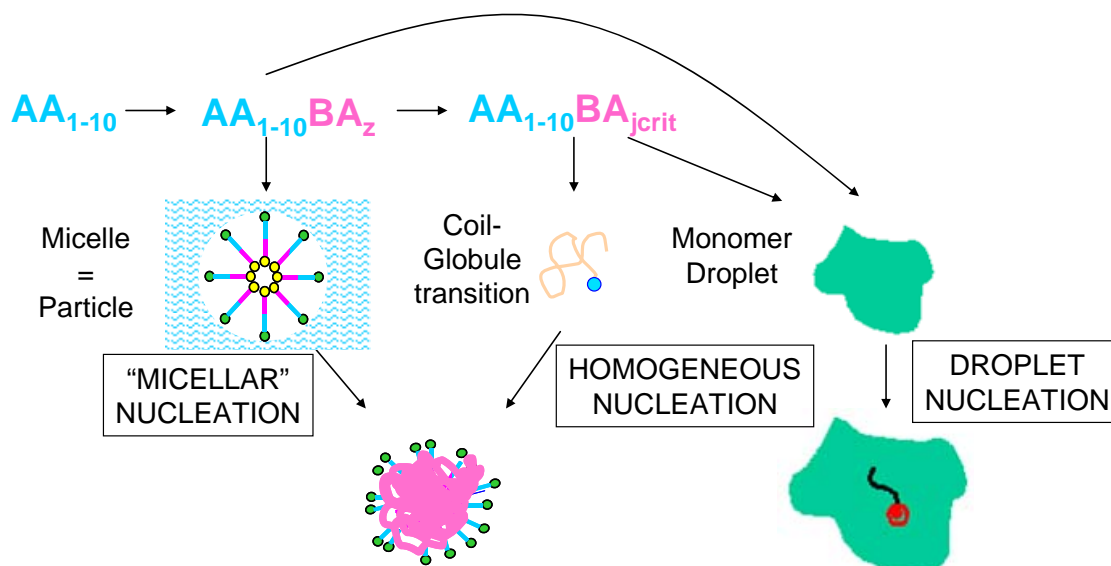

Figure 3.2: Possible nucleation mechanisms for amphipathic macro-RAFT agents (BA based example).

For the controlled feed RAFT mediated experiments with the pre-formed amphipathic RAFT agents the nucleation mechanism is visualized in Figure 3.3. As the starting amphipathic

macro-RAFT agents are both water-soluble and surface active, the macro-RAFT agents are most likely present as aggregates. However, the aggregates have a transient existence, since the aggregates of the macro-RAFT agents are still labile and the individual RAFT molecules can migrate between micelles through the aqueous phase or by coalescence and redispersion. During the nucleation stage some of these micelles take-up a z-meric radical and grow under RAFT control. Migration remains possible until at least one macro-RAFT molecule grows to a length at which it is no more labile. The assembly of macro-RAFT molecules then becomes a true particle, and these growing particles can subsequently cannibalize labile di-blocks from the transient aggregates. The still labile macro-RAFT species will stabilize newly formed surface area on the growing particles. This process continues until all macro-RAFT agents are non-labile and incorporated into the particles, which is in the spirit of the original Smith-Ewart theory.

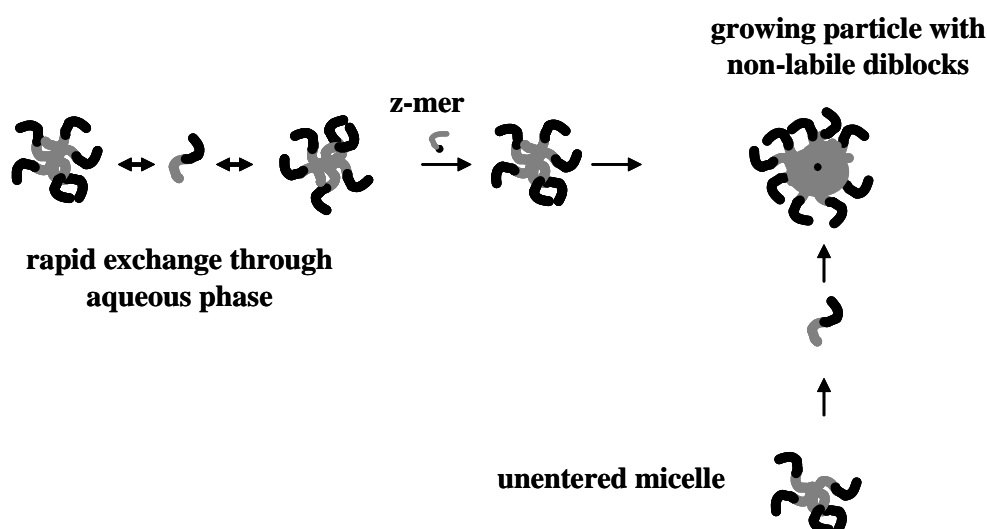**Figure 3.3: Proposed particle formation mechanism for amphipathic macro-RAFT agents.**

3.3.1 Derivation of a particle number expression from the mechanism

The process described above has been mathematically formulated and published[14] and the derivation of an expression for the particle number in *ab-initio* RAFT controlled radical polymerization in emulsion is repeated here. The Maxwell Morrison theory is the basis for

the nucleation rate in this controlled radical system that needs external initiation. It is assumed that each z-meric species will enter and initiate an aggregate of amphipathic macro-RAFT agents; therefore the number of particles (N_p) is described by the amount of initiator (I) in equation (3.1):

$$N_p = 2k_d[I]\left\{\frac{\sqrt{2k_d[I]k_{t,w}}}{k_{p,w}[M]_w}+1\right\}^{1-z} t\, N_A \qquad (3.1)$$

Here $[M]_W$ is the monomer concentration in the water phase, k_d is the initiator dissociation rate coefficient, $k_{t,W}$ and $k_{p,W}$ are water phase termination and propagation, respectively. N_A is Avogadro's number.

The initiation time (t) is restricted to the available amount of labile macro-RAFT agent in the reaction mixture. In accordance with Smith-Ewart theory, cessation of the nucleation stage is assumed to be ended once all macro-RAFT agents have either been irreversibly adsorbed onto a growing particle, or have participated in the formation of a particle. It is assumed that this is the case once a critical degree of polymerization is attained for all the macro-RAFT agents.

$$\overline{X}_n = X_{crit} \qquad (3.2)$$

where $\overline{X}_n$ is the number-average degree of polymerization of (both dormant and growing) chains. It is assumed that during the nucleation stage all surface area is completely covered by the hydrophilic end groups of the macro-RAFT agent. The number of RAFT capped chains per particle is:

$$n_{cap} = \frac{A_s}{A_e} \qquad (3.3)$$

where A_S is the area of a monomer swollen single particle and A_e is the surface covered by one RAFT capped chain. The value of A_e depends on e.g. initiator type and on the number of hydrophilic monomer units. One has

$$A_s = \pi^{1/3}\left(6V_S\right)^{2/3} \tag{3.4}$$

where V_s is the monomer swollen volume of a single particle. By mass conservation and assuming isometric mixing of polymer and monomer, one has[5]

$$V_S = \left(\frac{\overline{X}_n n_{cap} M_0}{\rho_P N_A}\right)\left(\frac{\rho_M}{\rho_M - [M]_p M_0}\right) \tag{3.5}$$

where ρ_P and ρ_M are the density of polymer and monomer respectively. M_0 is the monomer molecular weight, and $[M]_P$ is the monomer concentration in the particles. The ratio $\rho_M/\left(\rho_M - [M]_p M_0\right)$ represents the contribution of monomer to the swollen particle volume. Combination of equations (3.3)-(3.5) yields

$$V_S = 36\pi\left(\frac{\overline{X}_n M_0}{A_e \rho_P N_A}\frac{\rho_M}{\rho_M - [M]_p M_0}\right)^3 \tag{3.6}$$

The particle growth rate is found by assuming that all particles grow at the same rate, i.e. ignoring compartmentalization effects except those arising from a value of the average number of radicals per particle, $\overline{n}$. The growth rate at time t is then given by

$$\frac{d\overline{X}_n}{dt} = \frac{k_p [M]_p \overline{n}}{n_{cap}} \tag{3.7}$$

Solving equation (3.7) with $\overline{n}$ independent of time gives

$$\overline{X}_n^3 = \overline{X}_n^3 \big|_{t=0} + Bt;$$

$$B = \frac{k_p[M]_p \overline{n} A_e^3}{12\pi} \left(\frac{M_0}{\rho_P N_A} \frac{\rho_M}{\rho_M - [M]_p M_0} \right)^{-2} \tag{3.8}$$

Substitution of t from equation(3.8) into equation (3.1) leads to an expression for the number of particles nucleated

$$N_p = 2k_d[I]\left\{ \frac{\sqrt{2k_d[I]k_{t,w}}}{k_{p,w}[M]_w} + 1 \right\}^{1-z} \frac{\overline{X}_n^3 - \overline{X}_n^3 \big|_{t=0}}{B} N_A \tag{3.9}$$

3.3.2 Sample implementation

The styrene based controlled feed amphipathic macro-RAFT experiments with the most hydrophobic macro-RAFT agents (10AA+10STY) were simulated with the developed model, see section 3.3.1. The reactions that were carried out by Sprong et al.[2] at 80 °C produced around 10^{19} particles per liter; see Figure 3.4. The reaction conditions together with physically and chemically reasonable parameters, see Table 3.1, were implemented into the model for experiments with varying amounts of initiator. The simulated values for the number of particle are compared with the experimentally obtained number of particles in Figure 3.4.

Table 3.1: Parameters used for model calculation.

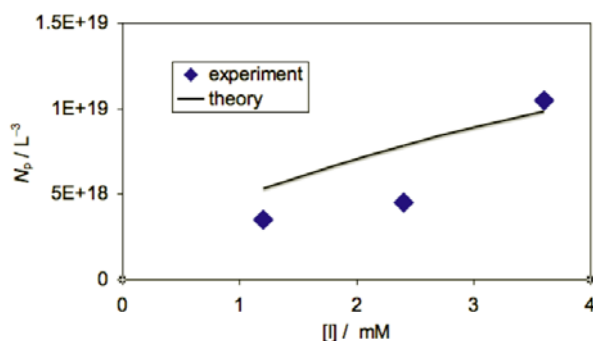| Property	Value	Ref
T	80 °C	
k_d	8.97×10^{-5} s^{-1}	15, 16
$k_{p,W}$	6.5×10^2 M^{-1}s^{-1}	17
$k_{t,W}$	2.0×10^9 M^{-1}s^{-1}	18
M_0	104 g mol^{-1}	
A_E	0.4 nm^2	19
ρ_M	906 kg m^{-3}	16
ρ_P	1.04×10^3 kg m^{-3}	16
$[M]_W$	5.6×10^{-3} mol L^{-1}	20
$[M]_P$	5.8 mol L$^{-1,}$	21
$X_{n|t=0}$ and X_{crit}	10 (start) and 20 (fitted)	
z	2	10
$\overline{n}$	1 (assumption)	

Figure 3.4: Particle number for amphipathic RAFT system (10AA+10STY).

The predicted number of particles is in the same order magnitude as the experimental results for small scale experiments with controlled feed of styrene[2]. For this first test of the model parameters for styrene were taken from literature, $[M]_w$[20],$[M]_P$[21] (temperature dependence was not taken into account). Since the calorimetric experiments, see chapter 2, demonstrated that, even during the slow controlled feed conditions, the overall monomer concentration increased to a value where monomer droplets are formed, the saturated concentration in styrene particles was taken as the concentration of monomer in the particles. The rate coefficients k_d[16] and k_t[18, 22, 23] were obtained from literature as well. For the "headgroup" area of the amphipathic RAFT agent a value of a typical ionic stabilizer SDS was used[19]. Furthermore the number of radicals per particle was taken as one, neglecting termination during the period of nucleation. A more advanced approach based on the work of Stuart Thickett[24, 25] is presented in chapter 6.

3.4 *Conclusions*

A model inspired by Smith and Ewart's nucleation theory has been derived for the particle formation mechanism of the amphipathic macro-RAFT system under controlled feed conditions. It is assumed that the preformed amphipathic macro-RAFT molecules are present in the form of micellar assemblies at the start of nucleation. Entry by z-meric species initiates particle formation by growing the macro-RAFT agents to such a degree of polymerization of

the hydrophobic block that the macro-RAFT is no longer labile. Remaining labile macro-RAFT assemblies will be cannibalized by the growing particles. Cessation of nucleation is assumed once all macro-RAFT agents are adsorbed onto the particles and are no longer labile.

A first implementation of the model using physically reasonable parameters shows promising results. However, it is important to verify the various parameters experimentally before any mechanistic postulates can be confirmed or refuted.

Although accurate rate data were obtained for the system by calorimetric measurements, see chapter 2, they are of limited value for the study of the duration of the particle formation, since the system under investigation was run at non monomer saturated conditions. It is therefore important to obtain accurate data for the time evolution of the molecular weight distribution, the particle size and the particle size distribution for these amphipathic macro-RAFT systems. Useful data for the nucleation mechanism can be deduced from these experimental data.

3.5 *References*

1.   Ferguson, C. J.; Hughes, R. J.; Nguyen, D.; Pham, B. T. T.; Gilbert, R. G.; Serelis, A. K.; Such, C. H.; Hawkett, B. S. *Macromolecules* **2005,** 38, 2191-2204.
2.   Sprong, E.; Leswin, J. S. K.; Lamb, D. J.; Ferguson, C. J.; Hawkett, B. S.; Pham, B. T. T.; Nguyen, D.; Such, C. H.; Serelis, A. K.; Gilbert, R. G. *Macromolecular Symposia* **2006,** 231, 84-93.
3.   Harkins, W. D. *Journal of the American Chemical Society* **1947,** 69, 1428-44.
4.   Smith, W. V.; Ewart, R. H. *Journal of Chemical Physics* **1948,** 16, 592-9.
5.   Gilbert, R. G., Emulsion Polymerization. In 1995; p 384.
6.   Hansen, F. K.; Ugelstad, J. *Journal of Polymer Science, Polymer Chemistry Edition* **1978,** 16, 1953-79.
7.   Fitch, R. M.; Tsai, C. H. *Polym. Colloids, Proc. Symp.* **1971**, 73-102.
8.   Hansen, F. K. *Chemical Engineering Science* **1993,** 48, 437-44.
9.   Hawkett, B. S.; Napper, D. H.; Gilbert, R. G. *Journal of Polymer Science, Polymer Chemistry Edition* **1981,** 19, 3173-9.
10.   Maxwell, I. A.; Morrison, B. R.; Napper, D. H.; Gilbert, R. G. *Macromolecules* **1991,** 24, 1629-40.

11. Adams, M. E.; Trau, M.; Gilbert, R. G.; Napper, D. H.; Sangster, D. F. *Australian Journal of Chemistry* **1988,** 41, 1799-813.

12. Ferguson, C. J.; Hughes, R. J.; Pham, B. T. T.; Hawkett, B. S.; Gilbert, R. G.; Serelis, A. K.; Such, C. H. *Macromolecules* **2002,** 35, 9243-9245.

13. Foerster, S.; Abetz, V.; Mueller, A. H. E. *Advances in Polymer Science* **2004,** 166, 173-210.

14. Gilbert, R. G. *Macromolecules* **2006,** 39, 4256-4258.

15. Lewis, F. M.; Matheson, M. S. *Journal of the American Chemical Society* **1949,** 71, 747-8.

16. Brandrup, J.; Immergut, E. H.; Editors, *Polymer Handbook, Fourth Edition*. 1998;

17. Buback, M.; Gilbert, R. G.; Hutchinson, R. A.; Klumperman, B.; Kuchta, F.-D.; Manders, B. G.; O'Driscoll, K. F.; Russell, G. T.; Schweer, J. *Macromolecular Chemistry and Physics* **1995,** 196, 3267-80.

18. Sangster, D. F.; Davison, A. *Journal of Polymer Science, Polymer Symposia* **1975,** 49, 191-201.

19. Piirma, I.; Chen, S. R. *Journal of Colloid and Interface Science* **1980,** 74, 90-102.

20. Lane, W. H. *Industrial and Engineering Chemistry, Analytical Edition* **1946,** 18, 295-6.

21. Hawkett, B. S.; Napper, D. H.; Gilbert, R. G. *Journal of the Chemical Society, Faraday Transactions 1: Physical Chemistry in Condensed Phases* **1980,** 76, 1323-43.

22. Dainton, F. S.; James, D. G. L. *Journal of Polymer Science* **1959,** 39, 299-312.

23. Dainton, F. S.; Eaton, R. S. *Journal of Polymer Science* **1959,** 39, 313-20.

24. Thickett, S. C.; Gilbert, R. G. *Macromolecules* **2006,** 39, 6495-6504.

25. Thickett, S. C.; Gilbert, R. G. *Macromolecules* **2006,** 39, 2081-2091.

Chapter 4

Characterization of macro-RAFT agents

Abstract: *The results of the characterization efforts to quantify the initial and time-evolution of the molecular weight distribution of the macro-RAFT agents are reported here. Various characterization techniques have been used to obtain insights into the duration of the nucleation time. Intrinsic quantitative techniques such as CE, HPLC and SEC were applied to obtain the molecular weight distribution of the RAFT-capped polymers. However with none of these techniques baseline separation could be obtained, even for the simplest of starting blocks, the hydrophilic macro-RAFT agent. Trends and qualitative data were obtained for the macro-RAFT agents before and during the reactions by SEC. The differences in SEC elution times demonstrated that far more macro-RAFT agent was involved in the initial nucleation stage for the more hydrophobic (10AA+10STY) system than for the purely hydrophilic (10AA) ones. Mass spectrometric techniques (MALDI-ToF and ESI) proved to be valuable tools for confirming the successful synthesis of the various macro-RAFT species, although no quantitative data can be obtained from these techniques.*

4.1 *Introduction*

Calorimetric measurements of the controlled feed amphipathic macro-RAFT experiments, described in chapter 2, provide insights into the starting time of the initial particle formation for the various macro-RAFT systems. However, since the calorimetric amphipathic macro-RAFT experiments have to be run under controlled feed conditions to prevent droplet polymerization, it is impossible to obtain information about the duration of the nucleation phase that can be related to the model. In this chapter nucleation time is studied indirectly by characterization of the synthesized polymers. The results of these characterization efforts of the macro-RAFT species are here reported. Not only should this provide insight into the time evolution of the molecular weight distribution, it could also allow quantification of the initial macro-RAFT species. This quantitative information can be used to determine the mechanisms that are at the basis of nucleation in the amphipathic RAFT systems.

Mass Spectrometry

The individual macro-RAFT species of the produced distribution can be readily identified by mass spectrometry. Developments in the field of soft ionization techniques such as electrospray ionization (ESI) and matrix-assisted-laser-desorption/ionization (MALDI) in the last decade have tremendously increased the application of mass spectrometry for the characterization of synthetic polymers[1]. It has become possible to bring intact, predominantly singly charged, polymers in the gas phase without degradation of the polymer molecule. This allows obtaining structural information on polymer chains as a function of its molar mass, i.e. repeat units, end-group masses, copolymer compositions as well as the overall molar weight distribution (MWD). Various authors have reported that accurate molar-mass distributions can be obtained for polymers with low polydispersities (PDI < 1.2)[2-9]. However, mass discrimination is a known problem, particularly for very small and very large molecules,

resulting in both underestimation and overestimation of the average molecular weight. For this reason mass spectrometry techniques are mostly seen as a complementary source of qualitative data about the polymer in combination with traditional quantitative chromatographic techniques like HPLC and SEC.

Quantitative detection techniques like ultra-violet (UV) and diffential refractive index (DRI) detectors can be used in combination with chromatographic separation techniques like SEC. Since the macro-RAFT agents contain the UV active carbon sulfur double bond, polymeric species containing a RAFT moiety can be readily detected. The separation of RAFT and non-RAFT polymeric species can either be performed by measuring at two different wavelengths (one for the RAFT agent and one for the polymer e.g. 254 nm for styrene) or by application of an additional universal detector like refractive index.

Before quantitative molecular weight data can be obtained, the various polymer species have to be separated. This separation can be performed based on different properties of the polymer. Four different separation techniques are discussed that were used or tried for the characterization of the macro-RAFT species.

Capillary Zone Electrophoresis

Since the macro-RAFT species all contain a hydrophilic poly(acrylic acid) block, it is possible to use capillary electrophoresis (CE) for separation purposes. Capillary zone electrophoresis or free solution capillary electrophoresis is the simplest form of CE. By applying a voltage over a capillary, polymeric species are accelerated or retarded based on their charge and hydrodynamic volume. The resulting velocity of the polymeric species relative to the average liquid velocity is referred to as the electrophoretic mobility. The hydrodynamic volume of a polymer is proportional to the mass of the molecule when no

branching or crosslinks are present. Together with the electro-osmotic flow (EOF), a plug flow of the electrolyte solution through the capillary due to the applied voltage, the electrophoretic mobility can be used with great efficiency to separate compounds with a very similar structure. The efficiency of capillary electrophoresis separations is typically much higher than the efficiency of other separation techniques like HPLC. Unlike HPLC, in capillary electrophoresis there is no mass transfer between phases. In addition, the flow profile in EOF-driven systems is flat, rather than the rounded laminar flow profile characteristic of the pressure-driven flow in chromatography columns.[10] As a result, EOF does not significantly contribute to band broadening as in pressure-driven chromatography.

Liquid chromatography

Alternatively the macro-RAFT species can be separated by liquid chromatography. All chromatographic processes relate to the selective distribution of the solute between the mobile and the stationary phase of a chromatographic system[11]. In an ideal situation, size exclusion chromatography (SEC) separation is accomplished purely based on entropic effects. The volume of the pores of the stationary phase accessible by the solute depends on its hydrodynamic volume. The smaller the hydrodynamic volume of the solute, the larger the accessible volume of the pores in the stationary phase is and the longer the elution time will be. The opposite process of ideal size exclusion chromatography is liquid adsorption chromatography (LAC), where in the ideal case separation is only based on enthalpic effects. Here the adsorptive characteristics of the (macromolecular) solute onto the stationary phase govern the retention time. The larger the solute, the more interaction it will have with the stationary phase, the longer the elution time will be.
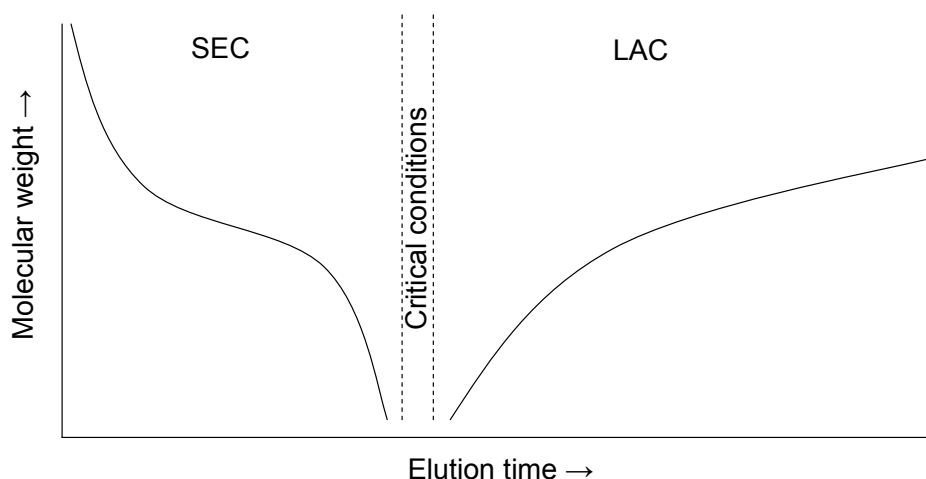
Figure 4.1: Chromatographic behaviour molar mass versus retention time for the different modes, SEC, critical mode and LAC.

However, SEC and LAC are often mixed-mode chromatographic methods, where either entropic or enthalpic interactions dominate the other process[12]. When the enthalpic and entropic interactions are exactly in balance, chromatography in critical mode is attained. In this situation the solute starts to adsorb onto the stationary phase and the adsorption forces are exactly compensated by entropic losses. At critical conditions all species with different molecular weights elute at the same time. The three modes of liquid chromatography are illustrated by Figure 4.1.

By using the various characterization techniques by themselves or in combination with each other, qualitative and quantitative data on the molecular weight distribution of the macro-RAFT species and the time evolution thereof can be obtained. When quantitative data of the lower molecular weight species of the macro-RAFT agents can be obtained, the disappearance of the lower molecular weight species may point to particle formation, since any macro-RAFT agent involved in nucleation or adsorption on a particle is expected to grow very quickly to a more hydrophobic species that is insoluble in the aqueous phase. With quantitative data, one would also be able to study which particular macro-RAFT species are initially involved in the nucleation process for the various macro-RAFT systems.

4.2 *Experimental*

4.2.1 Capillary Zone Electrophoresis

Capillary zone electrophoresis experiments were carried out using a Hewlett Packard[3D] CE system equipped with a diode array detector. The capillary was thermostatted at 25 °C for all separations. Poly(vinyl alcohol) (PVA) and bare silica capillaries (50·μm internal diameter, HP) of a total effective length of 56 cm were used. The bare silica capillary was pre-treated by rinsing for 5 minutes with an aqueous 0.1 M NaOH solution and with a buffer solution before use. The PVA capillary was only rinsed with buffer solution before use. Boric acid (pH 9.3) and phosphate buffers (pH 5-9) were prepared ranging in concentration from 20 to 100×10^{-3} mol L^{-1}.

4.2.2 Liquid Chromatography

Size Exclusion Chromatography

Poly(n-butyl acrylate) samples were analysed using a Shimadzu system fitted with a series of Waters columns (HR4, HR3 and HR2). Molecular weights were determined from refractive index data analysed with Polymer Laboratories Cirrus software, with all molecular weights being relative to polystyrene standards and converted to poly(n-butyl acrylate) using "universal calibration"[11] and the following Mark-Houwink parameters[13]: styrene, $K = 11.4 \times 10^{-5}$ dL g^{-1}, $\alpha = 0.716$; n-butyl acrylate $K = 12.2 \times 10^{-5}$ dL g^{-1}, $\alpha = 0.70$. It should be noted that universal calibration with the Mark-Houwink relationship is not valid for lower molecular weights, the Dondos-Benoit relationship, which is linear in this range, could be used as an alternative[14]. A 5 volume % mixture of acetic acid and THF mixture was used as mobile phase and to dissolve the dried polymer SEC samples.

Styrene samples were analysed with the same eluent as the n-butyl acrylate samples on a Waters system equipped with a UV and DRI detector system and with two 7 μm linear S PFG columns and a 7 μm PFG precolumn (Polymer Standards Service, Germany). Molecular weights were determined from both the UV and DRI data analysed with Waters Millenium software, with all molecular weights being relative to polystyrene standards.

High Performance Liquid Chromatography

High performance liquid chromatography (HPLC) analyses of macro-RAFT agents were carried out on an Agilent 1100 series system comprising a degasser, a quarternary pump, an autosampler (1 μL injection volume) and a UV diode array detector. For data collection and processing the software package HP Chemstation (Hewlett Packard) was used. The stationary phase was a Zorbax RX-C8 column (Agilent) (2.1 ×150 mm) with 5 μm particles and the mobile phase was a MeOH/H_2O gradient with 0.1% acetic acid at a flow rate of 0.25 ml min^{-1}, see Table 4.1.

Table 4.1: Water methanol gradient used for HPLC separation of macro-RAFT agents.

Time	H_2O [Volume %]	MeOH [Volume %]
0	50	50
25	0	100
27	0	100
30	50	50

4.2.3 Mass spectrometry

Electrospray mass spectrometer analysis (ESI-MS) of the n-butyl acrylate based macro-RAFT agents were carried out using a Finnigan Mat LCQ MS detector with Finnigan LCQ Data processing and Instrument Control software. Samples were dissolved in 50:50 v/v MeOH/H_2O and fed into the electrospray ionization unit at 0.2 mL min^{-1}. The electrospray

voltage was 5 kV, the sheating gas was nitrogen at 415 kPa, and the heated capillary was at 200 °C

The ESI-MS analysis of the styrene based macro-RAFT agents were carried out on a HPLC-MS setup. This combination is equipped with an Agilent MSD type SL with an atmospheric pressure electrospray interface. The polymer was eluted in a gradient of a water methanol mixture with the addition of 0.1 % of acetic acid and fed into the electrospray ionization unit at 0.25 mL min^{-1}. The electrospray voltage was 4 kV, nitrogen was used as sheating gas at a nebulising pressure of 207 kPa, and the capillary was heated at 350 °C. The data was processed with HP Chemstation (Hewlett Packard) software.

MALDI-ToF analysis was carried out on a Voyager DE-STR from Applied Biosystems. The matrix trans-2-[3-(4-tert-Butylphenyl)-2-methyl-2-propenylidene]malononitrile (Fluka) was used since it absorbs the laser energy well and facilitates ionization of a range of polymers[15]. The matrix was dissolved in THF at a concentration of 40 mg mL^{-1}. The macro-RAFT agents were dissolved in a MeOH/THF mixture of 4:1 volume ratio at a RAFT concentration of 1 mg mL^{-1}. In the MALDI-ToF-MS experiment, the matrix and the polymer solutions were premixed in a ratio of 1:1. The premixed solutions were handspotted on the target plate and left to dry. All spectra were recorded in the reflector mode.

4.3 *Results & Discussion*

4.3.1 Mass spectra of the initial macro-RAFT agents

The initial macro-RAFT agents could be readily analysed by mass spectroscopy techniques like ESI-MS and MALDI-ToF-MS, resulting in a non-quantitative indication of the distribution of macro-RAFT species produced. Nevertheless the ESI-MS data confirmed the formation of the initial hydrophilic macro-RAFT agents (see section 2.2.2). Figure 4.2 shows

an ESI-MS spectrum of a macro-RAFT agent that was designed to contain a hydrophilic

acrylic acid block of a degree of polymerization (DP) of 10. However, Figure 4.2 shows a

singly charged distribution of a peak DP of 11 and a doubly charged peak DP of 13 acrylic

acid units. This difference in peak DP indicates that the longer hydrophilic blocks are more

easily ionized in the negative mode of ESI-MS, indicating some mass discrimination.
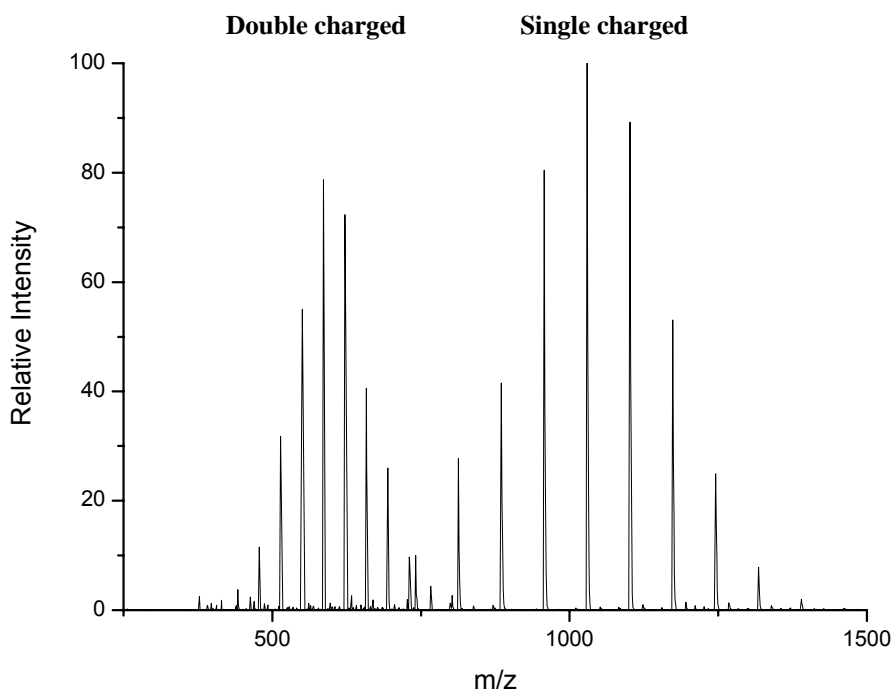

Figure 4.2: Electrospray mass spectrum of hydrophilic macro-RAFT agent designed to contain on average 10 acrylic acid groups; see section 2.2.2.

It is therefore likely that the single charged distribution in Figure 4.2 is probably also

showing a too high peak molecular weight for the hydrophilic macro-RAFT agents.

ESI-MS demonstrated to be a very useful tool to establish the success of the formation of

macro-RAFT agents of varying degrees of hydrophobicity. In Figure 4.3, ESI-MS spectra of

the various n-butyl acrylate based macro-RAFT agents are collected. Clearly the average

molecular weight increases for the more hydrophobic n-butyl acrylate based macro-RAFT
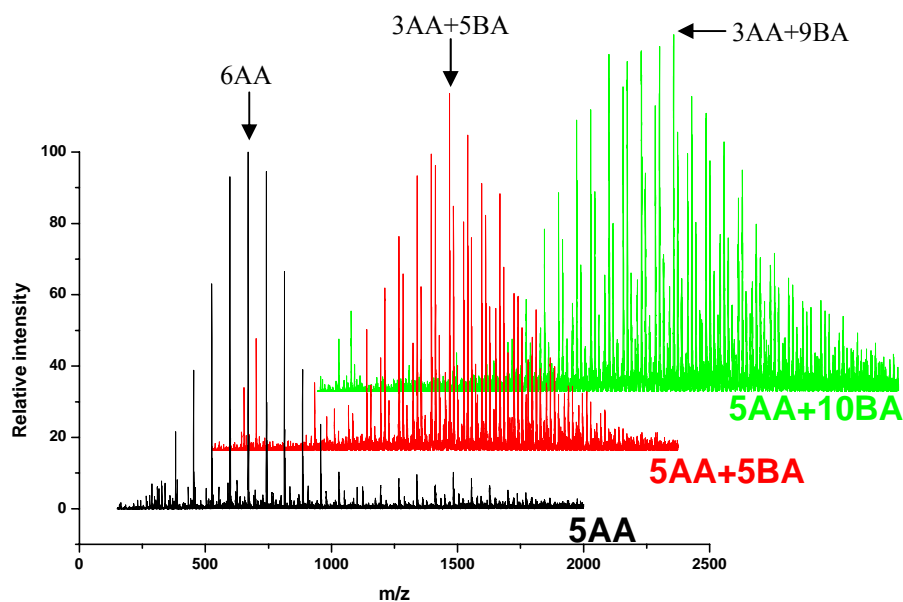
agents.

Figure 4.3: Electrospray spectra of n-butyl acrylate based macro-RAFT agents; see section 2.2.2.

The ESI-MS systems used in this study had an upper molecular weight range of 2000 g mol^{-1}.

For this reason the more hydrophobic preformed di-block macro-RAFT agents (e.g.

10AA+10STY) were analysed by MALDI-ToF-MS. In Figure 4.4 a typical example of a

MALDI-ToF mass spectrum of the more hydrophobic macro-RAFT (10AA+10STY) is

shown. This macro-RAFT agent was synthesized with the hydrophilic macro-RAFT (10AA)

as precursor; see Figure 4.2. Only after assigning each peak with a specific macro-RAFT

species these MALDI-ToF-MS spectra become informative. However, with a distribution

around the peak degree of polymerization of 10 styrene units on top of the distribution of the

initial hydrophilic macro-RAFT agents peak assignment becomes a very laborious task. This

task has been alleviated by using a MALDI/ESI MS interpretation program developed in-

house[16], that transforms the mass spectrum into a contour plot of the analysed polymeric

species. The transformation is performed by fitting the observed spectrum with possible

combinations of both monomers, the RAFT agent as well as the z-group and initiator based

end-groups, resulting in a fingerprint of the analysed block copolymeric macro-RAFT agent

(10AA+10STY); see Figure 4.5. The contour plot's intensity (z-axis) is constructed of the

relative intensities of the mass spectrum; these data are not quantitative and therefore care should be taken when interpreting these plots.
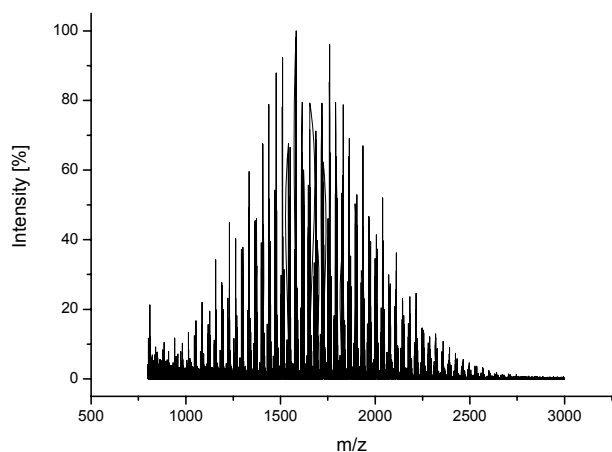

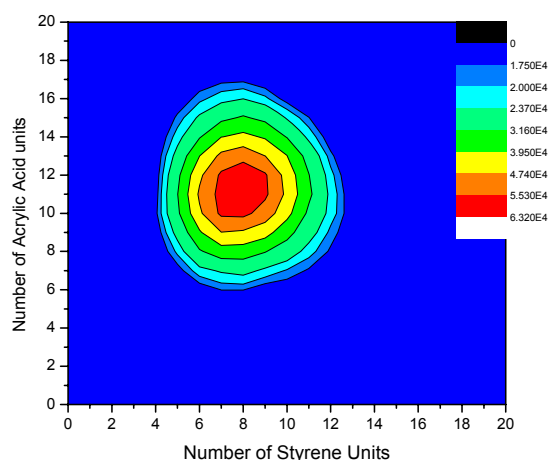**Figure 4.4: MALDI-ToF mass spectrum of the preformed di-block (10AA+10STY) amphipathic macro-RAFT agent.**

Figure 4.5: Contour plot of the preformed di-block (10AA+10STY) amphipathic macro-RAFT agent, with on the x and y axis the number of respective monomeric units attached to the RAFT moiety.

4.3.2 Quantification of the initial macro-RAFT agents

Quantitative molecular weight analysis of the initial macro-RAFT agents has been attempted with various methods. First of all a combination of LAC and SEC was tried to quantitatively analyse the BA based preformed di-block macro-RAFT agents. A multi-dimensional polymer characterization setup (Polymer Standards Service) based on an Agilent 1100 series system was used. The idea was to separate the species in the first dimension only on the length of the hydrophilic block by running the LAC at the critical conditions for BA[17]. The separation procedure was then continued by SEC analysis of the fractions of the first separation to obtain the overall molecular weight per hydrophilic block length. However, critical conditions for a model system based on pure BA macro-RAFT agents, where the hydrophilic (5AA) macro-RAFT agent will still separate, could not be obtained, see appendix II. This is due to the fact that at the critical conditions for BA in the presence of a RAFT group at an apolar (C18 functionalized nucleosil column, Agilent) stationary phase, the hydrophilic macro-RAFT (5AA) does not dissolve in the mobile phase (49.9% ACN and 50.1 THF by

volume). Both hydrophilic (5AA) and hydrophobic (BA) macro-RAFT agents did dissolve in acidic water/THF mixtures, but good conditions for separation based on hydrophilic block length do not agree with critical conditions for the BA blocks. On more hydrophilic stationary phases (CN- and OH-functionalized nucleosil columns, Agilent) no critical conditions could be obtained with acidic water/THF mixtures as eluent for the BA based macro-RAFT agent. Therefore, unfortunately no reasonable results could be obtained for this kind of two-dimensional analysis.

Finding critical conditions for the amphipathic species proved to be impossible. Use of polar organic eluents, e.g. dimethyl sulfoxide or dimethyl acetamide, might be an interesting direction for future research into the analysis of amphipathic species under critical conditions. In literature the use of these organic solvents has not been reported for amphipathic species to the best of the author's knowledge.

For a quantitative analysis of the initial hydrophilic macro-RAFT agent, the molecular weight distribution can be determined by separation based on charge and hydrodynamic volume using capillary electrophoresis or a variation thereof[18]. Capillary zone electrophoresis has been successfully used to characterize oligo(acrylic acid) macro-RAFT agents[19]. Lower buffer concentrations were used in the present study. With the reduced buffer concentration of 50 $\times 10^{-3}$ mol L^{-1} of borate buffer at a pH of 9.3 the optimal separation conditions were obtained, see Figure 4.6.

Although a better separation performance towards oligomeric acrylic acid macro-RAFT agents is reported[19] by CZE than could be obtained by aqueous phase SEC, poly(acrylic acid) blocks of a higher than oligomeric degree of polymerization could not be separated to baseline, i.e. elution peaks partially overlap. This lack of baseline separation makes it impossible to obtain quantitative insight into the initial molecular weight distribution of the

hydrophilic macro-RAFT agent. As a consequence more complex amphipathic RAFT agents cannot be analysed quantitatively in term of molecular weight distribution by capillary zone electrophoresis.
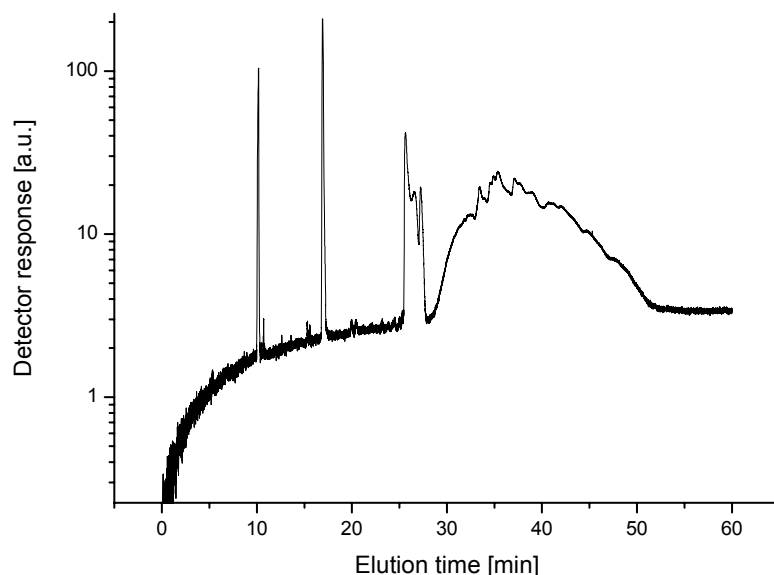

Figure 4.6: Electropherogram of hydrophilic macro-RAFT (5AA) in a borate buffer of 50×10^{-3} mol L^{-1} at a pH of 9.3; detailed information on this macro-RAFT agent can be obtained in section 2.2.2.

Better separation of the initial hydrophilic macro-RAFT agent, could be obtained from high performance liquid chromatography over an apolar (Zorbax RX-C8, Agilent) column with a water/methanol gradient; see Table 4.1. The more hydrophobic the macro-RAFT agent is, the more interaction it has with the stationary phase, and therefore elution takes place at a later time. For this reason the RAFT agent without any hydrophilic block elutes last. The difference in the UV signal and the total ion count confirms the formation of some homo-poly(acrylic acid), that elutes first; see Figure 4.7. Unfortunately, only for the first oligomer baseline separation is obtained, elution peaks of macro-RAFT agents with two or more acrylic acid units are not completely separated.
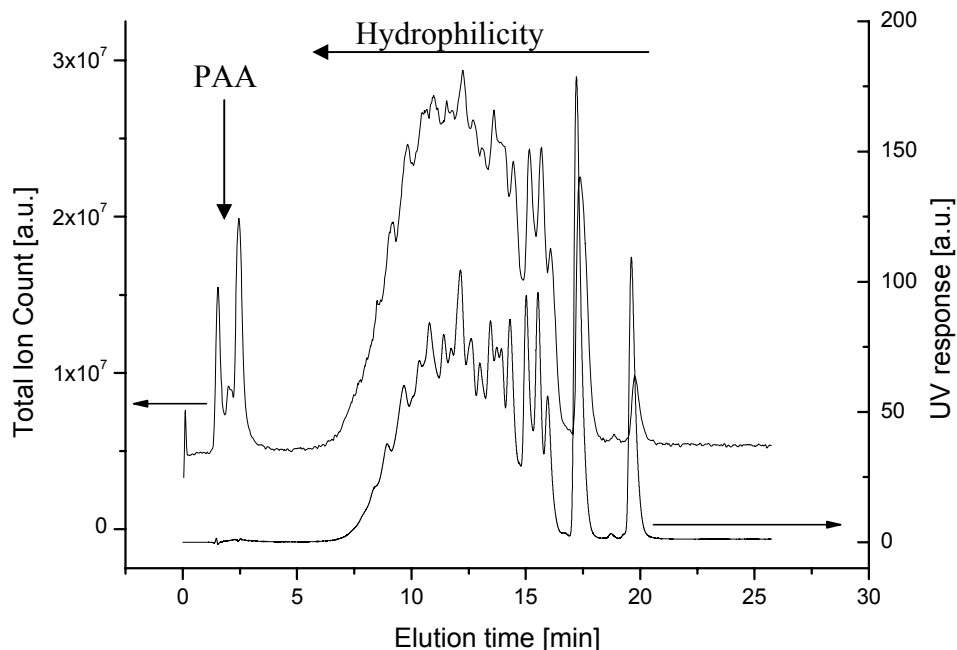
Figure 4.7: Total Ion Current and UV trace of initial hydrophilic macro-RAFT (10AA) after HPLC separation over a C8 column with a H$_2$O/MeOH gradient. For synthesis of macro-RAFT see section 2.2.2.

Individual elution peaks can be observed on top of the main trace in the chromatogram. However, the more hydrophilic the macro-RAFT is, the poorer the separation becomes. This is demonstrated by the broader distributions obtained by MS for the individual peaks of the more hydrophilic macro-RAFT agents, as shown in Figure 4.8.
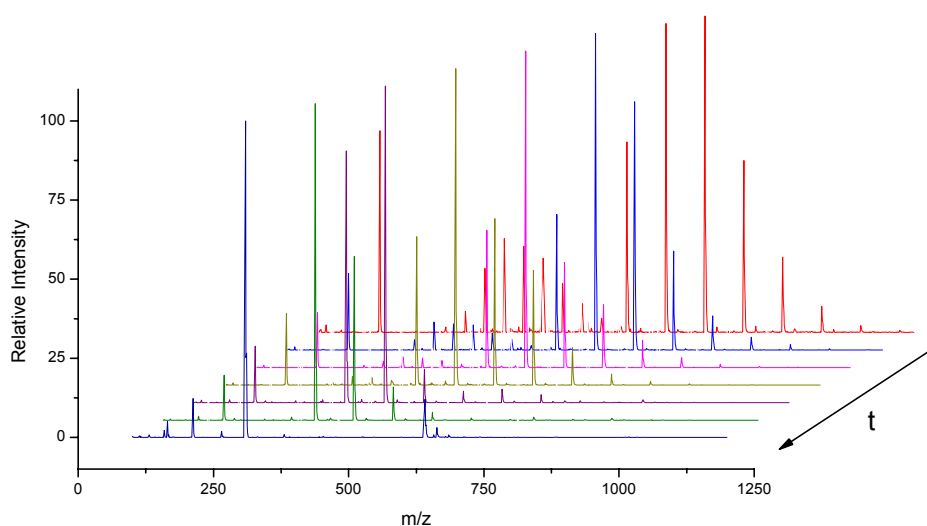

Figure 4.8: Mass spectra of the individual peaks of the HPLC elution peaks in Figure 4.7 of the initial hydrophilic macro-RAFT agent (10AA). The RAFT agent, with the longest elution time is printed in the foreground. The most hydrophilic macro-RAFT agent (with the broadest distribution) is in the background.

4.3.3 Time evolution of the molecular weight distribution

Size exclusion chromatography (SEC) was used to monitor the overall time evolution of the molecular weight distribution of the macro-RAFT agents during polymerization. In order to minimize the interaction of the hydrophilic block of the macro-RAFT species with the column the SEC separations were performed in a 5 weight % acetic acid/THF mixture[20]. In the presence of acetic acid, all acrylic acid groups are protonated.

The n-butyl acrylate controlled feed experiments were confirmed to be performed under RAFT controlled radical polymerization conditions by a steadily increasing molecular weight distribution as determined by SEC, see Figure 4.9. This is in agreement with previously reported results for the n-butyl acrylate based amphipathic RAFT agent system[21].
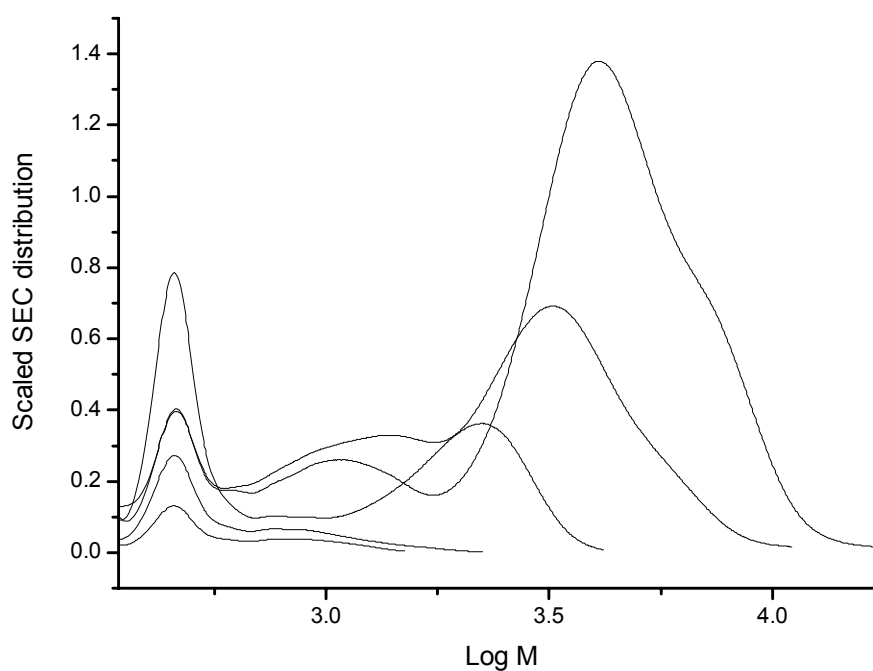

Figure 4.9: Increasing molecular weight distribution with conversion in a controlled feed BA experiment; see section 2.2.2 for details on synthesis.

For a better understanding of the differences in nucleation behaviour of the hydrophilic and more hydrophobic macro-RAFT agents, samples of styrene based experiments were analysed under the same acidic SEC conditions; see Figure 4.10 and Figure 4.11. The polymerizations

starting with 10AA and 10AA+10STY macro-RAFT agents respectively both show controlled behaviour, since both show a decreasing elution time (indicating higher average MWD) with conversion. However the average molecular weight is much higher for the hydrophilic macro-RAFT system, indicating that less macro-RAFT agent is involved in the initial nucleation phase.
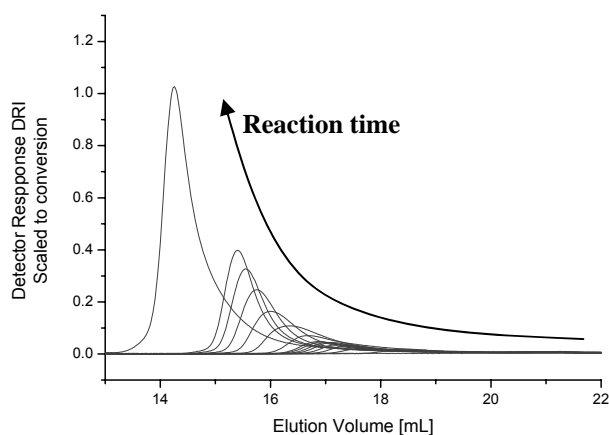

Figure 4.10: Time evolution of MWD of a styrene controlled feed experiment in the presence of hydrophilic macro-RAFT (10AA).
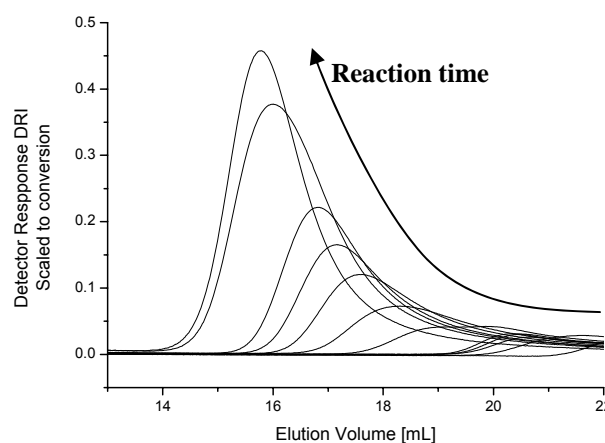
Figure 4.11: Time evolution of MWD of a styrene controlled feed experiment in the presence of more hydrophobic macro-RAFT (10AA+10STY).

This is even more clearly observable when the SEC data of both the hydrophilic and the more hydrophobic macro-RAFT agent are compared for the samples taken just before and just after the initial particle formation; see Figure 4.12. These samples were taken after the same reaction time during the respective experiments and both polymerizations went to starved conditions after the initial nucleation phase, so the same amount of monomer had reacted. However, there is a big difference in the molecular weight distributions, indicating the participation of a large amount of macro-RAFT agents in the initial nucleation phase for the more hydrophobic macro-RAFT agent (10AA+10STY). The actual difference would be quantified by taking the ratio of the average molecular weight for the two systems if the macro-RAFT agent's elution behaviour were the same as the polystyrene standards. Unfortunately, although the SEC analyses were performed under acidic conditions, the elution time of the more hydrophobic macro-RAFT agent (10AA+10STY) before particle

formation and after particle formation were well below the expected elution time for molecules of that molecular weight. Apparently even though the acrylic acid block is protonated by the addition of the acetic acid to the eluent, it still interacts with the stationary phase. As a consequence the apparent average molecular weight is significantly lower than the real molecular weight. This would not be a problem if the SEC columns used had a linear calibration curve in the region of the eluding macro-RAFT agents, since both contain the same hydrophilic block, but this is not the case. With the retardation caused by the interaction with the stationary phase, the macro-RAFT agents end up in the even lower molecular weight range where SEC columns generally can not discriminate well, since molecules in that low molecular weight range can penetrate into all the pores of the stationary phase.

It can be concluded that SEC analysis provides valuable information about the controlling performance of the amphipathic macro-RAFT agents in *ab-initio* emulsion polymerization. Unfortunately SEC does not provide quantitative answers for the macro-RAFT systems, however, qualitative information can be deduced from the measurements. During the nucleation stage the hydrophobic macro-RAFT agent (10AA+10STY) is involved in much larger amounts than the hydrophilic macro-RAFT agent (10AA), as demonstrated by the SEC.
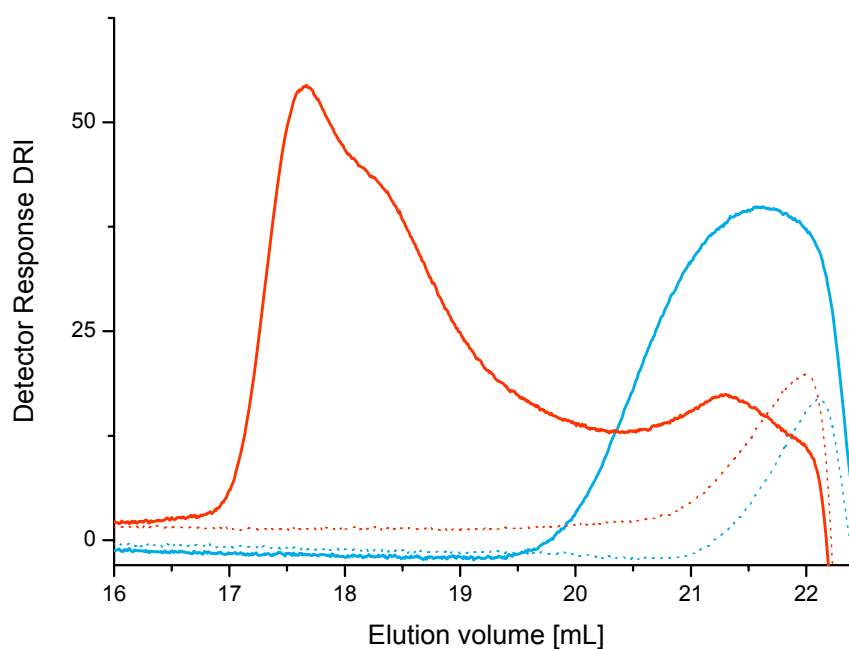
Figure 4.12: Chromatogram of both hydrophilic (10AA) (red) and more hydrophobic (10AA+10STY) (blue) macro-RAFT just before (dotted lines) and just after (solid lines) the initial nucleation. See section 2.2.2 for synthesis details.

4.3.4 Determination of particle formation time

By combining the above discussed size exclusion chromatography with MALDI-ToF mass spectrometry, we attempted to identify the type of macro-RAFT agent involved in the initial nucleation stage. The disappearance of the low MW fraction of the macro-RAFT agent could also provide a way of estimating the nucleation time when using the amphipathic RAFT systems as surfactant precursors. Fractions of the SEC separated samples were collected using a Cygnet fraction collector. The collected fractions were dried and dissolved in a MeOH/THF mixture and analysed by the described MALDI procedure; see section 4.2.3.
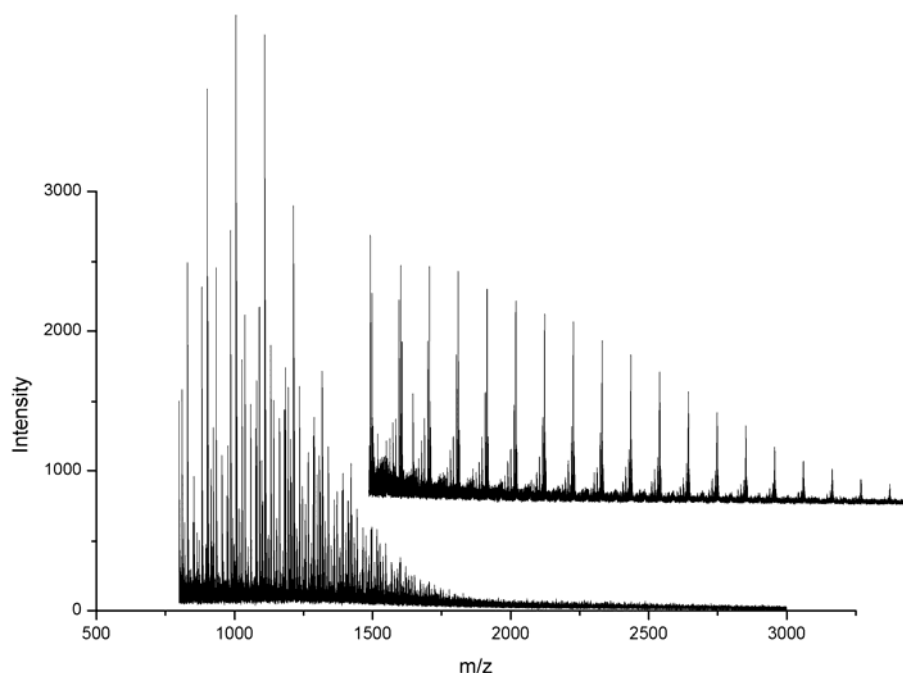
Figure 4.13: MALDI-ToF-MS analysis of low MW SEC fractions (21-23 min) for the more hydrophobic macro-RAFT agent (10AA+10STY). In the foreground the distribution before particle formation around a peak DP (xSTY+2AA), in the background after particle formation a series of xSTY+8AA.

Only for some SEC fractions MALDI-ToF mass spectra were obtained. Unfortunately these measurements proved to be very concentration dependent, which was hard to control for the SEC fractions. The resulting spectra confirmed the predicted results: before particle formation the complete range of the macro-RAFT agents was still present, after particle formation only the more hydrophilic macro-RAFT agents could be distinguished. The data that could be collected support the assumptions in the particle formation mechanism, but due to the lack of results (due to the concentration issues) no firm quantitative answers can be given, only qualitative trends. It was demonstrated that it is not possible to answer questions about the precisely defined species involved in the nucleation stage to collect enough information about the development of the macro-RAFT agent by the MALDI-ToF-MS analysis of the fractions to determine nucleation time.

4.4 *Conclusions*

In conclusion, mass spectrometry, either by ESI-MS or MALDI-ToF-MS, is a reliable tool to establish that a macro-RAFT agent has been successfully prepared. The MS techniques provide insights into the molecules molecular weight synthesized, particularly in combination with the visualisation program. The obtained contour plots, the fingerprints of the polymeric species, are an easy way to compare spectra. However, for the amphipathic RAFT agents with a poly(acrylic acid) hydrophilic block, the MS measurements in the negative mode showed the tendency to ionize longer hydrophilic blocks more easily, confirming the presence of mass discrimination in MS techniques; a not unexpected result. So, all data produced by the MS techniques can only be used for qualitative purposes.

It proved to be difficult to obtain accurate information about the molecular weight and composition distribution of the macro-RAFT agents; neither capillary electrophoresis, high performance liquid chromatography nor size exclusion chromatography could provide definitive data due to the lack of baseline separation for the initial hydrophilic macro-RAFT agent, let alone the more hydrophobic, more complex ones. It was therefore impossible to obtain quantitative data on the molecular weight of the macro-RAFT agent and the time-evolution thereof. However, size exclusion chromatography provided qualitative data about the initial nucleation stage for the controlled feed styrene experiments. The differences in SEC elution times demonstrated that far more macro-RAFT agent was involved in the initial nucleation stage for the more hydrophobic (10AA+10STY) system than for the pure hydrophilic (10AA) ones.

While MALDI-ToF-MS analyses of low MW fractions of the SEC samples could not shed any light on the particle formation time, they did qualitatively confirm the faster incorporation of the more surface active macro-RAFT species into the particles during the

initial nucleation stage. However, due to the lack of reproducible results these data have to be treated with care.

The problems observed in characterizing these amphipathic block macro-RAFT agents can be summarized as the Heisenberg effect in polymer characterization. Either mass spectrometric techniques are used and exact molecular information about the polymeric species is obtained, but no quantitative answer about the molecular weight distribution, or an intrinsic quantitative method is used with a lack of resolution to separate the macro-RAFT species to baseline, making assignment of all the peaks hardly possible.

4.5 *References*

1.   Hanton, S. D. *Chemical Reviews (Washington, D. C.)* **2001,** 101, 527-569.
2.   Byrd, H. C. M.; McEwen, C. N. *Analytical Chemistry* **2000,** 72, 4568-4576.
3.   Lehrle, R. S.; Sarson, D. S. *Polymer Degradation and Stability* **1996,** 51, 197-204.
4.   Tang, X.; Dreifuss, P. A.; Vertes, A. *Rapid Communications in Mass Spectrometry* **1995,** 9, 1141-7.
5.   Belu, A. M.; DeSimone, J. M.; Linton, R. W.; Lange, G. W.; Friedman, R. M. *Journal of the American Society for Mass Spectrometry* **1996,** 7, 11-24.
6.   Schriemer, D. C.; Li, L. *Analytical Chemistry* **1997,** 69, 4176-4183.
7.   Shimada, K.; Lusenkova, M. A.; Sato, K.; Saito, T.; Matsuyama, S.; Nakahara, H.; Kinugasa, S. *Rapid Communications in Mass Spectrometry* **2001,** 15, 277-282.
8.   Rashidzadeh, H.; Guo, B. *Analytical chemistry* **1998,** 70, 131-5.
9.   Axelsson, J.; Scrivener, E.; Haddleton, D. M.; Derrick, P. J. *Macromolecules* **1996,** 29, 8875-8882.
10.   Skoog, D. A., *Principles of Instrumental Analysis. 3rd Ed.* 1985;
11.   Pasch, H.; Trathnigg, B., *HPLC of Polymers.* Springer-Verlag: Berlin, 1997;
12.   Berek, D. *Macromolecular Symposia* **2004,** 216, 145-163.
13.   Beuermann, S.; Paquet, D. A.; McMinn, J. H.; Hutchinson, R. A. *Macromolecules* **1996,** 29, 4206-4215.
14.   Tsitsilianis, C.; Dondos, A. *Journal of Liquid Chromatography* **1990,** 13, 3027-37.
15.   Willemse, R. X. E.; Staal, B. B. P.; van Herk, A. M.; Pierik, S. C. J.; Klumperman, B. *Macromolecules* **2003,** 36, 9797-9803.
16.   Willemse, R. X. E.; Staal, B. B. P.; Donkers, E. H. D.; Van Herk, A. M. *Macromolecules* **2004,** 37, 5717-5723.
17.   Muller, A. H. E.; Roos, S. G.; Schmitt, B. *Polymer Preprints (American Chemical Society, Division of Polymer Chemistry)* **1999,** 40, 140-141.
18.   Cottet, H.; Simo, C.; Vayaboury, W.; Cifuentes, A. *Journal of Chromatography, A* **2005,** 1068, 59-73.
19.   Castignolles, P.; Gaborieau, M.; Hilder, E. F.; Sprong, E.; Ferguson, C. J.; Gilbert, R. G. *Macromolecular Rapid Communications* **2006,** 27, 42-46.

20. Ferguson, C. J.; Hughes, R. J.; Pham, B. T. T.; Hawkett, B. S.; Gilbert, R. G.; Serelis, A. K.; Such, C. H. *Macromolecules* **2002,** 35, 9243-9245.
21. Ferguson, C. J.; Hughes, R. J.; Nguyen, D.; Pham, B. T. T.; Gilbert, R. G.; Serelis, A. K.; Such, C. H.; Hawkett, B. S. *Macromolecules* **2005,** 38, 2191-2204.

Chapter 5

Physical properties of the solution and latex

Abstract: *In this chapter the physical properties of the initial macro-RAFT solution and the latexes obtained from these have been examined. The surface tension during the controlled feed RAFT-mediated emulsion polymerization has been studied by bubble tensiometry. Not surprisingly, there proved to be a much larger amount of surface active species present in the amphipathic macro-RAFT system than in the hydrophilic system. The time-evolution of the particle size distribution for the styrene-based macro-RAFT systems has been investigated by offline (cryo-)TEM, DLS and HDC measurements. It has been demonstrated that the majority of the particles is formed within half an hour from the onset of nucleation. The surface coverage by the amphipathic macro-RAFT agents of the latexes was examined by Maron titration. The derived specific surface area of the amphipathic macro-RAFT agent (10AA+10STY) was in the range of 1-2 nm^2.*

5.1 *Introduction*

The results of studies concerning the physico-chemical properties of the macro-RAFT solutions and latexes prepared starting from these macro-RAFT solutions are reported here. Specifically particle size and fractional surface coverage of the macro-RAFT based latex particles and surface tension of the solutions were investigated.

For a meaningful discussion of the developed particle formation model, accurate parameters are required. Values for the particle formation time, the average particle sizes and the specific headgroup area of the macro-RAFT agents have to be determined. Average particle sizes can be obtained by various methods e.g. electron microscopy, hydrodynamic fractionation and light scattering. An alternative method for the determination of the average particle size is soap titration, the so called Maron titration[1, 2]. By combining the results of soap titrations with the average particle size determined with one of the previously mentioned techniques, estimates for the average headgroup area of the macro-RAFT agents can be obtained. Note that the macro-RAFT agents stabilizing the particles are predominantly present at the surface of the particles. Monitoring the evolution of the particle size distribution provides valuable information about the particle formation time in the RAFT-mediated emulsion polymerization. Surface tension measurements give access to details about the amount of surface active species in the aqueous phase. All this information will help to test the assumption in the developed particle formation mechanism that micelles are present in the solution before particle formation takes place.

5.1.1 Surface tension

Surface tension is the effect within the surface layer of a liquid that causes that layer to behave like a stretched membrane under tension[3]. This effect allows insects, such as the water

strider, to walk on water and allows objects more dense than

water such as needles to float on the surface of water. This

tension, acting parallel to the surface, arises from the attractive

forces between the molecules of the liquid[4], and can be

influenced by surfactants. The concentration of surface active

species in the aqueous solution can be monitored by surface

tension measurements. In this research a bubble tensiometer

(SensaDyne) was used. This bubble tensiometer works via the

maximum bubble pressure method[5]. By measuring the surface
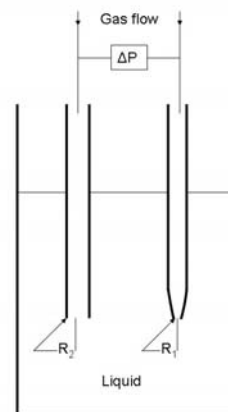

Figure 5.1: Schematic representation bubble tensiometer.

tension within the bulk of the test fluid, one avoids some sources of error such as surface

contaminants or surface foam. This method is based on the measurement of the maximum

bubble pressure of an inert gas that is blown inside the fluid. By measuring the pressure as the

bubbles are formed through two probes of different radii that are immersed in the test fluid, a

differential pressure signal is produced, which is directly related to the surface tension of the

fluid. This procedure overcomes the need for the gravitational constant and liquid density

terms of the fluid that are in the original equation that characterizes the maximum bubble

pressure technique by Schrödinger[6].

5.1.2 Maron titration

Maron titration is a method for the determination of the surface area and average particle size

of synthetic latexes[1, 2]. The method involves the titration of a latex with a soap solution until

the critical micelle concentration (CMC) is attained, as determined by monitoring either the

surface tension or the electrical conductance of the sample. When the critical micelle

concentration, C_{CMC} is known, the titrated soap adsorbed on the latex particles, S_a (expressed

in moles soap per gram of latex particles) can be calculated with equation (5.1), assuming that the soap preferentially adsorbs onto the surface of the latex.

$$C = \left(S_a - \left(\frac{C_{CMC}}{\rho} \right) \right) m + C_{CMC} \qquad (5.1)$$

In equation (5.1) C is the total concentration of added surfactant (moles per litre of latex solution), m is the concentration of polymer (grams per litre of latex solution) and ρ the density of the latex particles (grams litre^{-1}). The surface covered by the titrated SDS per gram of latex particles (A_{SDS}, in m^2 gram^{-1}) can be expressed as:

$$A_{SDS} = S_a \times A_E \times N_A \qquad (5.2)$$

In equation (5.2) A_E is the specific surface area of SDS (10^{-18} m^2) and N_A is the number of Avogadro. However, in equation (5.1) and (5.2), the dependence of the specific surface area and the CMC on the electrolyte concentration is not taken into account. This will be discussed in paragraph 5.3.3.

5.1.3 Determination of particle size distribution

There are basically two types of particle sizing devices: those that physically separate particles based on their size, and those that infer the size without physical separation. In the case of monodisperse samples, both of these approaches should give the same answer. However, if the sample is not monodisperse then care must be taken when interpreting the output from non-separating instruments.

Transmission Electron Microscopy

Transmission electron microscopy (TEM) is the most direct and reliable method for the measurement of particle size distributions (PSD), but unfortunately also one of the most

laborious. Within the vacuum of the TEM microscope, an electron beam is generated, accelerated and focussed onto the specimen. Proportional to the electron density of the sample the electrons of the beam are absorbed, scattered or transmitted. The transmitted electrons are subsequently focussed and used to form a magnified image of the specimen of up to 100 to 500000 times[7] the original size. Samples prepared for TEM always have to be dried onto a metal grid, which disturbs the state of the emulsions studied. In TEM, it is essential to avoid distortion of the particles by the electron beam, which can readily occur for polymers with a relatively low glass transition temperature (T_g) such as poly(n-butyl acrylate) or even higher T_g polymers that require staining for contrast. Cryogenic transmission electron microscopy (Cryo-TEM) can be used to overcome these problems. Under cryogenic conditions a sample is petrified within amorphous ice by fast cooling in liquid ethane. Once the samples are petrified in liquid ethane they are stored in liquid nitrogen until the Cryo-TEM measurements. Special liquid nitrogen cooled sample holders are used to keep the polymer latex particles frozen in the amorphous ice during the TEM measurements, in this way Cryo-TEM allows investigation of aqueous dispersions in their natural state[8].

Capillary hydrodynamic fractionation

Two similar hydrodynamic separation methods were used for the determination of PSD of the macro-RAFT latexes. Both techniques rely on the same physical principle: particles of different sizes travel at different speeds through a capillary. This is caused by the velocity profile over the area of the capillary and the differences in the time the particles spent in the different areas (see Figure 5.2). Since smaller particles have a smaller exclusion layer near the wall of the capillary, where the velocity is the lowest, their elution times are the longest. After separation the concentration of the particles is determined by measuring the eluent's light absorption characteristics. One of the two techniques used here based on the above

principle is hydrodynamic chromatography (HDC); it uses a packed column with non porous

particles for the separation, whereby the type of packed column determines the range of

separation. The interstitial channels in the packed bed can be visualized as a series of small

capillaries and within each capillary, the same velocity gradient exists described by a

parabolic flow profile, see Figure 5.2. Capillary hydrodynamic fractionation (CHDF) is the

other technique, and employs a long narrow capillary, able to separate particles in the size

range of 20-1000 nm. Both techniques require calibration using a set of standards made up of

hard-sphere latex particles (e.g. polystyrene or PMMA), each standard having a well known
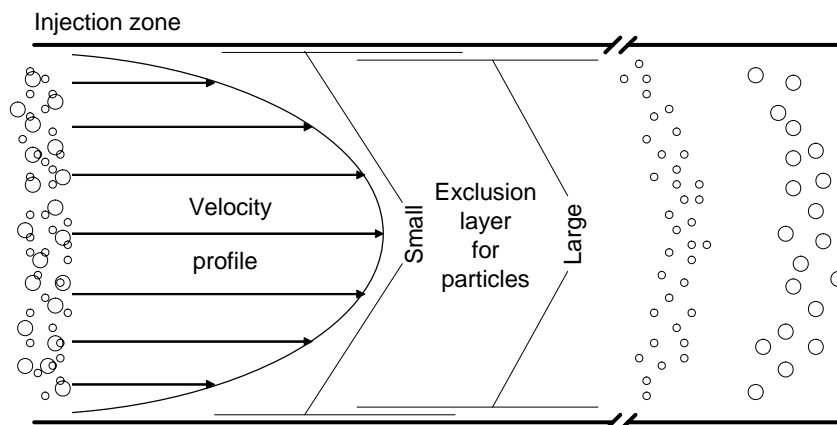
narrow particle size distribution.

Figure 5.2: Illustration of the velocity profile and the separation of large particles from small particles in a capillary tube (after Dos Ramos[9]).

Photon correlation spectroscopy

Photon correlation spectroscopy (PCS, also known as dynamic light scattering, DLS) is a

form of dynamic light scattering, where the motion of colloidal particles is investigated by

comparison of successive light scattering signal measurements. The degree of correlation

between the measurements and the speed of change is controlled by the diffusion coefficient

of the particles and hence by the average particle size. However, light scattering techniques

provide only a z-average particle size (which is more sensitive to larger particles). This value

is subsequently converted into a particle size distribution by the software of the equipment, by making various assumptions about the functional form of the PSD, which may or may not be valid.[10]

5.2 *Experimental*

5.2.1 Characterization of colloidal particles

A hydrodynamic chromatograph (HDC, Polymer Laboratories) equipped with a packed column was used for the analysis of latexes, equipped with a low particle size cartridge (type 1, separation range 5 to 300 nm). The HDC was calibrated by polystyrene standards in a range of 20 – 350 nm (Duke Scientific).

Average particle size and particle size distribution were also determined by DLS, performed mostly on a Malvern 4700 light scattering instrument equipped with a Malvern Multi-8 7032 correlator operating at a scattering angle of 90° at a temperature of 21 °C. Some samples were analysed by a Brooker N4 plus system, operating at a scattering angle of 90° and a temperature of 20 °C.

TEM samples were prepared by drying latexes ranging in solid content between 0.01% and 0.1% onto a carbon coated copper grid (200 mesh, Electron Microscopy Sciences). Poly(n-butyl acrylate) samples were stained with zinc uranyl acetate. TEM measurements were performed on a Philips CM 10, 12 and 120 Biofilter electron microscope, and a FEI Sphera and Titan electron microscope. Cryo-TEM samples were diluted and petrified using a Vitrobot[11]; Cryo-TEM measurements were performed on a Philips CM12 electron Microscope at Maastricht University.

5.2.2 Surface Tension measurements

All surface tension measurements of the latexes or dilutions thereof were performed using a SensaDyne® Model 6000 surface tensiometer. Measurements of the latexes were performed in a 50 or 100 mL glass beaker. The small samples taken during the reaction were measured inside a custom made low volume glass setup, see Figure 5.3. This setup enabled accurate surface tension measurements with sample sizes as small as 3 mL. Before the measurements the apparatus was calibrated with ethanol and water as standards at about 20 °C.
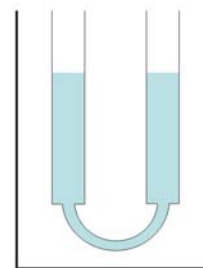

Figure 5.3: Schematic representation low volume glassware.

5.2.3 Maron titrations

All Maron titrations were performed with the SensaDyne Surface Tensiometer as described in section 5.2.2. The tensiometer was used in combination with a Watson Marlow low-volume peristaltic pump (type 101U), two Promax digital timers and a magnetic stirring plate. In the preparation of the measurements, 30 mL of the macro-RAFT latex or a dilution thereof was added to a 50 mL beaker. The measurements were started by determination of the starting surface tension by bubble tensiometer (note that calibration is not necessary, since the CMC is determined by trend analysis of the data). Surface tension values were continuously recorded every five seconds. A soap solution of sodium dodecyl sulfate (SDS, Merck) was pumped into the solution for a period of 1 minute, while the solution was stirred for 5 minutes. After the addition of the soap solution the surface tension was measured for 15 minutes without any further additions. This addition and measurement cycle was repeated for up to 24 times. The surface tension measurements were averaged over the addition-free time for every SDS concentration without taking into account the first and the last minute of this period.

5.3 *Results & Discussion*

5.3.1 Concentration of surface active species

The evolution of the surface tension during the reaction can provide information about the amount of surface-active species in the reaction mixture and the particle formation mechanism in general. Samples taken during the controlled feed styrene experiments were analysed by bubble tensiometry. The most hydrophobic macro-RAFT agent (i.e. 10AA+10STY) proved to be highly surface active at the start of the reaction, see Figure 5.4. This was not only demonstrated by the low surface tension readings but also by foam formation at the top of the solution. After about an hour reaction time, the surface tension had risen almost to that of pure water (i.e. $73.05 \cdot 10^{-3}$ N m^{-1} at 18 °C[12]). This could be explained by the aqueous-phase polymerization of the macro-RAFT agents. This aqueous phase polymerization leads to more hydrophobic macro-RAFT agents with lower critical micelle concentrations than the original 10AA+10STY macro-RAFT agent. For the hydrophilic macro-RAFT agent hardly any increase of the surface tension was observed. A slight increase in the surface tension was observed for both macro-RAFT agent systems after the initial particle formation. A possible explanation for the observed increase of the the surface tension is adsorption of aqueous phase macro-RAFT agents onto the initially nucleated particles and the disappearance of monomer droplets that were present before the initial particle formation.
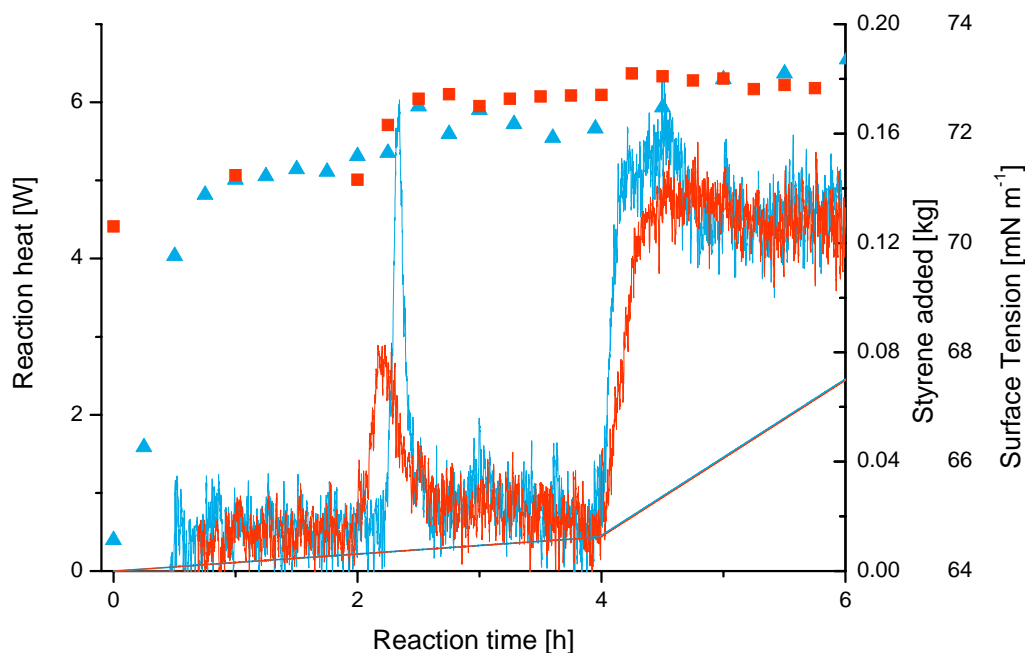
Figure 5.4: Surface tension during the *ab-initio* semi-batch emulsion polymerization of styrene as measured off-line by bubble tensiometry, both the reaction heat (thin lines) and surface tension (symbols) are shown for the hydrophilic (10AA, red, squares) and more hydrophobic macro-RAFT (10AA+10STY, blue, triangles) systems.

Mechanistically, the surface activity of most hydrophobic macro-RAFT agents seems to support the postulate in chapter 3, that these macro-RAFT agents are already present as micelles before the initial particle formation starts. On the other hand, the hydrophilic macro-RAFT agents first have to grow in the aqueous phase to become sufficiently surface active, before they can either participate in nucleation or adsorb onto existing growing particles. Since the composition of the macro-RAFT agents is a distribution (see Figure 4.2 and Figure 4.3) and growth is statistical, these species will only become gradually surface active enough to participate in nucleation or adsorption.

5.3.2 Particle sizes

Even before any particle sizing measurements were performed on the latex products it was obvious that the particle sizes of the latex products from the various macro-RAFT agents showed considerable differences. The larger particles were produced by the reactions

containing only hydrophilic macro-RAFT agents(e.g. 5AA or 10AA). These scattered the light much more than the smaller particles obtained by the more hydrophobic amphipathic macro-RAFT agents. The results are white latexes for the hydrophilic macro-RAFT agents and transparent yellow latexes with a blue tinge for the most hydrophobic macro-RAFT agents (see Figure 5.5 and Figure 5.6).

Figure 5.5: Optical properties n-butyl acrylate macro-RAFT latexes (5AA, left, 5AA+10BA right).

Figure 5.6: Optical properties styrene macro-RAFT latexes (10AA, left, 10AA+10STY right).

The difference between the particle sizes obtained with hydrophilic (5AA or 10AA) and hydrophobic (5AA+10BA or 10AA+10STY) macro-RAFT agents was quantified by several particle sizing techniques, see Figure 5.7. After comparing the results of the various particle sizing methods (see Table 1), the fastest particle separation method, hydrodynamic fractionation over a packed column, was chosen to analyse most latexes. Normally, when comparing particles with different techniques e.g. TEM and DLS, one should take into account the difference between the swollen and unswollen particle size of a latex. However, since after the initial particle formation the controlled-feed reactions in fact run at starved conditions, the fractional conversion is almost complete at any time in the reaction. This means that there is virtually no monomer left to swell the latex particles. In this case the swollen and unswollen particle size are the same.

Table 5.1: Particle sizing techniques compared.

Latex	TEM [nm]		HDC [nm]	DLS[nm]
	$<d_n>$	$<d_{vv}>$	$<d_{vv}>$	$<d_z>$
JLTUe006 (10AA+10STY)	27.4	29.8	24	42 ± 4

Here $\langle d_n \rangle$ is the number average diameter and $\langle d_{vv} \rangle$ is the volume weighted average diameter as defined in equation (5.3) and (5.4), d_z.is the intensity weighted average diameter as measured by PCS. The PCS data shown below represent the weighted contribution as derived from the intensity signal, the intensity weighted average is however much larger because of the presence of a small fraction of particles (>100 nm).
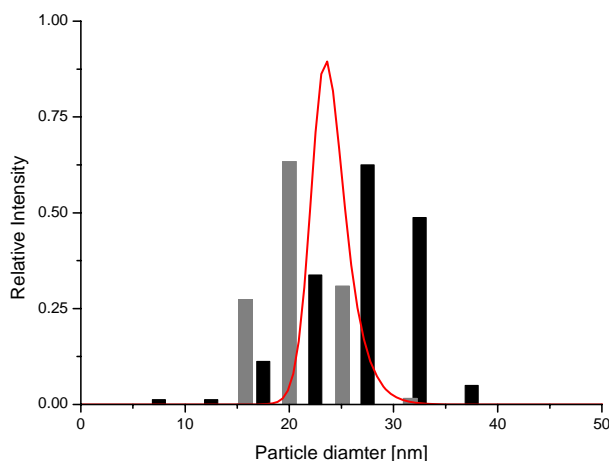

Figure 5.7: Overlay of particle size distributions as determined by TEM (black bars), DLS (gray bars) and HDC (line).

The visual observations are confirmed by the measurements of the particle size distribution, the more hydrophobic macro-RAFT agents produce much smaller particles, than the hydrophilic ones. An overview of the combined results is shown in a box chart in Figure 5.8; the borders of the box in the chart for the various macro-RAFT systems is defined by the 25th and 75th percentiles of the average weighted diameters of the various latexes as measured by TEM, HDC and DLS and the whiskers are determined by the 5th and 95th percentiles of these measurements.
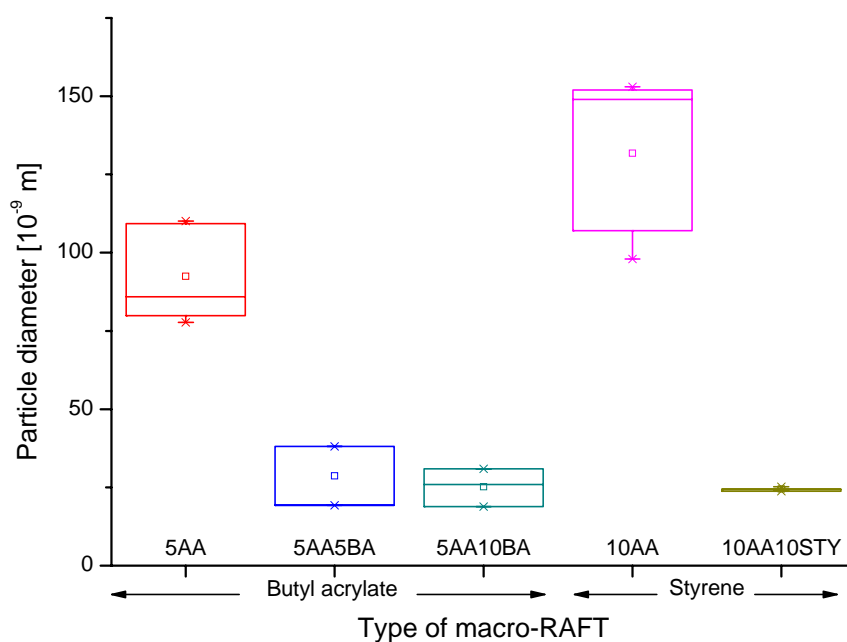
Figure 5.8: Average particle sizes for the macro-RAFT agents.

Figure 5.8 clearly demonstrates that the more hydrophobic the macro-RAFT agent is, the more particles are created during the reaction, resulting in smaller particles. The propagation rate coefficient of the monomer also seems to play a role for the hydrophilic macro-RAFT systems. The n-butyl acrylate system has on average more particles than the corresponding styrene system. This could be explained by the large polymerization rate difference during the initial aqueous phase polymerization. Because of the high propagation rate coefficient of n-butyl acrylate (33700 L mol^{-1} s^{-1} at 60 °C[13]) compared[14] to styrene (663 L mol^{-1} s^{-1} at 80 °C[15]), the aqueous phase macro-RAFT agents will become surface active quicker for the BA system than for the styrene polymerisation. As a consequence more macro-RAFT species will be available at the start of nucleation for the n-butyl acrylate system than for styrene, resulting in more particles. This supports the theory of the two competing processes involved during the particle formation, *i.e.* new particle formation by stinging of micelles or homogeneous nucleation and adsorption of surface active macro-RAFT agents by growing particles. When more surface active macro-RAFT agents are available at the start of the nucleation stage, more particles can be created. Slow aqueous phase polymerization of

styrene will results in fewer but bigger particles. However, the more hydrophobic macro-RAFT systems for both the n-butyl acrylate and the styrene systems show similar sizes for the final particles. The difference in propagation rate coefficient does not seem to play any role in this case, which suggests that the final particle number is predominantly determined by the initial amount of micelles present.

To obtain insight into the particle formation process, the evolution of the PSD has to be monitored during the reaction. Initially the particles will be very small, especially for the hydrophobic macro-RAFT agents. Therefore relying on a method that is calibrated for particles with a diameter larger than 20 nm is not preferred. This is why transmission electron microscopy was chosen for determining the particle size during the reaction. Preliminary results using conventional TEM (see Figure 5.9) showed fairly large aggregates of particles. However, cryo-TEM images (see Figure 5.10) confirmed that the observed aggregates are simply the result of the drying of the latex onto the TEM grid during sample preparation. In order to obtain accurate particle size distributions from TEM images, the aggregates have to be split up into individual particles which are then measured. This proved to be difficult using commercial software. However, the Java based open source image processing program ImageJ[16] was able to perform this task. A detailed description of the TEM image analysis and particle counting process and how it can be automated is provided in appendix III.
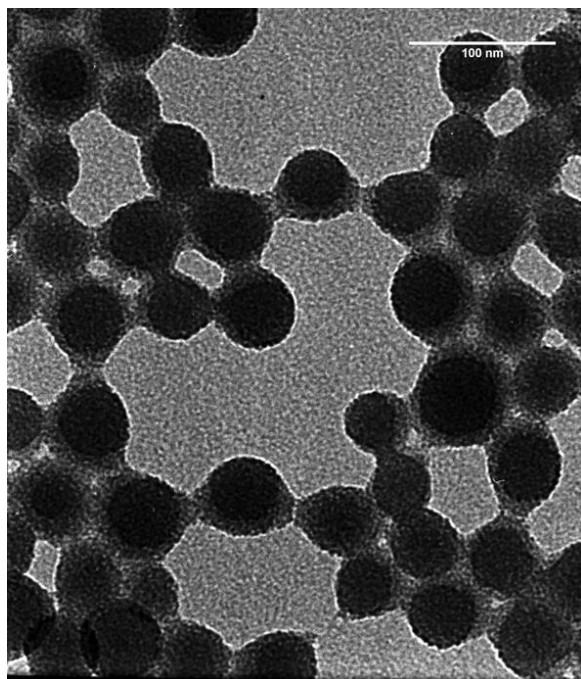
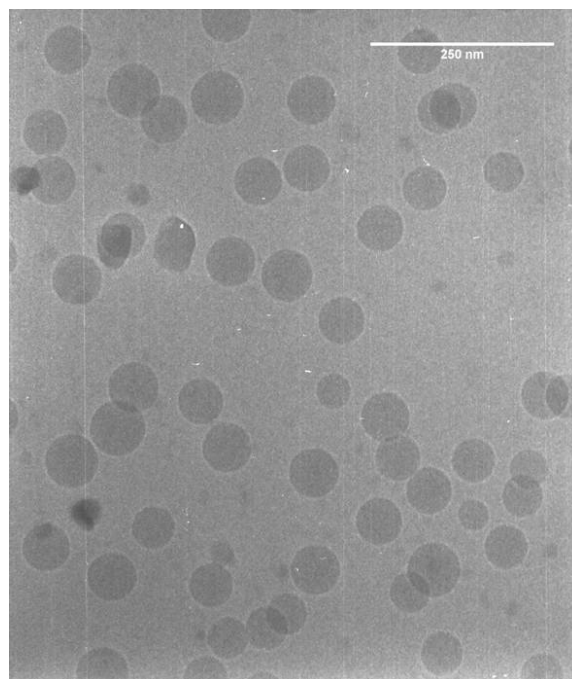**Figure 5.9: TEM of electrosteric stabilized polystyrene particles, (10AA, JLTUe026U).**

Figure 5.10: Cryo-TEM of electrosteric stabilized polystyrene particles, (10AA, JLTUe026U).

All TEM images of the hydrophilic macro-RAFT agent in the controlled-feed styrene experiments were analysed by the ImageJ based method. Figure 5.11 shows a typical example the evolution of the particle sizes of the semi-batch emulsion polymerization of styrene in the presence of the hydrophilic macro-RAFT agents. To obtain reliable results TEM images with enough contrast are required. Some samples of this experiment and most samples of the hydrophobic macro-RAFT did not meet this criterion, and were analysed manually using the same tools in ImageJ.

The particle size distributions of the hydrophilic macro-RAFT based latexes show a steadily increasing average particle size. The number average $<d_n>$ and volume weighted average $<d_{vv}>$ diameter[17] were calculated from the TEM measured perimeters, assuming spherical particles using equation (5.3) and (5.4).

$$< d_n > = \frac{\sum n_i d_i}{\sum n_i} \qquad (5.3)$$

$$< d_{vv} > = \frac{\sum n_i d_i^4}{\sum n_i d_i^3} \qquad (5.4)$$

When the volume weighted average particle sizes are converted into particle numbers, it is shown that very quickly after the initial particle formation the final number of particles is reached, suggesting a fairly short particle nucleation time.
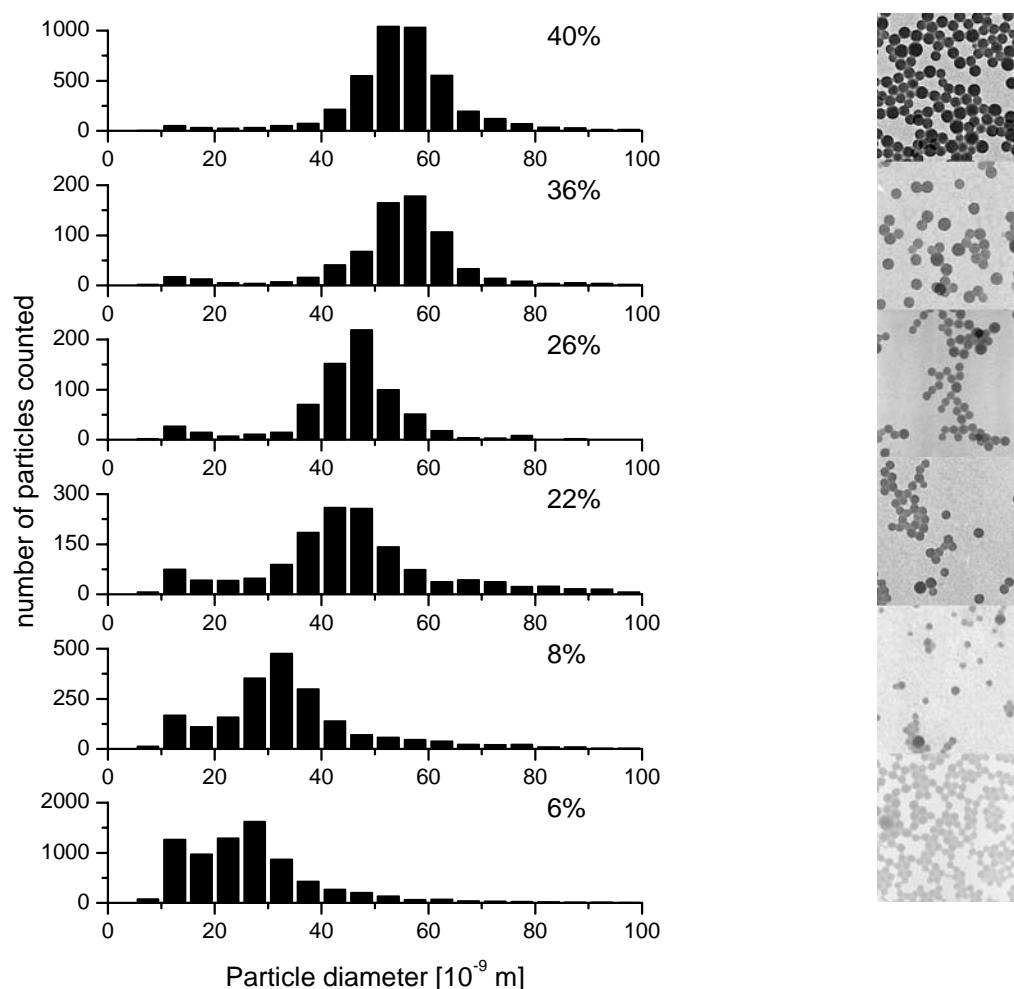

Figure 5.11: Particle size distributions for hydrophilic macro-RAFT (10AA) system as a function of the fraction of the total amount of styrene fed. The cut-outs on the right hand side are the corresponding TEM pictures at a size of 773 x 773 nm per square.

The average particle diameter (both number and weight average) are collected in Table 2. The average particle size of the hydrophobic macro-RAFT systems also increases gradually during the reaction; see Table 2 and Figure 5.12.

Table 5.2: Average diameters for the styrene macro-RAFT based latexes as a function of the total amount of monomer fed [%].

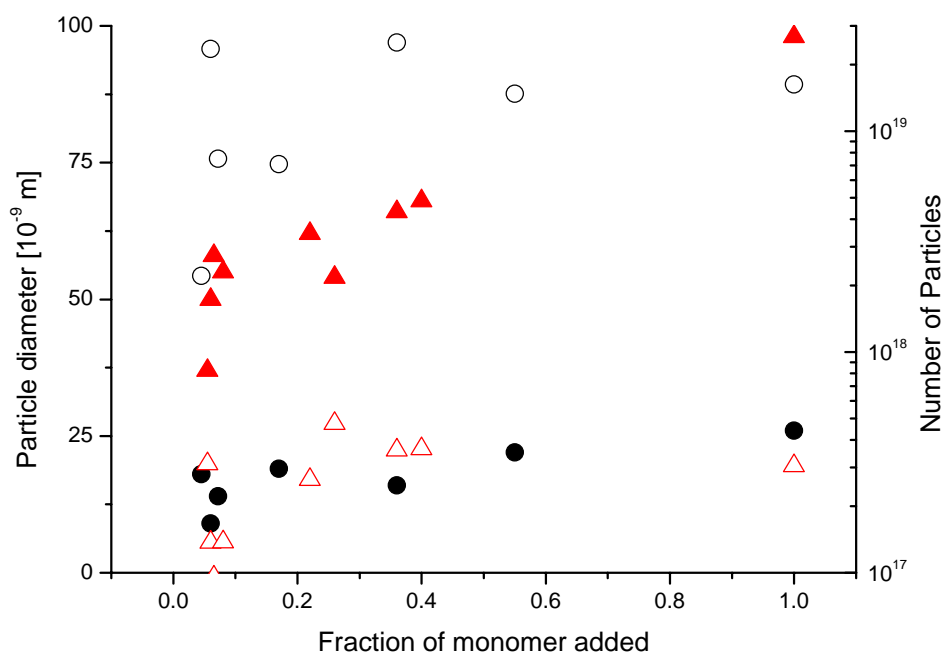| Monomer fed 10AA macro-RAFT	$<d_n>$ [nm]	$<d_{vv}>$ [nm]	Monomer fed 10AA+10STY macro-RAFT	$<d_n>$ [nm]	$<d_{vv}>$ [nm]
5.5	23	37	4.5	11	18
6.0	27	50	6.0	8.7	9
6.5	36	58	7.2	11	14
8.0	35	55	17	15	19
22	46	62	36	15	16
26	45	54	55	20	22
36	54	66	100	22	26
40	55	68			
100	89	98			

Figure 5.12: Trends in the volume weighted average particle diameter and number for both macro-RAFT systems, circles for the hydrophobic macro-RAFT, N_p (open) and $<d_{vv}>$ (solid) and triangles for the hydrophilic one, N_p (open) and $<d_{vv}>$ (boxed).
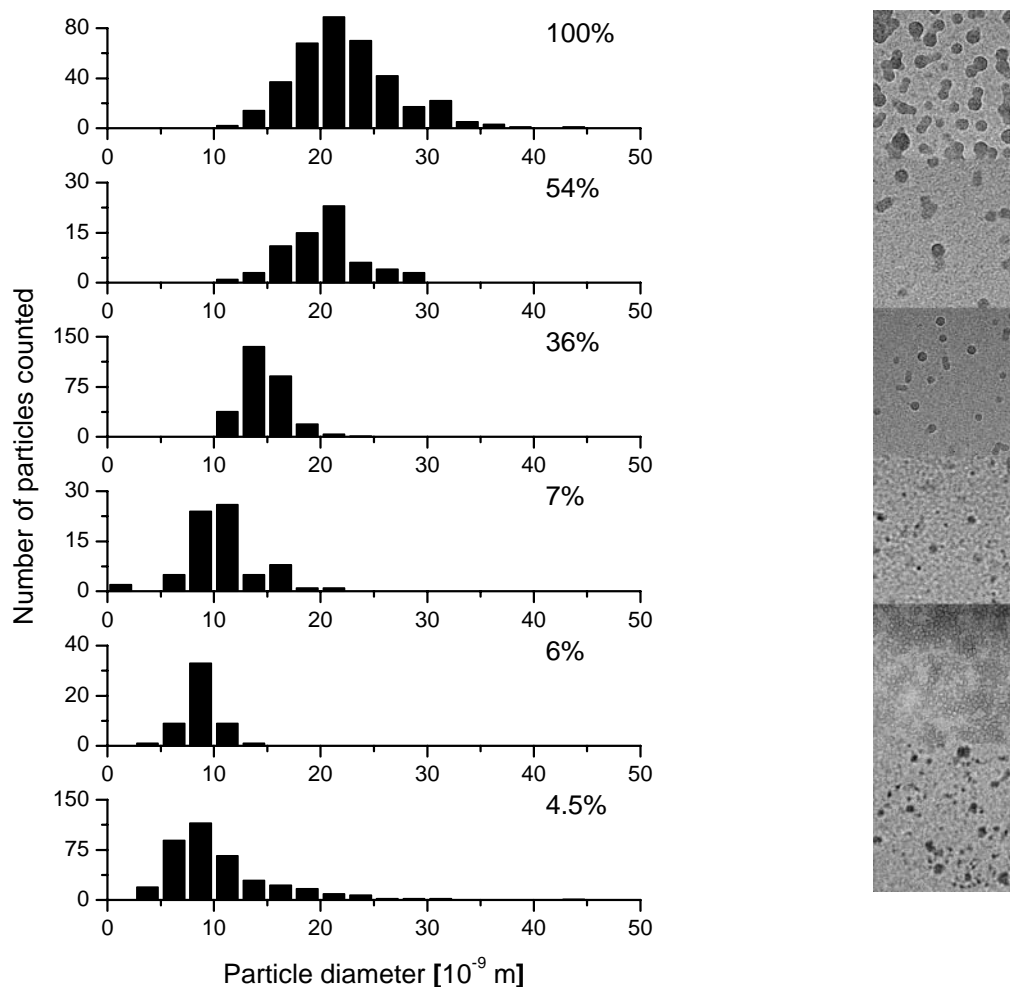
Figure 5.13: Particle size distributions for hydrophobic macro-RAFT (10AA+10STY) system as a function of the fraction of the total amount of styrene fed. The cut-outs on the right hand side are the corresponding TEM pictures, shown at a size of 288 x 288 nm per square.

However, during the reactions with the hydrophobic macro-RAFT agents many more particles were nucleated initially. These initially nucleated particles grew steadily during the reaction. Mechanistically these similar trends in particle growth but big differences in particle numbers can be explained by the lack of micelles present for the hydrophilic macro-RAFT (10AA) system. Because of this, the particles that were initially formed, grew and adsorbed the remaining aqueous phase macro-RAFT agents as they became surface active enough, preventing more nucleation.

5.3.3 Surface area per macro-RAFT agent

Now that the particle sizes of the polystyrene latexes are known, the area that one macro-RAFT molecule occupies on the surface of the latex particle can be obtained from Maron titrations. The surface of the particles covered with macro-RAFT agents can be calculated by subtraction of the free area determined by soap titration from the average area per particle as determined by the TEM analysis, neglecting surface excess effects, see equation (5.5). In order to obtain reliable results, one has to take into account the shielding effect of electrolytes in solution, particularly since all macro-RAFT based latex particles are negatively charged (acrylic acid groups neutralized with NaOH). The influence of the electrolyte concentration was measured by bubble tensiometry for the concentration range of the latexes. The CMC values decreased with electrolyte concentration in agreement with literature data[18], see Figure 5.14. For all calculations of the aqueous-phase surfactant concentration at the CMC, the influence of the electrolyte concentration was taken into account. The electrolyte effect was quantified by fitting the literature data to a first order exponential decay. With increasing electrolyte concentration the surface area per SDS molecule decreases. This effect was also taken into account by fitting literature data to a linear exponential decay, see Figure 5.15.
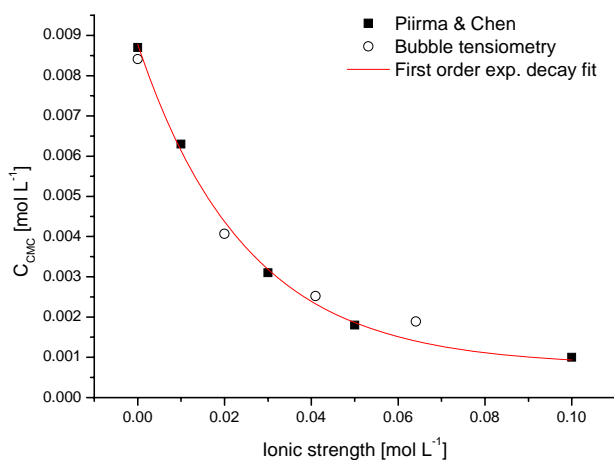

Figure 5.14: Influence of ionic strength on the CMC of SDS, literature values compared with bubble tensiometry.
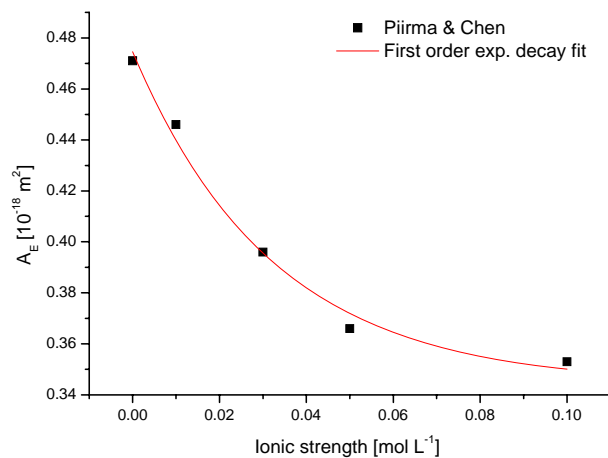
Figure 5.15: Influence of ionic strength on the surface area covered by one surfactant molecule (SDS).

The critical micelle concentration for SDS in the presence of the macro-RAFT latexes has been determined from the intersection of the straight lines of the concentration-dependent and –independent sections. This procedure was performed for three different concentrations of each latex, resulting in CMC plots such as given in Figure 5.16, that can be represented in a Maron plot, see Figure 5.17.
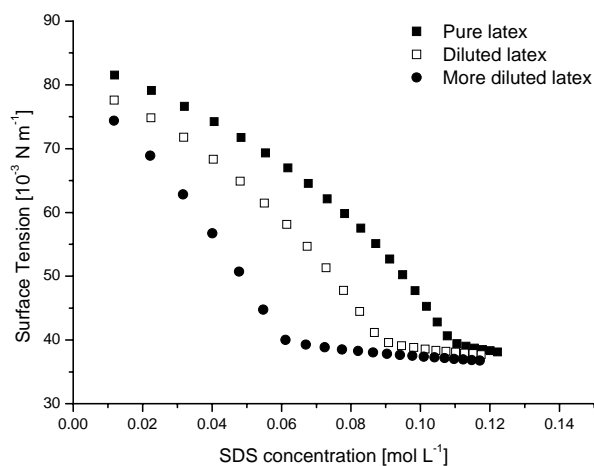

Figure 5.16: Surface saturation determined by Maron titration of a macro-RAFT latex (10AA+10STY) and dilutions thereof.
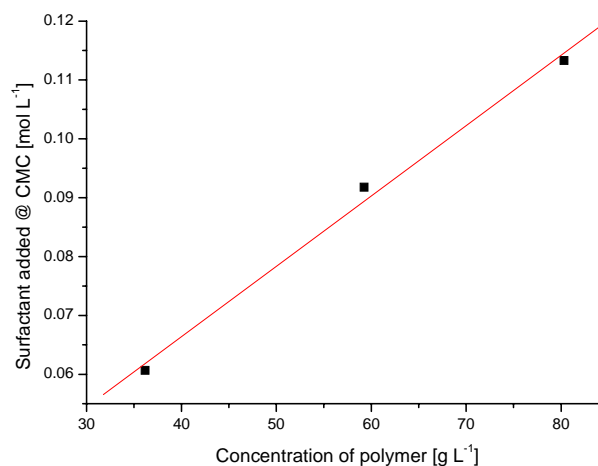
Figure 5.17: Maron plot of a macro-RAFT latex (10AA+10STY) and dilutions thereof.

The molecular area of the macro-RAFT agents ($A_{E\ Macro-RAFT}$) was calculated using equation (5.5):

$$A_{E\ macro-RAFT} = \frac{N_p \pi r^2 - A_S}{n_{macro-RAFT}}$$

(5.5)

Here N_p and r are respectively the number of particles and the particle radius as determined by an external technique (e.g. TEM or HDC). A_S is the area occupied by SDS on the particle surface as determined by the Maron titration. The value obtained for the molecular area of the macro-RAFT agent is the lowest boundary value, since for the calculation all hydrophilic groups of the macro-RAFT agents are assumed to be on the surface of the particles, whereas it is also possible for macro-RAFT agents to become "buried in" inside the particles, in particular for the macro-RAFT agents with the shortest hydrophilic block of poly(acrylic

acid). Previous studies revealed a strong dependence of the surface area of SDS on the particle size diameter[18-20]. This is probably due to the curvature of the particle surface, facilitating tight packing of the surfactants. Unfortunately a value for surface area of SDS for particles as small as those obtained from the hydrophobic macro-RAFT agents is not known. The values collected in Table 3 were obtained from the earlier mentioned electrolyte dependent surface area of SDS reported by Piirma and Chen[18].

Table 5.3: Maron titration results for styrene based latexes synthesized with 10AA+10STY macro-RAFT agents.

Latex name [JLTUe#]	CMC [10^{-2} mol L^{-1}]	[NaOH] @CMC [10^{-2} mol L^{-1}]	[Polymer] @CMC [10^1 g L^{-1}]	Occupied Area by SDS [10^1 m^2 g^{-1}]	$<d_{vv}>$ [nm]*	Min. area / macro-RAFT [nm^2]	Est. area / macro-RAFT [nm^2]
006	11.34	3.07	7.38	35.5	24.0 [b]	-5.97	1.2
006	8.99	2.48	5.98	35.2	24.0 [b]	-5.76	1.6
006	5.76	1.52	3.67	36.7	24.0 [b]	-6.48	1.7
008	10.90	3.13	7.64	32.9	24.5 [b]	-4.89	1.4
008	8.94	2.51	6.13	34.1	24.5 [b]	-5.49	1.7
008	6.21	1.64	4.01	36.4	24.5 [b]	-6.69	1.5
027	11.33	3.04	8.03	32.7	25.7 [a]	-5.62	2.2
027	9.18	2.42	5.92	36.4	25.7 [a]	-7.64	1.4
027	6.07	1.48	3.61	39.5	25.7 [a]	-9.36	1.0

*As determined by: [a] TEM, [b] HDC

It is clear that the negative apparent surface areas (Min. area) for the smaller particles have no physical meaning, but the data show that the area occupied per SDS molecule is much smaller for smaller particles. When a value of 0.24 nm^2 is used for the specific surface area of SDS, as obtained by extrapolation of the particle size dependent surface area by Piirma et al.[18], more realistic surface areas in the range of 1 to 2 nm^2 for the macro-RAFT agents are obtained (Est. area). However, a systematic study is needed to validate the specific surface area used for SDS.

5.4 *Conclusions*

It has been demonstrated by bubble tensiometry that the more hydrophobic macro-RAFT agents are already surface active at the start of the reaction. The hydrophilic macro-RAFT agents show no significant sign of surface activity during the reaction.

Particle size measurements show a clear trend for the controlled feed experiments in the presence of macro-RAFT agents: the more hydrophobic (or surface active) the initial macro-RAFT agent is, the more particles are nucleated. Comparing the two monomer systems i.e. styrene and n-butyl acrylate, it has been shown that the use of monomers with higher propagation rate coefficients leads to more particles for the hydrophilic macro-RAFT systems. This is probably due to the faster aqueous phase polymerization of the hydrophilic macro-RAFT agents, resulting in more surface active macro-RAFT agents at the start of nucleation. However, this effect does not play a role for the more hydrophobic macro-RAFT systems, indicating a different dominant particle formation mechanism.

The majority of all particles were already formed within the first half hour after the start of the initial particle formation, which was after about 5 % of the total monomer was added during the controlled fed styrene experiments.

Mechanistically the above conclusions seem to confirm the postulated particle formation mechanism; the aqueous phase macro-RAFT depletion can be due to either new particle formation or adsorption onto growing particles. The presence of micelles stimulates the rapid formation of many particles. In the absence of these the rate of polymerisation within the existing particles determines the eventual number of particles.

Furthermore, the surface area occupied by one molecule of the macro-RAFT agents with on average 10 acrylic acid units has been determined for small particles to be 1-2 nm^2, based on

an extrapolated specific surface area for SDS at the surface of the small particles obtained

($\approx$ 25 nm in diameter). The results of this work point to a much lower value for the specific

surface area of SDS molecules at smaller particles, which is due to the curvature of the

particles.

5.5 *References*

1. Maron, S. H.; Elder, M. E.; Ulevitch, I. N. *Journal of Colloid Science* **1954,** 9, 89-103.
2. Abbey, K. J.; Erickson, J. R.; Seidewand, R. J. *Journal of Colloid and Interface Science* **1978,** 66, 203-204.
3. Hunter, R. J., *Introduction to Modern Colloid Science*. 1993;
4. Atkins, P.; de Paula, J., *Atkins' Physical Chemistry, 7th Edition*. 2002;
5. Klus, J. P.; Gibbons, E. E.; Brodsky, E. L.; Janule, V. P. Surface tensiometer. 81-232091 4416148, 19810206., 1983.
6. Schrödinger, E. *Annalen der Physik* **1915,** 351, 413-418.
7. Silverman, L.; Billings, C. E.; First, M. W., *Particle Size Analysis in Industrial Hygiene*. 1971;
8. Talmon, Y. *Berichte der Bunsen-Gesellschaft* **1996,** 100, 364-72.
9. DosRamos, J. G.; Silebi, C. A. *Journal of Colloid and Interface Science* **1990,** 135, 165-177.
10. Weiner, B. B. *Special Publication - Royal Society of Chemistry* **1992,** 102, 173-85.
11. Butter, K.; Bomans, P. H. H.; Frederik, P. M.; Vroege, G. J.; Philipse, A. P. *Nature Materials* **2003,** 2, 88-91.
12. Weast, R. C.; Editor, *CRC Handbook of Chemistry and Physics. 64th Ed*. 1984;
13. Buback, M.; Kurz, C. H.; Schmaltz, C. *Macromolecular Chemistry and Physics* **1998,** 199, 1721-1727.
14. Van Herk, A. M. *Macromolecular Theory and Simulations* **2000,** 9, 433-441.
15. Buback, M.; Gilbert, R. G.; Hutchinson, R. A.; Klumperman, B.; Kuchta, F.-D.; Manders, B. G.; O'Driscoll, K. F.; Russell, G. T.; Schweer, J. *Macromolecular Chemistry and Physics* **1995,** 196, 3267-80.
16. Rasband, W. S. *National Institutes of Health, Bethesda, Maryland, USA http://rsb.info.nih.gov/ij/* **1997-2006**.
17. Jung, C. W.; Jacobs, P. *Magnetic resonance imaging* **1995,** 13, 661-74.
18. Piirma, I.; Chen, S. R. *Journal of Colloid and Interface Science* **1980,** 74, 90-102.
19. van Zyl, A. J. P.; de Wet-Roos, D.; Sanderson, R. D.; Klumperman, B. *European Polymer Journal* **2004,** 40, 2717-2725.
20. Landfester, K. *Macromolecular Symposia* **2000,** 150, 171-178.

Chapter 6

Nucleation mechanism revisited

Abstract: *In this chapter the experimental results obtained for the specific surface area and the time-evolution of the particle size distribution were implemented in an expression for particle numbers in these amphipathic macro-RAFT systems. This expression[1] is based on the model for nucleation of amphipathic macro-RAFT agents as derived in chapter 3. It is demonstrated that the specific surface area of the macro-RAFT species has a very large influence on the results of the model calculations. Furthermore it is demonstrated by the experimentally derived number of RAFT agents per particle that the time constant for transport of block copolymeric surface active macro-RAFT agents through the aqueous phase is large as compared with the time constant of nucleation for common initiator concentrations. As a result it is possible to use these macro-RAFT agents to obtain a latex with both a narrow molecular weight distribution and a predefined narrow particle size distribution. The overall mechanistic consequences of this research are discussed and suggestions are provided for possible future work.*

6.1 *Introduction*

In this chapter the data obtained for the amphipathic RAFT system from the study of the time-evolution of the molecular weight distribution and the particle size distribution and other physical properties of the latexes are used to test the assumptions in the model for particle number. The experimental data is compared with other work employing the amphipathic RAFT agents in emulsion[2-4] and these are subsequently compared with the modelling results.

6.1.1 Mechanistic results

It was demonstrated in section 3.3.2 that the derived relation between nucleation time and particle number[1] could predict the number of particles well in a RAFT mediated styrene emulsion polymerization with amphipathic preformed di-blocks using reasonable physico-chemical parameters[4] (A_E=0.4 nm^2, $\bar{n}$ =1 and monomer concentration given by the saturated values for large particles). However, with the knowledge gained by monitoring the time evolution of molecular weight distribution and particle size distribution a more detailed mechanistic comparison between model calculations and experimental results can be obtained. It was postulated in chapter 3 that until particle nucleation ceases, the number of z-meric species[5] entering macro-RAFT aggregates equals the number of particles at time t; see equation (6.1).

$$N_p = 2k_d[I]\left\{ \frac{\sqrt{2k_d[I]k_{t,w}}}{k_{p,w}[M]_w} + 1 \right\}^{1-z} t\, N_A$$

(6.1)

The values of t in equation (6.1) at which nucleation ceases were derived by using the assumption that the nucleation time is determined by the time it takes for all macro-RAFT agents to be taken up by the growing particles. In this situation, all macro-RAFT molecules

are assumed to have attained a critical degree of polymerization at which migration between particles/micelles no longer occurs; for the complete derivation see section 3.3.1.

$$t = \frac{\overline{X}_{crit}^{\,3} - \overline{X}_{n}^{\,3}\big|_{t=0}}{B};$$

$$B = \frac{k_p [M]_p \overline{n} A_E^{\,3}}{12\pi} \left(\frac{M_0}{\rho_P N_A} \frac{\rho_M}{\rho_M - [M]_p M_0} \right)^{-2}$$

(6.2)

For the case where one starts with water soluble amphipathic macro-RAFT molecules that are no longer mobile through the aqueous phase on the timescale of nucleation, $X_n \geq X_{crit}$, the number of particles is defined by the initial number of aggregates, since no transfer of macro-RAFT molecules is possible through the aqueous phase.

6.2 *Comparison of modelling and experimental results*

Before comparing the modelling results with literature data and experimental results, the boundaries set by nucleation times derived from experimental observations and particle numbers are explored to establish an operating window for the modelling data reported in section 6.2.1.

To provide a structured discussion on the model and the obtained experimental results, the first aspect to consider was the aggregation behaviour of the amphipathic macro-RAFT agents as these are the precursors for the particles. Literature data for this aggregation number has been obtained from SANS experiments on a similar amphipathic macro-RAFT system[3]. Based on these SANS results an average specific surface area was calculated, which in turn could be compared with the experimental data obtained from the Maron titrations of chapter 5. This comparison provides one of the parameters for the nucleation model as described in section 6.2.2.

Once aggregates are present, phase equilibrium will be established between the aqueous-phase monomer, monomer in the droplets (if present) and monomer inside the hydrophobic cores of the aggregates. The thermodynamic forces governing the distribution of the monomer among the different phases are described by the Morton equation[6]. This equation can be used to estimate the monomer concentration in the initial aggregates of macro-RAFT agents that are the precursors for the latex particles in section 6.2.3 although it is emphasized that the Morton equation is only semi-quantitative.

The aggregates swollen with monomer will become particles upon entry of a z-meric radical as was put forward by Maxwell and Morrison[5]. However, Thickett et al.[7-10] have demonstrated that for these electrosterically stabilized systems radical transport into and out of the particle is affected by the presence of the poly(acrylic acid) at the particle surface. The influence of this effect on the average radical concentration per particle is discussed in section 6.2.4.

Now that the parameters for the model governing the nucleation stage have been defined, the particle numbers in the resulting latexes can be compared with the model predicted values and the assumptions on the basis of the nucleation model can be tested. The influence of the various parameters is evaluated by a sensitivity analysis. Based on the results of the sensitivity analysis and a comparison of the expected and obtained number of RAFT molecules per particle, recommendations are put forward for possible future work. In addition possibilities for improvement of the model describing nucleation in these amphipathic RAFT systems are formulated.

6.2.1 Defining the operating window

It was demonstrated by TEM measurements that the majority of particles was formed within half an hour after nucleation had commenced, as shown by the time evolution of the PSD in Figure 5.12. In Figure 6.1 this half hour time limit is visualized for the nucleation time. In the same graph the experimentally obtained particle numbers from the TEM measurements of the styrene latexes based on the amphipathic macro-RAFT system (10AA+10STY) are presented as experimental boundaries. Also presented is the theoretically produced number of z-mers (Maxwell Morrison) with time. All data necessary for the calculation of the number of z-meric species with time in a styrene based system are readily available in literature, see table 3.1. However, it should be mentioned that the value for z was chosen on the value for the initiator fragment of a persulfate radical, although that for azo-biscyanovaleric acid based radical used in the slightly basic reaction mixture may be different[11].
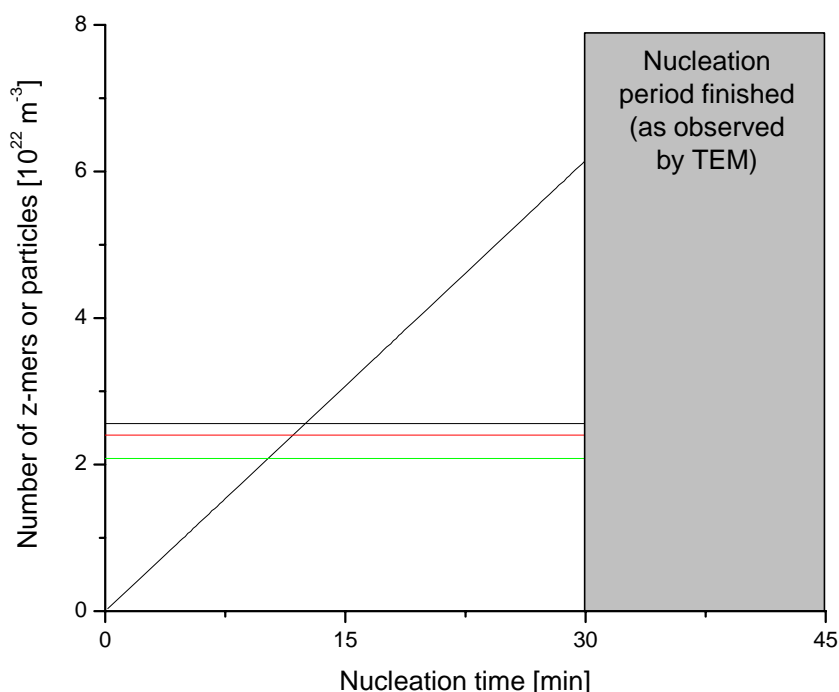

Figure 6.1: Experimental limits and values for particle numbers compared with z-mers produced in the reaction. The horizontal lines represent experimentally observed particle numbers: highest JLTUe006, JLTUe008 in between and JLTUe027 the lowest number of particles for styrene based amphipathic RAFT (10AA+10STY) experiments. The amount of theoretically produced z-mers (Maxwell-Morrison) with z=2 during nucleation is shown by the proportional relation with nucleation time (all other parameters are as in Table 3.1).

Testing the limits for nucleation time is not as straightforward, since the predicted nucleation time depends on many variables that are not accurately known for this particular system, and the experimental data only yield an upper bound. In the following sections, several of these parameters are discussed in more detail.

6.2.2 Surface covered by the macro-RAFT agents

In chapter 5 the "headgroup" area of the amphipathic macro-RAFT agents was determined by Maron titration[12, 13] using a bubble tensiometer. For the small particles, synthesized with the amphipathic macro-RAFT agents (10AA+10STY), no accurate value for this area could be obtained since no accurate value for the SDS surface area is known for these small particles ($d_p \approx 25$ nm). Previous studies revealed a strong dependence of the surface area of SDS on particle diameter[14-16]. This is probably due to the curvature of the particle surface facilitating tight packing of the surfactants. An estimate for the SDS surface area was obtained by extrapolating the data of Piirma and Chen[15]. When a surface area of 0.24 nm^2 per molecule was used for SDS, a specific surface area of 1-2 nm^2 was obtained per macro-RAFT molecule on the surface of these small particles.

Recently amphipathic macro-RAFT (8AA+8STY) micelles, present at the start of the reaction, have been studied by Ganeva et al.[3] using Small Angle Neutron Scattering (SANS). The styrene block was synthesized with deuterated styrene, which provided good contrast between the core and the shell of the micelles. In this study it was shown that the obtained scattering data of the micelles could best be fitted with a smeared core-shell and structure model supplied by NIST[17]. The best fit to the data corresponded to spherical micelles with a core radius of 3.4 nm and a shell thickness of 2.7 nm. A more detailed discussion on the accuracy of SANS data can be found in literature.[18, 19] The shell thickness inferred from the SANS data by these authors corresponds to a fully extended conformation of the hydrophilic

poly(acrylic acid) block (8AA). The aggregation number was calculated by assuming that the micelles can be represented by solid spheres with a core radius of 3.4 nm and a specific density of deuterated polystyrene (1.12 g ml^{-1})[20]. An aggregation number of around $1.2 \cdot 10^2$ (or $1.0 \cdot 10^2$ if the RAFT group is included in the calculation with the same density as deuterated polystyrene) macro-RAFT molecules was calculated for the micelles, corresponding to 1.2 nm^2 (or 1.4 nm^2 including the RAFT group) of the micellar surface stabilized per macro-RAFT agent. This aggregation number is in line with typical values for these kind of amphipathic polymeric species[21]. The specific surface area of the macro-RAFT agent corresponds very well with the range obtained by the Maron titrations, interpreted using an estimated surface area of 0.24 nm^2 per SDS molecule. By reprocessing the data of the Maron titrations using the SANS specific surface area for the amphipathic macro-RAFT agent, a value for the specific surface area of SDS can now be obtained for these small particles, as given in Table 6.1.

Table 6.1: Reprocessed Maron titration values for specific surface area of SDS based on SANS surface area of the macro-RAFT agent (1.4 nm^2).

Latex	$<d_{vv}>$ [nm]	[NaOH] [mol L^{-1}]	A_E of SDS [nm^2]
JLTUe006	24	0.031	0.24
JLTUe006	24	0.025	0.25
JLTUe006	24	0.015	0.25
JLTUe008	25	0.031	0.24
JLTUe008	25	0.025	0.25
JLTUe008	25	0.016	0.24
JLTUe027	26	0.030	0.24
JLTUe027	26	0.024	0.22
JLTUe027	26	0.015	0.22

The calculated surface areas per SDS molecule are all in the same range; however, the low electrolyte values for the largest particles (JLTUe027) deviate from the rest, as the surface area is very sensitive to the size of the particle. Therefore the two lowest sodium hydroxide concentrations for the other two latexes were used to calculate an average surface area per SDS molecule for particles of around 24 nm in diameter. This data point has been added to extend the trend observed by Piirma and Chen[15], as shown in Figure 6.2. It is shown that the

trend, of the decreasing surface area per SDS molecule on the surface of smaller particles, described in literature[14-16] extends to the range of the particles studied in this research.
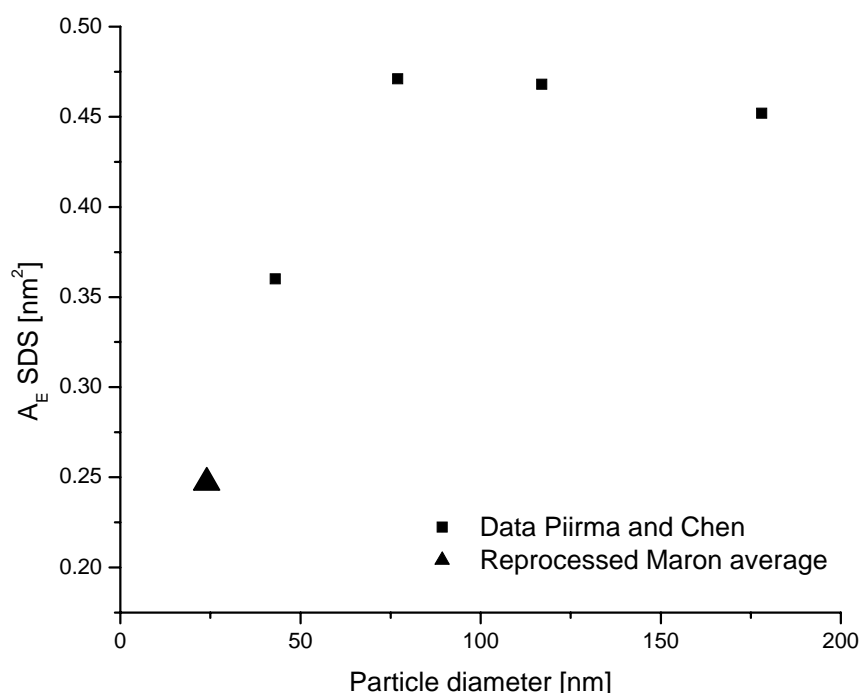

Figure 6.2: SDS surface area as a function of particle diameter based on Maron titrations.

6.2.3 Monomer concentration in the latex particles

In the calorimetric measurements of the amphipathic RAFT experiments (10AA+10STY), the heat flow for the initial peak indicating the onset of nucleation always corresponded to more monomer than can be dissolved in the aqueous phase, see e.g. figure E in Appendix I. In the presence of micellar aggregates of amphipathic macro-RAFT agents, the monomer will be taken up by the hydrophobic cores of the micelles. In the initial calculation the saturation concentration for larger particles (> 30 nm) was used as a parameter in the model. However, in case of an excess of monomer, the monomer concentration in the latex particles is controlled by thermodynamic considerations that are particle size dependent. The system will strive to minimize its Gibbs free energy, resulting in equilibrium between two opposing forces.[22] On one side there is the lowering of the surface free energy, which acts to keep the particles as small as possible. On the other side the reduction of the free energy of mixing

between the monomer and polymer, which causes the particles to swell to a size as large as possible and so pushes $[M]_p$ towards ρ_M/M_0. This saturation concentration of swelling of a latex particle in a monomer-rich system is described by the Morton equation[6].

$$\ln\left(1-\phi_p\right)+\phi_p+\chi\phi_p^{~2}+\frac{2\Gamma V_{sM}}{r_u RT}\phi_p^{~\frac{1}{3}}=0 \qquad (6.3)$$

Here Γ is the interfacial tension at the latex particle water surface, φ_p is the volume fraction of polymer in the polymer solution constituting the latex particles, V_{sM} is the partial molar volume of monomer (to a reasonable approximation, $V_{sM}=M_0/\rho_M$), χ is the Flory-Huggins interaction parameter and r_u is the average radius of the unswollen particles. Given values of Γ, χ and r_u, equation (6.3) can be solved iteratively to yield φ_p. From this, the corresponding value of $[M]_p$, see equation (6.4), can be calculated by mass balance; a complete derivation can be found in literature.[22]

$$\left[M\right]_p=\left(1-\phi_p\right)\frac{\rho_M}{M_0} \qquad (6.4)$$

Based on experimentally observed values of $[M]_p$ for larger styrene particles[23] and physically reasonable values for Γ and χ the size dependence of the monomer concentration in the particles has been deduced for a styrene emulsion system electrostatically stabilized by SDS at 50 °C. From the Morton equation a strong dependence of the $[M]_p$ on the unswollen particle radius is predicted; see Figure 6.3.
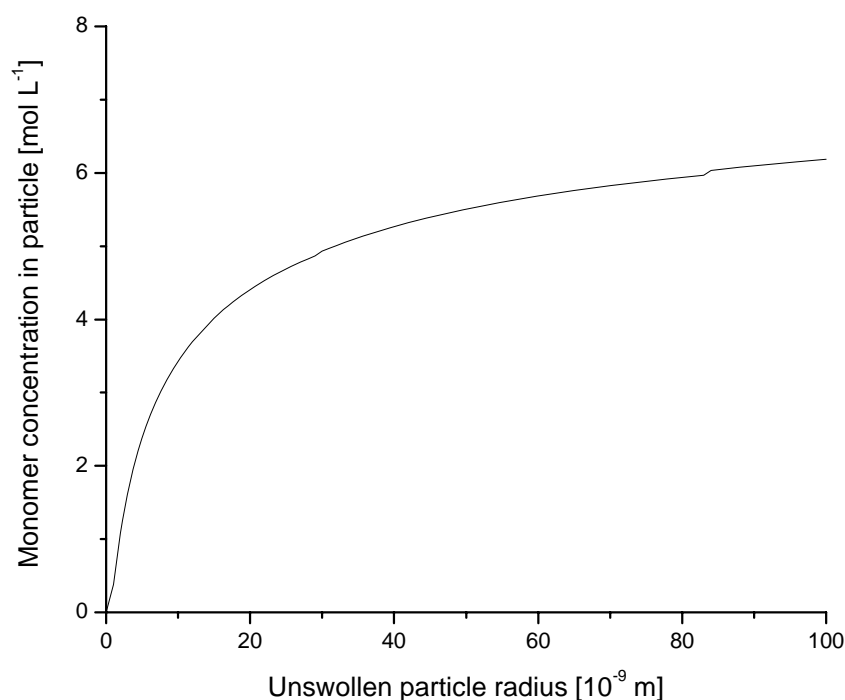
Figure 6.3: Saturation value of $[M]_p$ as a function of unswollen particle size as predicted using the Morton equation (eq. (6.3)), with $V_{sM} = M_0/ \rho_M$, $\Gamma = 20$ mN s^{-1}, $\chi = 0.45$, $\rho_M = 0.878$ g cm^{-3} and $r_u = 47$ nm; these are literature values for styrene/polystyrene system at 50 °C[23].

Since to the best of the authors knowledge it seems experimentally impossible to obtain a value for Γ at the water latex particle interface and it has been found that χ cannot be reliably assigned based on bulk calorimetric measurements;[24] hence it is necessary to calculate these system specific values based on measurements of $[M]_p$. So far it has been impossible to obtain accurate data for the monomer concentration in smaller latex particles, because of the lack of control to synthesize monodisperse small particles and the poor colloidal stability of such small particles. However, with the amphipathic macro-RAFT system such small particles can be reproducibly synthesized. Since these particles are electrosterically stabilized, colloidal stability is ensured. It is therefore in principle possible to test the Morton equation for particles in the lower size range (< 25 nm) using the amphipathic macro-RAFT system, although one should take into account the different stabilization technique applied for these electrosterically stabilized particles. This is an opportunity for future work to establish values for this important kinetic parameter for particle sizes typical for the nucleation stage of an emulsion polymerization.

The monomer concentration within the latex particle can be measured by applying one of a number of techniques, e.g. centrifugation combined with steam distillation, static vapor pressure[24], static swelling[25] or kinetic studies. Kinetic studies can be performed by e.g. reverse PLP-SEC[26, 27], where one knows the propagation rate coefficient, k_p, and determines the monomer concentration from the MWD after the pulsed laser polymerization experiments. However, kinetic studies by Thickett et al.[7, 9, 10] have demonstrated that the entry and exit of radicals is affected by the poly(acrylic acid) stabilizing groups for these electrosterically stabilized particles. Kinetic studies would have to take these effects into account before reliable measurements of the monomer concentration based on PLP-SEC are possible. The dependency of entry and exit on the stabilizing poly(acrylic acid) blocks leads to another important parameter for interpreting the model for the amphipathic macro-RAFT system, the average number of radicals per particle.

6.2.4 Average number of radicals per particle

The kinetics and mechanism for radical exit and entry in emulsion polymerization with electrosterically stabilized particles have been studied by Thickett et al.[7, 9, 10]. These authors performed seeded chemically initiated and γ relaxation experiments[28] with styrene. It was found that the electrosterically stabilized particles by poly(acrylic acid) chains have a significantly lower average number of radicals per particle than completely electrostatically stabilized particles (e.g. conventional SDS based emulsion polymerization).

In styrene emulsion experiments with electrostatically stabilized particles, the fate of radicals leaving the particle, in this type of zero-one system[22, 23, 29, 30], is to re-enter another particle without aqueous-phase termination (limit 2a). Radical loss is in this case only by bimolecular termination in particles already containing a radical, i.e. a propagating polymer chain. However, applying this radical loss mechanism leads to an unrealistically low radical entry

rate from the aqueous phase, compared to the expected z-meric species produced according to Maxwell-Morrison theory[5]. When radical loss was modelled as a first order process, i.e. after exit the radical is terminated in the aqueous phase (either by aqueous phase homo- or hetero termination), excellent agreement with an expected radical entry rate (Maxwell-Morrison theory) was obtained. The complete radical loss after exit can be rationalized by assuming preferential transfer of radicals to the poly(acrylic acid) stabilizing chains. In this way "midchain" radicals are formed that facilitate radical termination in the poly(acrylic acid) surface layer[31]. This point of view concerning termination in the poly(acrylic acid) surface layer was verified by a standard styrene bulk polymerization experiment in the presence of low molecular weight poly(acrylic acid). This experiment demonstrated that poly(acrylic acid) is a very good transfer agent as shown by the lower average molecular weights of polystyrene that were obtained after the bulk polymerization[9] compared to standard styrene bulk experiments.

In principle the same transfer reaction of a radical species to poly(acrylic acid) chains could occur during the initial synthesis steps of the macro-RAFT. However, as these reactions are performed in solution, all reactions are taking place in one phase. In the presence of the RAFT molecules radical transfer reactions will be dominated by the reversible addition fragmentation reaction steps, making the occurrence of transfer to poly(acrylic acid) most likely negligible. This hypothesis could be tested by NMR measurement to measure the amount of branches in the initial macro-RAFT species.

The steady state number of radicals per particle of a zero-one system undergoing first order radical loss by termination before re-entry can be represented by:

$$\bar{n} = \frac{\rho}{2\rho + k} \tag{6.5}$$

Here the average exit rate of radicals from the particle, *k*, in this sterically stabilized system is estimated according to a model reported by Thickett and Gilbert[10]. This model requires the particle size, which was assigned a constant average value, yielding k = 4×10^{-3} s^{-1}. The value of the average number of radicals entering the particle, ρ, was calculated from the Maxwell-Morrison model [5], which includes an explicit dependence on N_P, see equation (6.6), with z = 2 and the other parameters as collected in table 3.1.

$$\rho \approx \frac{2fk_d[I]N_A}{N_P}\left\{\frac{2\sqrt{fk_d[I]k_{t,W}}}{k_{p,W}[M]_W}+1\right\}^{1-z} \tag{6.6}$$

The average number of radicals per particle, represented by equation (6.5), depends in fact on the number of particles, see equation (6.6). When calculating the number of particles with the derived expression for particle number, represented by equation (6.1)and (6.2), one has to implement the resulting number of particles again in the calculations for the average number of radicals per particle and the resulting relation between equation (6.1) and (6.6) must be solved iteratively until convergence is reached.

6.2.5 Sensitivity analysis model parameters

All the above described properties were implemented in the expression for the number of particles. In order to determine the most influential parameters the calculations were performed with the derived values of $[M]_P$ and A_E, $\bar{n}$ was calculated iteratively for every obtained number of particles. Subsequently calculations for every parameter were repeated with a value 50% larger and smaller, keeping all other parameters equal to the default values, see Table 6.2.

Table 6.2: Sensitivity analysis of model parameters on the nucleation time and thus number of particles, iteratively solving the relation between N_p and ρ with a value of $k = 4 \cdot 10^{-3}$ s^{-1} as reported in literature[10].

Property	Value	t [s]	ρ [10^{-2} s^{-1}]	$\overline{n}$	N_P [·10^{20} m^{-3}]
-50%	967	19	3.8	0.48	6.6
[M]$_P$ [Mol m^{-3}]	1933	13	5.8	0.48	4.3
+50%	2900	12	6.3	0.49	3.9
-50%	0.59	132	0.6	0.37	45.2
A$_E$ [nm^2]	1.17	13	5.8	0.48	4.3
+50%	1.76	4	20.1	0.50	1.2
-5	15	4	17.6	0.49	1.4
X$_{crit}$	20	13	5.8	0.48	4.3
+5	25	27	2.7	0.46	9.3

The results in Table 6.2 demonstrate that the calculated nucleation time, and thence the particle number are extremely sensitive to the specific surface area of the macro-RAFT agent. As a consequence a very short nucleation time is obtained during which only a small fraction of the z-meric species necessary to initiate the experimentally found particles is generated. The small area of the macro-RAFT agent, cubed in the denominator of the nucleation time calculation, see equation (6.2), has a huge influence for the model calculations. Physically the inversely proportional influence of the cube of A$_E$ on the nucleation time can not be explained. A larger surface area of the macro-RAFT agent will only decrease the aggregation number of the macro-RAFT agents in the micelles[32]. As a consequence the total surface area generated by the growing particles would have to be larger for nucleation to cease, which would result in a longer nucleation time instead of a shorter one. Apparently, the assumptions on which the model is based have to be reconsidered.

The next biggest influence has the critical degree of polymerization for the macro-RAFT agent; the monomer concentration in the particles changes the particle number only marginally.

Another indication that the surface area has too large an influence on the particle number calculated by the model is the fact that the average number of radicals per particle is much higher in these calculations than was derived from experiments for a similar system by

Thickett et al.[9] using the same exit value. Average radical numbers per particle in the same range as the data of Thickett et al. were obtained for the model calculations when the SDS specific surface area was used in the initial calculations with reasonable physico-chemical parameters, see table 3.1.

6.2.6 Number of RAFT agents per particle

According to the nucleation model, all macro-RAFT agents involved in nucleation will be surface active and mobile through the aqueous phase until X_{crit} is reached. To test this assumption the experimentally obtained number of RAFT agents per particle are compared with literature values.[3, 4]

Table 6.3: Average number of RAFT molecules per particle for macro-RAFT systems of varying initial surface activity in semi-batch styrene experiments.

RAFT agent + concentration	[Initiator] mM	Particle diameter [nm]	RAFT/particle
10AA+10STY	2.5	24	145
(6.15 mM)	2.5	25	154
	2.5	26	177
8AA+8STY*	10.1	30	140
(2.5-3.3 mM)	5.1	30	121
	4.0	30	131
	3.0	28	119
	1.9	33	168
	1.0	36	237
	0.6	42	392
10AA+5STY (3x) ¤	2.4	37	524
10AA+5STY(1.5x) ¤	2.4	35	227
10AA+5STY(1x) ¤	2.4	34	138
10AA (2.5 mM)	2.5	98	10000

* Data Ganeva et al.[3] with corrected HDC particle size values, taking into account the shell thickness as determined by SANS.
¤ Data Sprong et al.[4]

It was demonstrated that the number of RAFT agents per particle depends on the initial surface activity of the amphipathic macro-RAFT agent. On one hand, if the initial macro-RAFT agents are already surface active at the start of the nucleation, the aggregates of macro-RAFT agents are precursors for particle formation upon entry of a z-meric radical. On the other hand, initial hydrophilic macro-RAFT agents will reside in the aqueous phase, where by relatively slow aqueous phase polymerization they will first have to attain a sufficiently long

hydrophobic block to become surface active and participate in nucleation process or adsorb onto existing growing particles.

It should be noted that the most hydrophobic macro-RAFT agents (10AA+10STY) contained on average a similar amount of RAFT agents as the aggregation number within the initial micelles, it seems therefore that in this particular case the time constant for transport of the macro-RAFT agents is high in comparison with the time constant of the nucleation of the micelles.[33, 34] This was demonstrated by Ganeva et al.[3]. These authors reported that by reducing the initiator concentration the nucleation time was extended, resulting in higher numbers of RAFT molecules per particle for systems with the same amount of hydrophobic macro-RAFT agent (8AA+8STY). Based on the experimental results the following nucleation situations are proposed for the macro-RAFT systems:

Case A: The initial macro-RAFT agents are too hydrophilic and are not surface active enough for participation in nucleation without further growth. In the case where the macro-RAFT agent is only a hydrophilic block, the shortest ones will become surface active first. After becoming surface active these macro-RAFT agents either aggregate or form a particle by homogeneous nucleation. High numbers of macro-RAFT agents per particle are expected, since the macro-RAFT molecules will only gradually become surface active enough to adsorb or nucleate.

Case B: The macro-RAFT agents are surface active and are still mobile in the aqueous phase. Nucleation can occur by stinging of micelles by a z-meric radical, macro-RAFT agents will adsorb onto growing particles. A strong dependence on initiator concentration is expected for the number of macro-RAFT molecules per particle, with a lower boundary formed by the aggregation number in the micelles.

Case C: The macro-RAFT agents are strongly hydrophobic (but still dissolve in the reaction medium), the macro-RAFT agents are already aggregated before the reaction starts. However, on the time scale of nucleation little or no transport of these RAFT agents occurs through the aqueous phase. Therefore the number of macro-RAFT agents per particle is equal to (or in the order of) the aggregation number in the micelles. This is the case in the model where $X_0 \geq X_{crit}$.

However, the synthesized macro-RAFT agents used in this study were always distributions of various degrees of polymerization of acrylic acid and in case of the preformed di-blocks, there is the further complication of a non-monodisperse distribution of styrene or n-butyl acrylate on top of the initial distribution of acrylic acid. Thus it is most likely that more than one of the situations discussed above play a role during the nucleation stage. For a systematic study it would therefore be necessary to fractionate the initial hydrophilic macro-RAFT agent and do that again after the formation of the di-block. With these macro-RAFT agents of a specific degree of surface activity the above situations could be verified.

Working with the most hydrophobic macro-RAFT agents in the presence of a sufficient amount of initiator enables one to form latexes with a predefined particle number, based on the initial aggregation number. The application of these kinds of macro-RAFT species provides therefore not only a procedure to form polymer with a narrow molecular weight distribution but also latex products with a predetermined number of particles.

When working with less surface active macro-RAFT systems that are still labile, one should take into account that a fraction of the macro-RAFT agents is probably too hydrophilic to participate in the nucleation process from the beginning. It is therefore important to include aqueous phase polymerization with hydrophobic monomers for this fraction in any future model describing nucleation for amphipathic macro-RAFT agents. One complicating factor

hereby is the lack of quantitative data on the composition and molecular weight distribution of the initial macro-RAFT agents. It has been demonstrated in chapter 4 that quantification of the initial molecular weight distribution for these block copolymers with a very hydrophilic block and a very hydrophobic block is no sinecure.

6.3 *Suggestions for future work*

It has been demonstrated here and elsewhere[2] that colloidal stable latexes of small particles with a narrow particle size distribution can be produced by semi-batch emulsion polymerizations in the presence of amphipathic RAFT agents. This technique can therefore be used to synthesize latexes with various small particle sizes. The saturation monomer concentration for all particles sizes can be measured for these electrosterically stabilized particles, which could provide valuable information for understanding nucleation conditions in regular emulsion polymerizations.

It proved to be difficult to obtain quantitative analytical results for the molecular weight distribution of block copolymeric macro-RAFT species with such large polarity differences. One possible approach for future quantification efforts could be to chemically modify[35, 36] the macro-RAFT species before analysis. Although previous studies in relation to the K_p of acrylic acid by the PLP-SEC method have proven that the modification process can have an influence on the apparent average molecular weight of the poly(acrylic acid), which was attributed to possible incomplete conversion of acid groups and the occurrence of side reactions influencing the polymer microstructure[37].

Once the behaviour of the styrene based macro-RAFT systems is completely understood, one could try to extend this knowledge to other monomeric system e.g. n-butyl acrylate where pseudo-bulk conditions are applicable.

6.4 *Conclusions*

It has been demonstrated by reprocessing the data of the Maron titrations with the specific surface area of an amphipathic macro-RAFT agent obtained from SANS measurements[3] that the estimation of 0.24 nm^2 per SDS molecule made in chapter 5 for the specific surface area of SDS at the surface area of small particles ($\approx$ 25 nm in diameter) was correct.

The experimental results of the specific surface area, A_E as determined by Maron titrations and SANS[3] and the derived values of $[M]_p$ and $\bar{n}$ for the amphipathic macro-RAFT systems have been implemented in the derived expression for particle numbers. It has been demonstrated that this expression is very sensitive towards the specific surface area of the macro-RAFT agent.

It has been demonstrated that surface active block copolymeric macro-RAFT agents are hardly mobile on the time-scale of nucleation as shown by the experimental number of macro-RAFT molecules per particle. As a consequence it is possible to predict the particle number using the initial aggregation number of the macro-RAFT agents, when working with the more hydrophobic and thus surface active macro-RAFT agents in the presence of a sufficient amount of initiator. The application of these kinds of macro-RAFT species provides therefore not only a procedure to produce polymer with a narrow molecular weight distribution but also latexes with a predefined number of particles.

6.5 *References*

1.   Gilbert, R. G. *Macromolecules* **2006,** 39, 4256-4258.
2.   Ferguson, C. J.; Hughes, R. J.; Nguyen, D.; Pham, B. T. T.; Gilbert, R. G.; Serelis, A. K.; Such, C. H.; Hawkett, B. S. *Macromolecules* **2005,** 38, 2191-2204.
3.   Ganeva, D. E.; Sprong, E.; Warr, G. G.; Such, C. H.; Hawkett, B. S. *submitted to Macromolecules*.

4. Sprong, E.; Leswin, J. S. K.; Lamb, D. J.; Ferguson, C. J.; Hawkett, B. S.; Pham, B. T. T.; Nguyen, D.; Such, C. H.; Serelis, A. K.; Gilbert, R. G. *Macromolecular Symposia* **2006,** 231, 84-93.

5. Maxwell, I. A.; Morrison, B. R.; Napper, D. H.; Gilbert, R. G. *Macromolecules* **1991,** 24, 1629-40.

6. Morton, M.; Kaizerman, S.; Altier, M. W. *Journal of Colloid Science* **1954,** 9, 300-12.

7. Thickett, S. C.; Gaborieau, M.; Gilbert, R. G. *submitted to Journal of American Chemical Society*.

8. Thickett, S. C.; Gilbert, R. G. *Macromolecules* **2005,** 38, 9894-9896.

9. Thickett, S. C.; Gilbert, R. G. *Macromolecules* **2006,** 39, 6495-6504.

10. Thickett, S. C.; Gilbert, R. G. *Macromolecules* **2006,** 39, 2081-2091.

11. van Berkel, K. Y.; Russell, G. T.; Gilbert, R. G. *Macromolecules* **2003,** 36, 3921-3931.

12. Maron, S. H.; Elder, M. E.; Ulevitch, I. N. *Journal of Colloid Science* **1954,** 9, 89-103.

13. Abbey, K. J.; Erickson, J. R.; Seidewand, R. J. *Journal of Colloid and Interface Science* **1978,** 66, 203-204.

14. van Zyl, A. J. P.; de Wet-Roos, D.; Sanderson, R. D.; Klumperman, B. *European Polymer Journal* **2004,** 40, 2717-2725.

15. Piirma, I.; Chen, S. R. *Journal of Colloid and Interface Science* **1980,** 74, 90-102.

16. Landfester, K. *Macromolecular Symposia* **2000,** 150, 171-178.

17. Kline, S. R. *Journal of Applied Crystallography* **2006,** 39, 895-900.

18. Mills, M. F.; Gilbert, R. G.; Napper, D. H.; Rennie, A. R.; Ottewill, R. H. *Macromolecules* **1993,** 26, 3553-62.

19. De Bruyn, H.; Gilbert, R. G.; White, J. W.; Schulz, J. C. *Polymer* **2003,** 44, 4411-4420.

20. Wallace, W. E.; Beck Tan, N. C.; Wu, W. L.; Satija, S. *Journal of Chemical Physics* **1998,** 108, 3798-3804.

21. Foerster, S.; Abetz, V.; Mueller, A. H. E. *Advances in Polymer Science* **2004,** 166, 173-210.

22. Gilbert, R. G., Emulsion Polymerization. In 1995; p 384.

23. Hawkett, B. S.; Napper, D. H.; Gilbert, R. G. *Journal of the Chemical Society, Faraday Transactions 1: Physical Chemistry in Condensed Phases* **1980,** 76, 1323-43.

24. Gardon, J. L. *Journal of Polymer Science Part A-1: Polymer Chemistry* **1968,** 6, 2859-2879.

25. Mathew J. Ballard, D. H. N. R. G. G. *Journal of Polymer Science: Polymer Chemistry Edition* **1984,** 22, 3225-3253.

26. Olaj, O. F.; Bitai, I.; Gleixner, G. *Makromolekulare Chemie* **1985,** 186, 2569-80.

27. Buback, M.; Gilbert, R. G.; Hutchinson, R. A.; Klumperman, B.; Kuchta, F.-D.; Manders, B. G.; O'Driscoll, K. F.; Russell, G. T.; Schweer, J. *Macromolecular Chemistry and Physics* **1995,** 196, 3267-80.

28. Lacik, I.; Casey, B. S.; Sangster, D. F.; Gilbert, R. G.; Napper, D. H. *Macromolecules* **1992,** 25, 4065-72.

29. Casey, B. S.; Morrison, B. R.; Maxwell, I. A.; Gilbert, R. G.; Napper, D. H. *Journal of Polymer Science, Part A: Polymer Chemistry* **1994,** 32, 605-30.

30. van Herk, A.; Editor, *Chemistry and Technology of Emulsion Polymerisation*. 2005;

31. von Sonntag, C. *Radiation Physics and Chemistry* **2003,** 67, 353-359.

32. Nagarajan, R. *Langmuir* **2002,** 18, 31-38.

33. Burguiere, C.; Pascual, S.; Bui, C.; Vairon, J.-P.; Charleux, B.; Davis, K. A.; Matyjaszewski, K.; Betremieux, I. *Macromolecules* **2001,** 34, 4439-4450.
34. Rager, T.; Meyer, W. H.; Wegner, G.; Mathauer, K.; Machtle, W.; Schrof, W.; Urban, D. *Macromolecular Chemistry and Physics* **1999,** 200, 1681-1691.
35. Plamper, F. A.; Becker, H.; Lanzendoerfer, M.; Patel, M.; Wittemann, A.; Ballauff, M.; Mueller, A. H. E. *Macromolecular Chemistry and Physics* **2005,** 206, 1813-1825.
36. Arakawa, R.; Egami, S.; Okuno, S. *Journal of Mass Spectrometry* **2006,** 41, 549-550.
37. Lacik, I.; Beuermann, S.; Buback, M. *Macromolecules* **2001,** 34, 6224-6228.

Appendices:

Appendix I: Supporting reaction curves
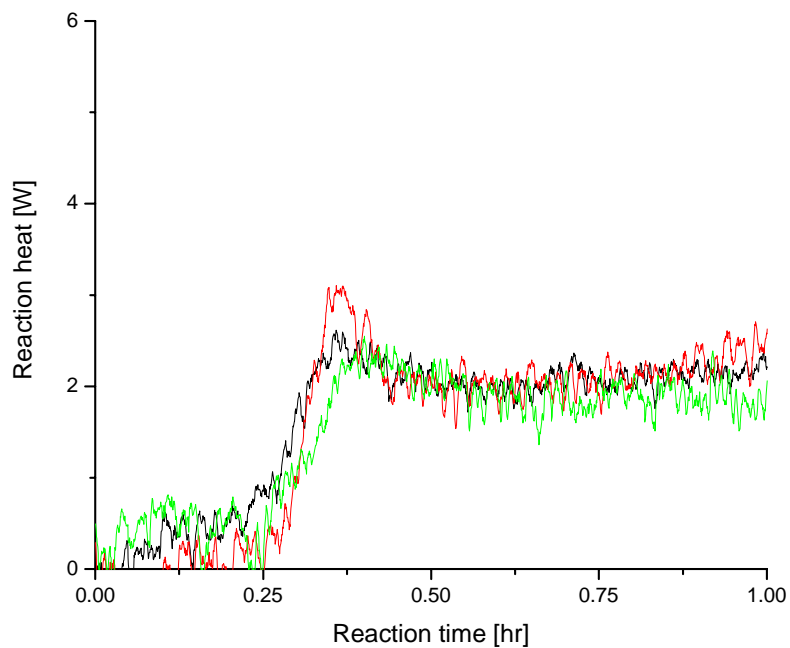
Figure A: Heat traces of controlled feed butyl acrylate experiments (at 60 °C) in the presence of preformed di-block macro-RAFT agents of 5 AA and 10 BA units. Nucleation start after about 15 min.
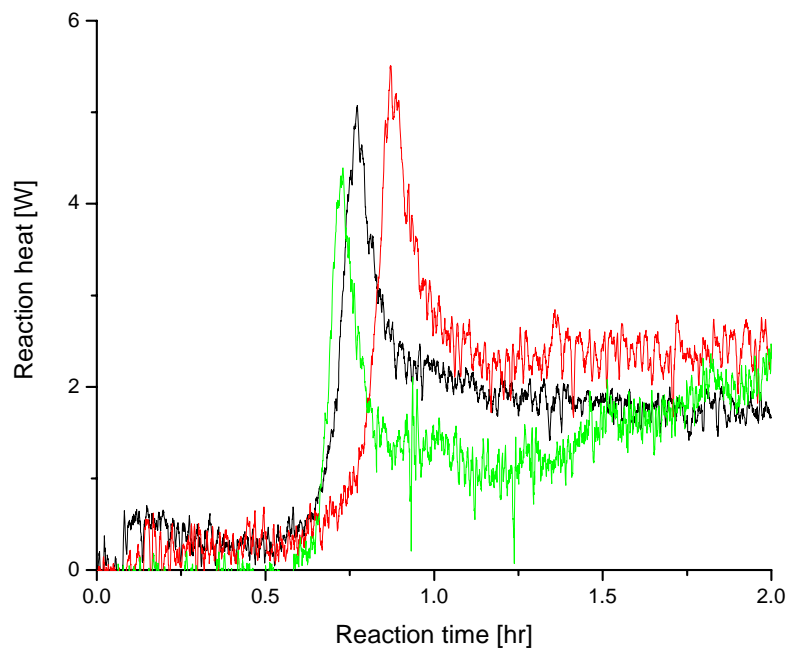
Figure B: Heat traces of controlled feed butyl acrylate experiments (at 60 °C) in the presence of preformed di-block macro-RAFT agents of 5 AA and 5 BA units. Nucleation start after about 35 min.
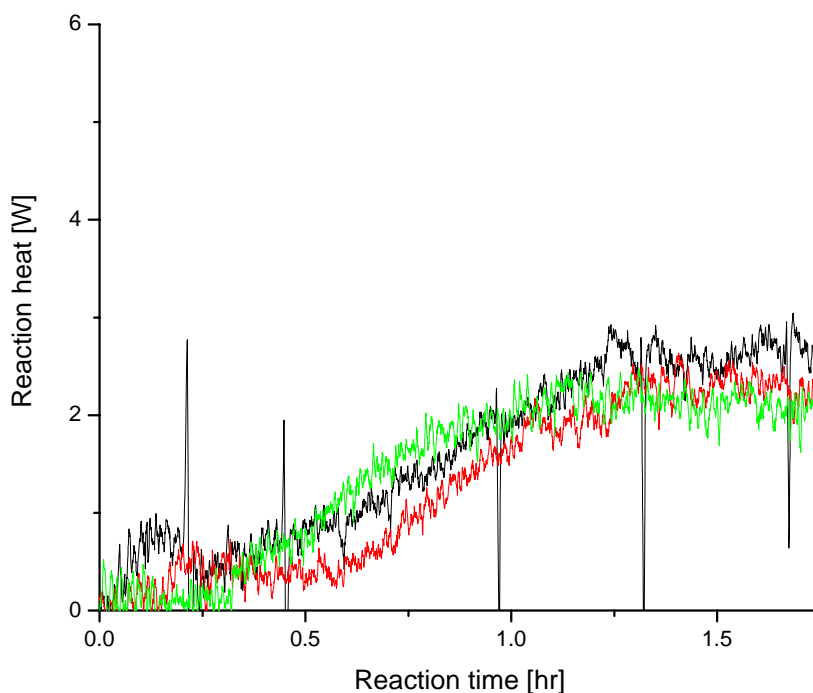
Figure C: Heat traces of controlled feed BA experiments (at 60 °C) in the presence of hydrophilic macro-RAFT agents of 5 AA units. Nucleation start after about 30 min. Notice that the dips in the heat signal are due to samples taken for off-line analysis.
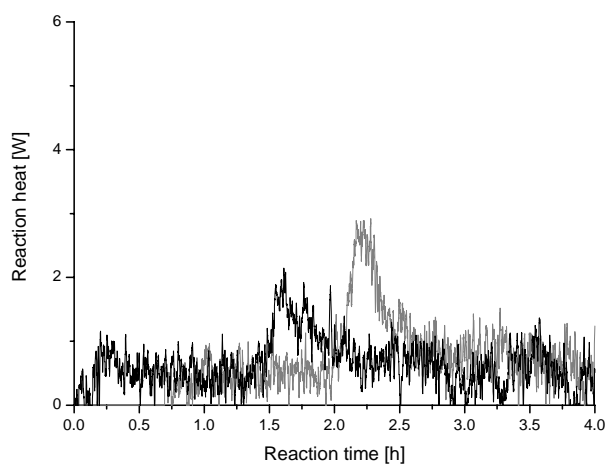
Figure D: Heat traces of controlled feed STY experiments (at 80 °C) in the presence of hydrophilic macro-RAFT agents of 10 AA units.
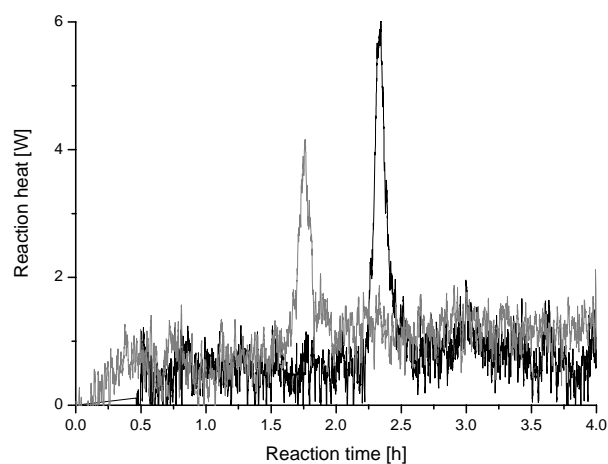
Figure E: Heat traces of controlled feed STY experiments (at 80 °C) in the presence of amphipathic macro-RAFT agents of 10 AA+10 STY units.

107

Appendix II: Separation of BA macro-RAFT agents under critical conditions

In order to find critical conditions for BA based macro-RAFT agents a model system was synthesized by solution polymerization. Butyl acrylate macro-RAFT agents were produced by polymerization of butyl acrylate in the presence of a RAFT agent (300:1, monomer:RAFT ratio) in toluene at 60 °C, designed to reach 20 % solid content at full conversion. All reactants, see Table 1, were added together in a round-bottom-flask and degassed with high purity argon before heating to the reaction temperature. Samples were taken at different times to obtain macro-RAFT agents with increasing average molecular weights.

Table 1: Recipe BA solution polymerization

Chemicals	Mass [g]
RAFT (C4)	0.028
Butyl acrylate	4.464
V-501	0.030
Toluene	17.43

Table 2: Sample information, times [min] and SEC results, Mn and Mw in 10^3 g mol^{-1}.

Sample	Time	Mn	Mw	PD
D	60	8.3	10.4	1.26
E	75	10.9	13.1	1.20
F	95	12.7	15.7	1.24
G	125	15.0	18.5	1.24
H	165	17.0	21.4	1.26
I	210	17.5	21.4	1.22

The samples were analyzed by SEC, see Table 2 and Figure G, under the conditions described in section 4.2.2. Subsequently a sample at low conversion (E) and one at higher conversion (I) were selected to find critical conditions for the BA macro-RAFT agents in HPLC, i.e. conditions where BA macro-RAFT agents of different molecular weights elute at the same elution volume.
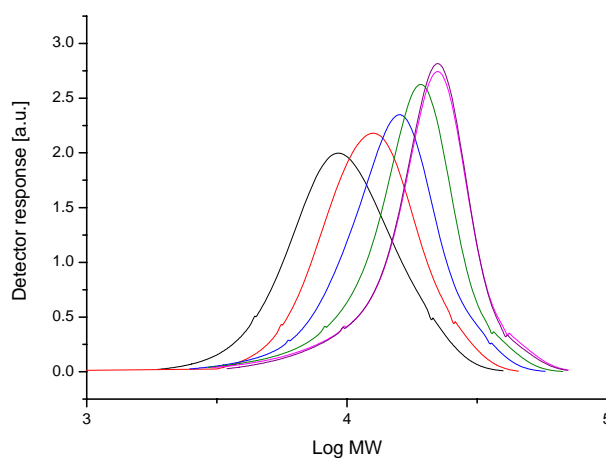
Figure F: SEC analysis of samples taken at different reaction times during BA solution polymerization at 60 °C in the presence of RAFT agent.

The critical conditions for BA macro-RAFT agents were investigated for three different static phases (C18-, CN- and OH-functionalized Nucleosil columns, Agilent).

Critical conditions for the BA based macro-RAFT agents could be obtained at literature conditions (ref 14, chapter 4) on the hydrophobic C-18 functionalized column, see Figure G. However, under these conditions hydrophilic macro-RAFT agents (5AA) are insoluble in the eluent, so no separation can be performed for the amphipathic macro-RAFT agents (which contain an array of hydrophilic and hydrophobic species). Both hydrophilic and more hydrophobic macro-RAFT agents dissolved in water/THF mixtures, but no critical conditions could be obtained for this eluent mixture for any of the used columns.
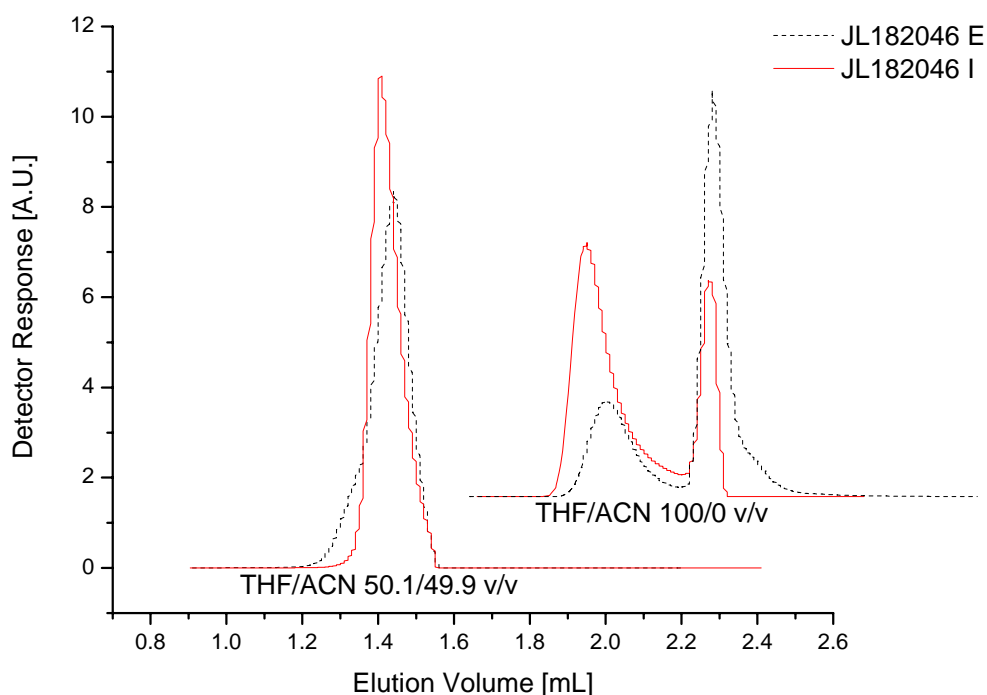
Figure G: Elution times of BA macro-RAFT agents over a C18-functionalized column at critical and non-critical eluent conditions.

Appendix III: TEM particle size distributions with ImageJ

The TEM image analysis is started by converting the raw image (see Figure E) to a binary image; this can be achieved using the automatic thresholding function. This divides the image into objects and background by taking a test threshold and computing the average of the pixels at or below the threshold and the pixels above it. It then computes the average of those two, increments the threshold, and repeats the process. This process of incrementing stops when the threshold is larger than the composite average. By applying a threshold to the raw TEM image small grayscale differences can introduce speckles on the particles, which can be removed by a process called appropriately despeckle. This is a median filter, which replaces each pixel with the median value in its 3×3 neighbourhood and is therefore a good method to remove "salt and pepper" noise in an image. After this process a cleaner binary picture is obtained, but all the connecting particles are still not measurable as individual particles. Watershed segmentation can be used to automatically separate or cut apart particles that touch. This works by first calculating the distance of each pixel to the nearest edge, to build up a so-called Euclidian distance map. It then dilates each of the local maxima as far as possible - either until the edge of the particle is reached, or the edge of the region of another local maximum in the Euclidian distance map. This algorithm works best for smooth convex objects that do not overlap too much. Most connected particles in the initial TEM picture were separated in this way (see Figure F).
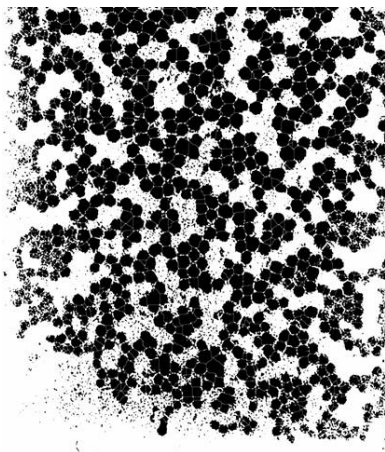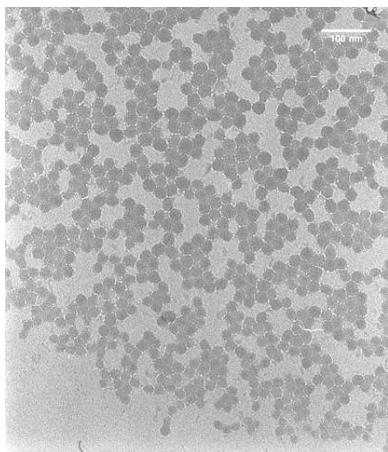
Figure H: Original TEM image.   **Figure I: Binary watershedded image.**   **Figure J: Minimum roundness and background removal.**

These individual particles can now be counted and measured by the inbuilt dedicated process. This works by scanning the image or selection until it finds the edge of an object. It then outlines the object and measures the area. For this process two important options and parameters can be set. In order to prevent false readings, the particles on the edge of the picture can be ignored. Remaining noise from the background of the original image and unseparated clusters of particles can be left out of the measurement by setting a minimum and maximum area for the measured particles. Care should be taken not to influence the PSD of the particles in this way. Another valuable parameter is the possibility of specifying the circularity of the particles as defined in equation (A.1).

$$circularity = 4\pi \left(\frac{area}{perimeter^2} \right) \hspace{2cm} (A.1)$$

In this way particles that were wrongly separated by the watershedding process can be left out of the particle size measurements. The resulting values for the areas of the particles were written to a spreadsheet. This multi-step image processing method was automated by creating a macro on the basis of the "batchsetscale" macro (available at the website of ImageJ).

111

// This macro batch processes a folder of images,
// setting the scales to a given specification.
// All the images must be in TIFF or DM3 format.
// After which it sets the treshold and despeckles it.
// The binary picture is subsequently analyzed for round particles of a minimum size.
// The resulting "masked" processed picture is saved as TIFF image and
// The resulting PSD data is saved as XLS data sheet.

```
requires("1.33n");
dir = getDirectory("Choose a Directory ");
list = getFileList(dir);
start = getTime();
setBatchMode(true); // runs up to 6 times faster
for (i=0; i<list.length; i++) {
    path = dir+list[i];
    //print(i+"  "+path);
    showProgress(i, list.length);
    open(path);
    title = getTitle();
    run("Set Scale...", "distance=0.614173228 known=1 pixel=1 unit=nm");
//depends on magnification, dm3 files generally do not need this step
    FileName = getTitle();
    run("Threshold");
    run("Despeckle");
    run("Watershed");
//select the range of particle sizes and circularity you want considered for measurement
    run("Analyze Particles...", "size=75-300000 circularity=0.4-1.00 show=Masks display
exclude clear");
        saveAs("Tiff", "D:\\"+FileName+" particilized.tif");
        saveAs("Measurements", "D:\\"+FileName+" PSD Results.xls");
    close();
 }
 // print((getTime()-start)/1000);
```

Acknowledgements / Dankwoord

First of all I would like to thank my supervisors Bob en Alex for giving me the opportunity to do a co-tutelle PhD between The University of Sydney and the Eindhoven University of Technology. This PhD project has been made possible with the financial support from the Key Centre for Polymer Colloids, the Foundation for Emulsion polymerization (SEP) and the European Graduate School (EGS). The Key Centre for Polymer Colloids was established and supported by the Australian Research Council's Research Centres Program. The support from Dulux Australia through the ARC linkage scheme together with their help in kind by providing me with enough RAFT agent to perform my experiments on the litre scale was really appreciated.

I could not have done this work without the support of many people, but first of all I would like to thank Bob my supervisor for his friendship and full commitment during my PhD even from the other side of the world, particularly the sharp analyses and discussions in the final write up were really appreciated. Maar ook in Nederland had ik een perfect team ter ondersteuning. Jan wil ik hierbij van harte danken voor alle leerzame discussies in de laatste twee jaar en de tijd en energie die je in mijn project en bij de tot stand koming van mijn boekje hebt gestoken. Jij bezit een buitengewone gave om mensen bij het verlaten van je kamer altijd weer vol positieve energie te laten vertrekken. Alex wil ik hierbij bedanken voor zijn vertrouwen en zijn steun als stille kracht van dit project, kritisch op het juiste moment en klaar voor een feestje bij een EGS weekend. Furthermore, I would like to thank all the members of the reading committee for their comments and suggestions.

Working in two places also means working with twice as many analytical set-ups, imaging techniques etc. I would like to express my gratitude for the technical help and advice from Binh and Duc with the TEM in Australia, and Peter Frederik, Paul Bomans and Hans Duimel for the (cryo-) TEM advice and measurements at Maastricht University. In Eindhoven, Niek Lousberg and Syed Imram Ali are gratefully acknowledged for providing me with TEM pictures in the final weeks of my PhD against all the odds. I would like to thank Keith, Hollie, Reza, Marion and Wieb for the various analyses and Henk for his help, thinking along during my characterization efforts. The helpful discussions with Bas and Robin and their support through the MALDI/ESI analysis software are much appreciated.

Curriculum Vitae

Joost Sieger Kaspar Leswin werd geboren op 15 maart 1978 te Eindhoven. Aan het Christiaan Huygens College te Eindhoven behaalde hij in 1996 zijn VWO diploma. In datzelfde jaar startte hij de opleiding Scheikundige Technologie aan de Technische Universiteit Eindhoven, waarbinnen hij zich specialiseerde in polymeerchemie. De studie werd succesvol afgerond in januari 2002. Na een klein jaartje te hebben gewerkt binnen PGI Nonwovens te Cuijk verkoos hij het onderzoek boven de productie. In maart 2003 startte hij een co-tutelle promotieonderzoek onder begeleiding van prof. dr. Robert Gilbert binnen de Key Centre for Polymer Colloids aan de universiteit van Sydney, Australië. In mei 2005 vervolgde hij zijn promotie onderzoek binnen de groep polymeerchemie aan de TU/e onder begeleiding van prof. dr. Alex van Herk en dr. Jan Meuldijk. De belangrijkste resultaten van zijn werk staan in dit proefschrift beschreven. Vanaf 1 juni 2007 zal hij in dienst treden als onderzoeker op het gebied van dispersies binnen BASF AG, Ludwigshafen, Duitsland.

Joost Sieger Kaspar Leswin was born on the 15th of March 1978 in Eindhoven, the Netherlands. In 1996 he obtained his secondary school certificate at the Christiaan Huygens College in Eindhoven. It the same year he started his degree in Chemical Engineering at the Eindhoven University of Technology. During his study he specialized in polymer chemistry and in January 2002 he obtained his masters degree. After working almost a year in industry at PGI Nonwovens, Cuijk, the Netherlands, he chose to continue his career in research. In March 2003 he started a co-tutelle PhD under the supervision of Prof. Dr. Robert Gilbert at the Key Centre for Polymer Colloids at the University of Sydney, Australia. In May 2005 he continued the project within the laboratory for polymer chemistry at the Eindhoven University of Technology under the supervision of Prof. Dr. Alex van Herk and Dr. Jan Meuldijk. The main results of his PhD-research are described in this thesis. From the 1st of June 2007 he will start working as a researcher in the field of dispersions at BASF AG, Ludwigshafen, Germany.